CZECH TECHNICAL UNIVERSITY IN PRAGUE
FACULTY OF BIOMEDICAL ENGINEERING
Department of Biomedical Technology

Master Thesis

2016 Jihyeon Seo

ČESKÉ VYSOKÉ UČENÍ TECHNICKÉ V PRAZE
FAKULTA BIOMEDICÍNSKÉHO INŽENÝRSTVÍ
Katedra biomedicínské techniky

Bridging the gap between rat and human EEG-fMRI epilepsy studies

Master thesis

Study programme: Biomedical and Clinical Technology
Field of study: Biomedical Engineering

Author of master thesis: B.Sc. Jihyeon Seo
Supervisor of master thesis: Ir. Willeke Staljanssens

Kladno 2016

Czech Technical University in Prague, Faculty of Biomedical Engineering

Department of Biomedical Technology | Academic year: 2015/2016

Diploma thesis assignment

(Master project thesis assignment)

Student:	**Jihyeon Seo**
Study branch:	Biomedical Engineering (CEMACUBE)
Title:	**Bridging the gap between rat and human EEG-fMRI epilepsy studies**
Title in Czech:	Překlenutí mezery mezi EEG-fMRI epileptickými studiemi u potkanů a člověka

Instructions for processing:

Perform scalp EEG-fMRI on rat in resting state. Perform scalp EEG-fMRI on rat when seizure is induced by kainic acid. Analyse the dataset of the Resting State with different methods. Analyse the dataset when the seizure was induced with different methods. Compare the result of the analysed resting state and the one of the analysed epileptic dataset.

References:

[1] Raedt, R., et al., Seizures in the intrahippocampal kainic acid epilepsy model: characterization using long-term video-EEG monitoring in the rat, Acta Neurologica Scandinavica, ročník 119, číslo 5, 2009, Květen, 293–303 s., doi:10.1111/j.1600-0404.2008.01108.x
[2] Rosazza, C., Minati, L., Resting-state brain networks: literature review and clinical applications, Neurological Sciences, ročník 32, číslo 5, 2011, Říjen, 773-785 s., doi:10.1007/s10072-011-0636-y
[3] Gotman, J., Epileptic networks studied with EEG-fMRI, Epilepsia, ročník 49, číslo s3, 2008, Březen, 42-51 s., doi:10.1111/j.1528-1167.2008.01509.x

Validity of assignment until date: 20.08.2017

Supervisor of diploma thesis: Ir. Willeke Staljanssens

..... Head of Department

..... Dean

In Kladno, 22.02.2016

Declaration

I hereby declare that I have completed this thesis with the topic “Bridging the gap between rat and human EEG-fMRI epilepsy studies” independently, and that I have attached an exhaustive list of citations of the employed sources to the Master thesis.

I do not have a compelling reason against the use of the thesis within the meaning of Section 60 of the Act No.121 / 2000 Coll., on copyright, rights related to copyright and amending some laws (Copyright Act).

In Kladno ……..……..……

Acknowledgements

First of all, I would like to express my deepest gratitude to my supervisor, Willeke Staljanssens for her consistent guidance and practical help on thesis work. Also, I want to thank prof. Robrecht Raedt for verification of seizure detection and also for some advice on EEG analysis. Other thanks go to Nathalie Van den Berge for her advice on fMRI data analysis. Thanks to all of them, I was able to finish this Master thesis.

Also, I would like to thank Benedicte Descamps, prof. Christian Vanhove for their practical support during the experiments. Without them, I could not have done the experiments as planned.

Most importantly, I would like to express how grateful I am towards my family. They have always supported me for whatever I wanted to do. Due to their unconditional love and support, I could have the privilege doing my Masters in two beautiful European countries, Czech Republic and Belgium and I was able to complete my Master thesis. Plus, I want to thank all my close friends who were always ready to cheer myself up during the thesis writing period.

Without all these people, I could not have become who I am today. This master thesis period has been extremely challenging but also enjoyable and worthwhile. I believe that this experience will prepare me better for whatever it comes during the next stages of my life. Thank you.

Bridging the gap between rat and human EEG-fMRI epilepsy studies

Jihyeon Seo

Abstract

Scalp EEG-fMRI has been widely used in clinical epilepsy studies to accurately localize and delineate the epileptogenic zone. On the other hand, in rat epilepsy studies, a pair of implanted electrodes in hippocampus has been used instead of scalp electroencephalogram (EEG) since the EEG signal can be directly measured from the seizure onset zone. However, the invasiveness of this EEG method is a major drawback. In our study, we introduced the Magnetic Resonance (MR) compatible scalp EEG cap that is designed in our lab to simultaneous scalp EEG-fMRI rat epilepsy studies. The aim of the thesis was to examine whether the scalp EEG cap could effectively record seizures and whether it could aid simultaneous EEG-fMRI studies to study functional connectivity of the brain in resting state and in seizures. For this purpose, we performed standalone EEG recording in resting state, standalone functional Magnetic Resonance Imaging (fMRI) scanning in resting state and simultaneous EEG-fMRI in resting state and in evoked seizures. Kainic acid (KA) was injected to rats intraperitoneally to induce seizures. The EEG recordings were analyzed whether they could capture seizure activity. In addition, we analyzed fMRI datasets using three different methods which were 10x10 Region of Interest (ROI) correlation analysis, General Linear Model (GLM) analysis and Independent Component Analysis (ICA). The EEG recordings were able to show the seizures which were seen with repeated sharp waves and peaks in delta and theta frequency region. Next, the ROI correlation analysis result of the seizure datasets showed increased correlation coefficients but also decreased coefficients compared to the ones of the resting state dataset of the same rat. In addition, we carried out GLM analysis with the seizure scans that are confirmed by EEG recording. The GLM analysis of a seizure dataset resulted in showing the functionally connected brain regions during evoked seizures such as neocortex, cingulate cortex, striatum, corpus callosum and hippocampus. Besides, ICA showed the similar brain regions that were functionally connected for the dataset. Also, when the GLM analysis could not show any significant functionally connected brain region for another seizure dataset, ICA could extract the voxels of which their time series were highly correlated. These findings suggest that the MR compatible scalp EEG cap could be used as a valuable tool in rat EEG-fMRI epilepsy studies and could play a role as an experimental platform to bridge the gap between preclinical epilepsy studies and clinical epilepsy studies.

Keywords: Epilepsy, Simultaneous EEG-fMRI, scalp EEG, functional connectivity

Contents

List of Figures

List of Tables

List of Abbreviations

- CNS = Central Nervous System
- PNS = Peripheral Nervous System
- fMRI = functional Magnetic Resonance Imaging
- EEG = electroencephalogram
- ECG = electrocardiogram
- ECoG = electrocorticogram
- iEEG = intracranial electroencephalogram
- SNR = Signal to Noise Ratio
- A/D = Analog/Digital
- MRI = Magnetic Resonance Imaging
- RF = radiofrequency
- BOLD = Blood Oxygen Level Dependent
- MR = Magnetic Resonance
- ILAE = International League Against Epilepsy
- IBE = International Bureau for Epilepsy
- AED = Anti-Epileptic Drug
- TMS = Transcranial Magnetic Stimulation
- VNS = Vagus Nerve Stimulation
- DBS = Deep Brain Stimulation
- TLE = Temporal Lobe Epilepsy
- KA = Kainic Acid
- PILO = pilocarpine
- SE = Status Epilepticus
- ROI = Region Of Interest
- GLM = General Linear Model

- ICA = Independent Component Analysis
- MAPSHIM = Multi Angle Projection SHIM
- GE-EPI = Gradient Echo – Echo Planar Imaging
- FOV = Field Of View
- TR = Time to Repeat
- TE = Time to Echo
- FWHM = Full Width Half Maximum
- RS = Resting State
- FFT = Fast Fourier Transformation
- SPM = Statistical Parametric Mapping
- HRF = Hemodynamic Response Function
- FWE = Family Wise Error

Chapter 1

Introduction

Background

Epilepsy is one of the major chronic neurological diseases and it affects approximately 65 million people worldwide [10]. Anti-epileptic drugs (AEDs) are prescribed to the patients as a treatment. However, it is known that 20-30 percent of the patients cannot achieve seizure freedom with AEDs and they are referred to as refractory epileptic patients [11]. Often, these patients go through resective surgery to remove the onset region of the seizures. Nevertheless, not all refractory epileptic patients are good candidates for the surgery. Patients who have an unclear seizure onset region or multiple seizure onset regions may not achieve seizure freedom after surgery and may have post-operative functional deficits in language and memory [12]. Therefore, the pre-surgical evaluation of epilepsy patients is crucial to delineate epileptogenic zone and to predict possible surgical outcome.

For precise localization and delineation of the epileptogenic zone, scalp EEG-fMRI has been a widely used approach in clinics. Electroencephalogram (EEG) measures the electrophysiological signals from the brain with high temporal resolution and functional Magnetic Resonance Imaging (fMRI) measures BOLD (Blood Oxygen Level Dependent) signals that tell us the hemodynamic response in the brain with high spatial resolution. Therefore, scalp EEG-fMRI has been used as a complementary, non-invasive, pre-surgical evaluation tool in clinical epilepsy studies [13]. On the other hand, preclinical rat EEG-fMRI epilepsy studies are usually done with implanted electrodes [14, 15]. However, the invasiveness of the method is a major drawback and to our knowledge, there has been no scalp EEG-fMRI epilepsy studies on rats. Therefore, we introduce a Magnetic Resonance (MR) compatible scalp EEG cap for rats that was designed in our lab last year [9] not only in standalone EEG recording but also in simultaneous EEG-fMRI measurements to provide a non-invasive experimental platform that is compatible with clinical EEG-fMRI epilepsy studies.

Aim of the thesis

The aim of the thesis is to test whether the scalp EEG could correctly record seizures and moreover facilitate EEG-fMRI studies to study functional connectivity in resting state and also in evoked seizures. Through this, we evaluate the potential usefulness of the MR compatible scalp EEG cap for rats in bridging the gap between preclinical epilepsy studies and clinical epilepsy studies. For this purpose, we analyzed EEG recordings and utilized three different data analysis methods for fMRI data which are 10 x 10 Region Of Interest (ROI) correlation analysis, General Linear Model (GLM) analysis and Independent Component Analysis (ICA).

Overview of the thesis

In chapter 2, we discuss the theoretical background to understand the topic of the thesis. In chapter 3, we describe all the experimental procedures in detail that we carried out ranging from the animal preparation, seizure induction, EEG recording, fMRI scanning, processing of EEG data to the processing of fMRI data. In chapter 4, we show the results of the data analysis. Afterwards in chapter 5, we interpret the results and discuss implications that they might have and also limitations of the current work and possible future works. Lastly in chapter 6, we draw a conclusion whether the MR compatible scalp EEG cap for rat would be useful in bridging the gap between rat and human EEG-fMRI epilepsy studies.

Chapter 2

Literature Review

2.1 The brain

In our body, there are two types of nervous system. One is the Central Nervous System (CNS) which consists of brain and spinal cord. The other is Peripheral Nervous System (PNS) which consists of cranial nerves and spinal nerves that connect CNS to the other body parts. The brain is the central organ in the CNS which controls a variety of bodily functions which will be discussed later. There has been a lot of research on the question how the brain regions are connected for its complex functions. The brain has been observed as a complex network-like organ and it is known that different regions of the brain communicate with each other even though they are distant away from each other. This is due to the functional connectivity which represents the similarities in patterns of activity in the regions of brain. The functional connectivity between different brain regions has been of one of the greatest interest in neuroscience along with advances in neuro imaging modalities such as functional Magnetic Resonance Imaging (fMRI) [16]. In this section, we will first discuss the neuron which is the basis form of the brain, the anatomy of the brain and the functional connectivity of the brain.

2.1.1 The neurons

The components of the neurons

Neurons are cells which are the core element of the brain. Neurons respond to electrochemical changes in the adjacent area. They are able to deliver the information to other neurons. This is possible due to their three components which are axon, dendrites and cell body. The cell body contains nucleus and cytoplasm. The dendrites acquire the input and then the axons send away the bioelectrical signals. The neurons may have several dendrites but they have only one axon. These three components of the neuron can be seen in figure 2.1. The ends of axons create the contact point with dendrites of other neurons and this is called synapse. The neurons communicate by sending and receiving electrochemical information at synapses. This information is carried by biological molecules called neurotransmitters [1].

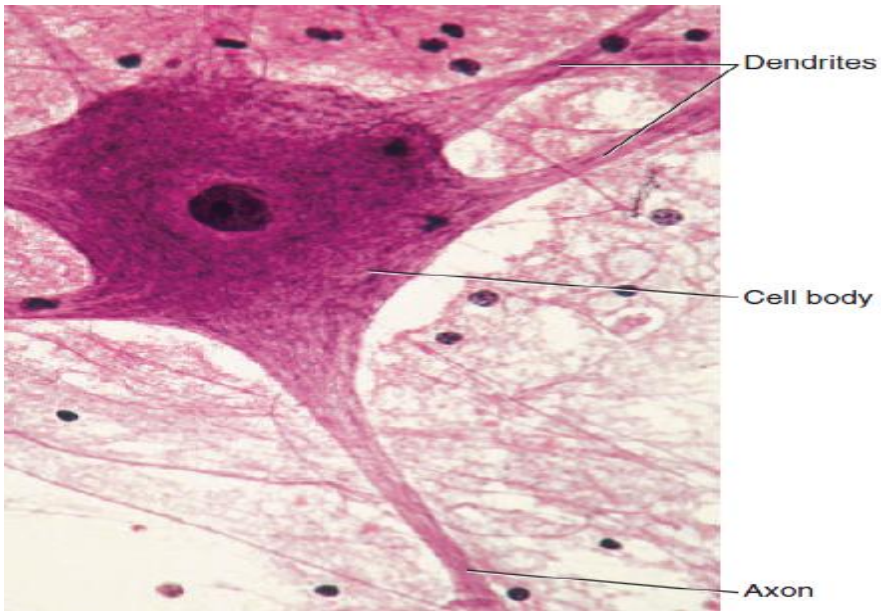

Figure 2.1: The neuron [1]

The classification of the neurons

The neurons can be classified by two different ways. One is by structural differences and the other is by functional differences.

The classification of the neurons by structural differences

The neurons can be classified into three groups by structural differences. First, the **bipolar neurons** are the neurons that have two processes branching from the cell body. One is axon and the other is dendrite. This type of neurons is found in eyes, nose and ears. The second type is **unipolar neurons**. Unipolar neurons have a single process from its cell body. This process is divided into two branches. One branch includes the dendrites and the other branch is the axon which enters the brain or the spinal cord. The cell bodies of the unipolar neurons accumulate outside of the CNS and this is called ganglia. The last type is **multipolar neurons**. The multipolar neurons have multiple processes extending from the cell body. Among these processes, only one process is axon and the others are dendrites. Most of the neurons whose cell bodies are located within the CNS are multipolar neurons. The three different structural types of neurons can be seen in figure 2.2 [1].

The classification of the neurons by functional differences

The neurons can also be classified into three groups that are determined by whether they transfer information into the CNS, within the CNS or out of the CNS. The first type is **sensory neurons** which are also called as afferent neurons. They carry information from peripheral body parts into the CNS. Most sensory neurons are unipolar but some are bipolar structurally. The second type is **interneurons** which are also called as association neurons. They are located within the CNS and they transport information from one part of the brain or the spinal cord to another part. Structural characteristic of the interneurons is multipolar. The last type is **motor neurons** which are also called efferent neurons. They carry information from the CNS to the effectors such as muscle or gland. Also they are multipolar [1].

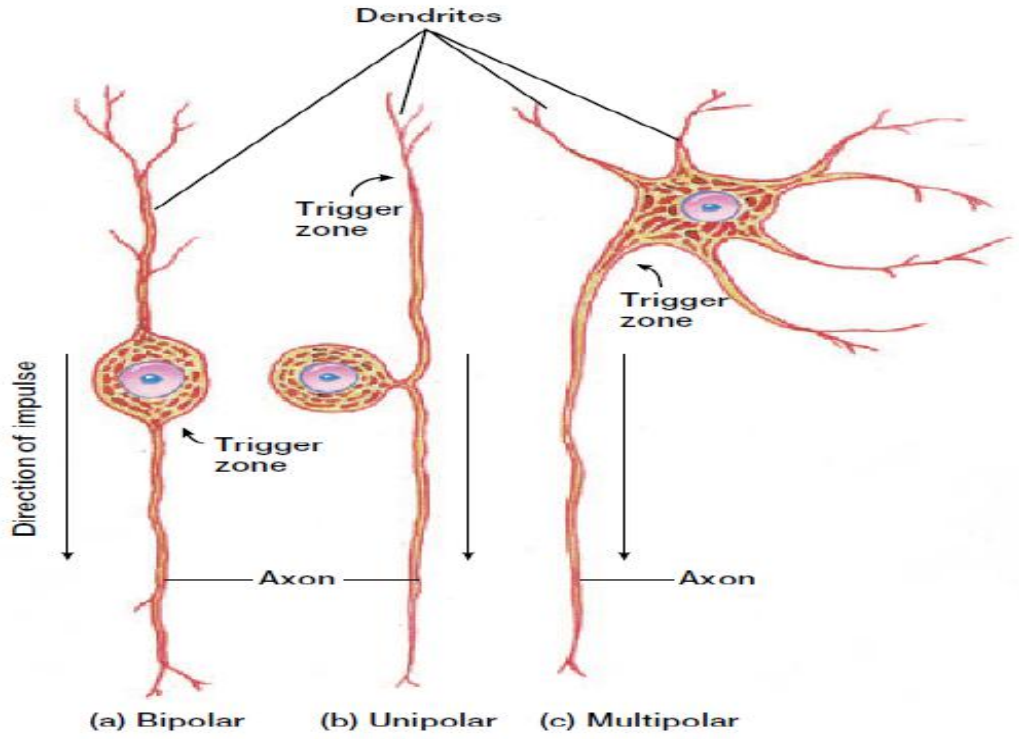

Figure 2.2: The structural types of neurons [1]
Trigger zone is a sensitive region of the axon where the nerve impulse is originated.

2.1.2 The anatomy of the brain

The major components of the brain are the cerebrum, the cerebellum and the brain stem. The whole structure of the brain can be found in figure 2.3. The **cerebrum** is the largest component of the brain. It is divided into left and right hemispheres. There is a structure of nerve fibers called corpus callosum that connects these two hemispheres. The cerebral hemispheres are divided into lobes. The name of the lobes is taken from the name of the skull bones that are overlying the lobes. There are frontal lobe, parietal lobe, temporal lobe and occipital lobe. The lobes of the cerebral hemispheres can be seen in figure 2.4. The outermost part of the cerebrum consists of thin layer of gray matter called **cerebral cortex**. Approximately 75% of all neuron cell bodies in the nervous system are in the cerebral cortex. There is a bulk of white matter that constitutes major part of the cerebrum under the cerebral cortex. This is made of stacks of nerve fibers which unite neuron cell bodies in the cerebral cortex with other parts of the nervous system. This white matter connects different parts of the cerebrum to each other [1].

The lobes of the cerebrum have different functions. First, the frontal lobes are responsible for controlling movements of voluntary skeletal muscles and higher intellectual processes. Second, the parietal lobes are responsible for sensation of touch, pressure, pain and temperature and verbal abilities. Third, the temporal lobes are in charge of hearing, remembering and interpreting sensory experiences. Lastly, the occipital lobes are responsible for vision and associating visual images with other sensory experiences.

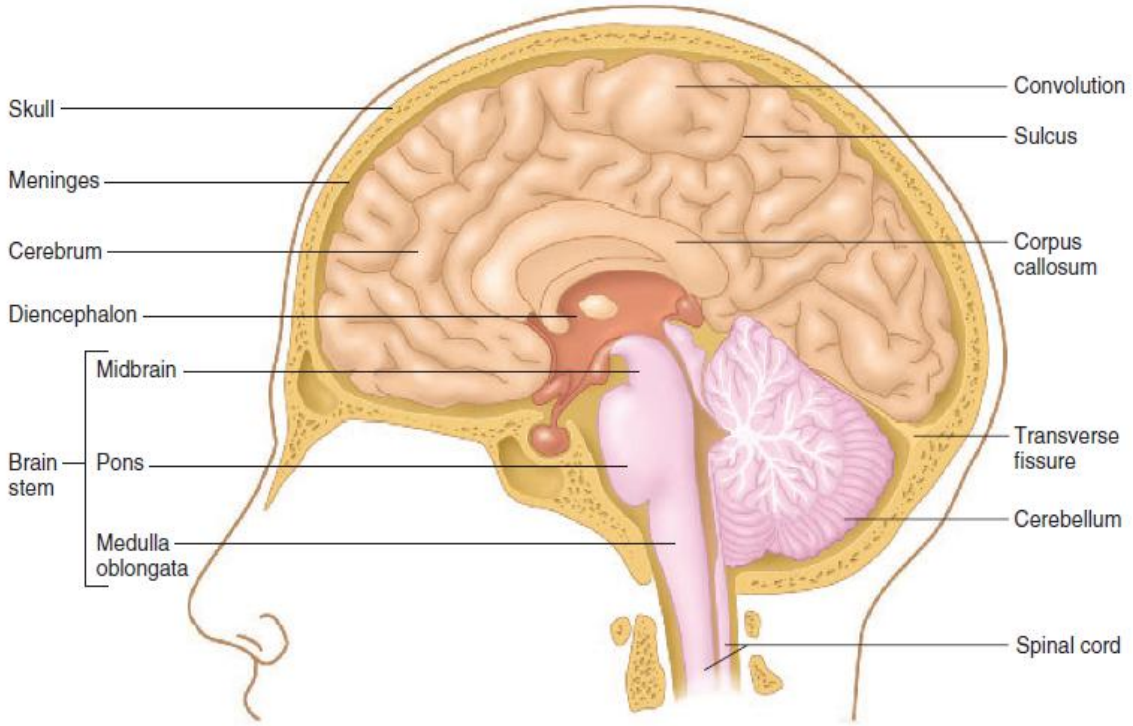

Figure 2.3: The whole structure of the brain [1]

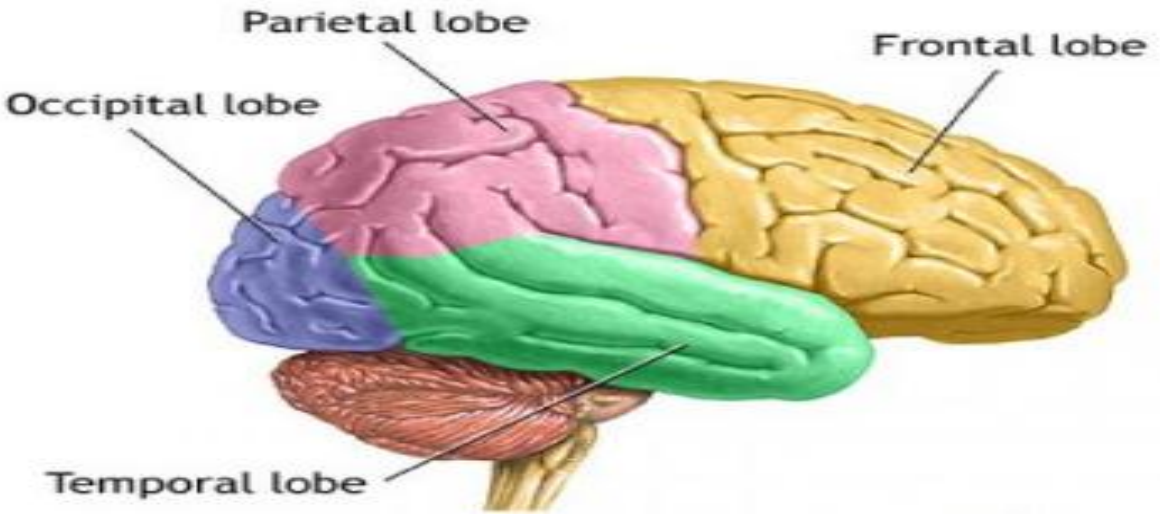

Figure 2.4: The lobes of the brain [2]

The second major component of the brain is the brain stem. The brain stem links the brain and the spinal cord. It is composed of the midbrain, pons and medulla oblongata. It contains several bundles of nerve fibers and loads of gray matter which are called nuclei. The last major component of the brain is the cerebellum. The functions of the brain stem include transporting impulses between the brain and spinal cord and reflexes. The cerebellum is located under the occipital lobe of the cerebrum and behind the pons and medulla oblongata of the brain stem. The major part of the cerebellum is white matter with a thin layer of gray matter which is called cerebellar cortex. The functions of the cerebellum are controlling muscle activities and posture and communicating with other parts of the CNS by nerve tracts [1].

2.1.3 Brain connectivity

The brain is believed to be a network-like organ which means that regions of the brain are connected to other regions of the brain. There are three types of connectivity of the brain that are widely discussed in neuroscience which are structural connectivity, functional connectivity and effective connectivity. **The structural connectivity** refers to the anatomical connections of brain regions by white matter. On the other hand, functional connectivity and effective connectivity are statistical concepts and these concepts can be used to find out brain regions that are connected even though they may not be structurally connected. **The functional connectivity** looks at the similarities in patterns of activity of different brain regions. While functional connectivity is not able to show directional relationship of the connectivity, **the effective connectivity** can reveal directional effect of one brain region over another [17].

2.2 Electroencephalogram (EEG) and functional Magnetic Resonance Imaging (fMRI)

2.2.1 Electroencephalogram (EEG)

Different types of EEG

Electroencephalogram (EEG) is a commonly used method in brain research that measures electrophysiological signals from brain. There are different types of EEG based on invasiveness such as scalp EEG, electrocorticogram (ECoG) and intracranial EEG (iEEG). The brief description of these three types of EEG is shown in figure 2.5. Scalp EEG is completely non-invasive and it is placed on the scalp of the subject so that it does not require surgical process which is an advantage. But since the EEG signal has to pass through the skull which has low conductivity, the signal to noise ratio (SNR) is very poor. Next, ECoG is partially invasive and it is placed on the surface of the brain which necessitates the surgery. However, it provides better SNR than scalp EEG since the signal is not captured after passing through the skull. Lastly, the intracranial EEG (iEEG) is invasive since it is implanted into the gray matter of the cerebral cortex. The advantage of iEEG is that the EEG signal is directly measured from the cerebral cortex which leads to higher SNR. Nevertheless, the surgical process to implant the electrodes is necessary and there is a risk that it could lead to some damage in brain functions. Therefore, in human studies, scalp EEG is preferred over the two EEG methods.

The source of the EEG signal

There is an abundant amount of specialized neurons called, apical pyramidal neurons, in the cerebral cortex. They are positioned parallel to each other and perpendicular to the surface of the brain. This can be seen in figure 2.6. As we discussed previously, neurons communicate with each other by means of neurotransmitter at synapses. This neurotransmitter crosses the synaptic cleft that binds to the post-synaptic membrane which is the membrane of the neuron located after the synapses. This induces the ion channel to open up the membrane and positively charged ions flow into the cells. As a result, the extracellular space around the neurons becomes relatively negatively-charged. In a remote part of the neuron, the ions leave the cells which makes the outside of the neurons positively charged. The combination of these processes creates electrical dipoles between different parts of the neuron. However, a single neuron is very small. Also, there is the thick skull as well as other layer of soft tissues. Therefore, the dipole of a single neuron is not detectable individually. Fortunately, there are so many pyramidal cells in the cerebral cortex, all lined up parallel to each other. Moreover, many of these cells often get stimulated at the same time. This way, the individually small dipoles summate to the dipole that is detectable on the scalp [18].

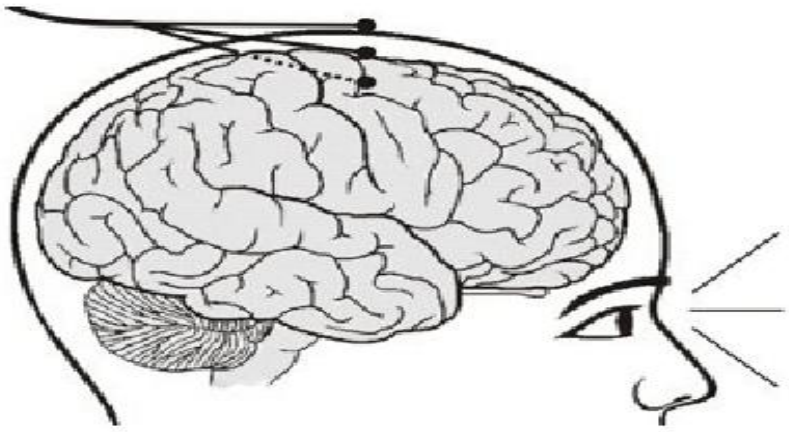

Figure 2.5: The different types of EEG depending on the invasiveness [3]
The scalp EEG (The highest bullet), the ECoG (The middle bullet) and the iEEG (The lowest bullet)

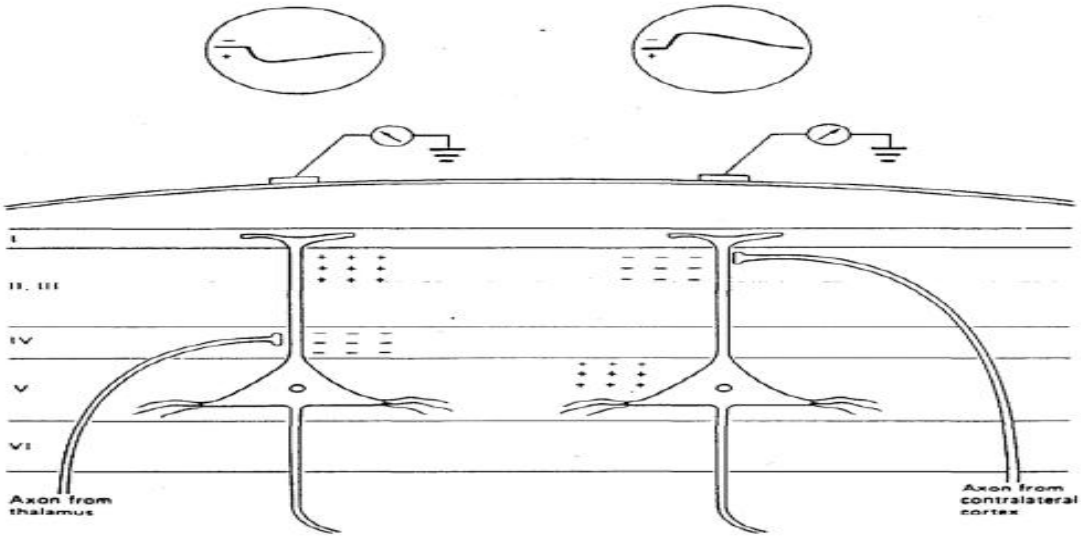

Figure 2.6: The pyramidal neurons that majorly contribute to the EEG signal [4]

The EEG recording system

The EEG recording system consists of electrodes with conductive gel, amplifiers with filters, A/D converter and a recording device (e.g. laptop). In human EEG system, if it is a routine checkup, only 6 to 8 electrodes are used. But when a more accurate test is required, 32 or 64 electrodes are used. In the case of high density EEG system, the number of electrodes even reaches 128 or 256. The human EEG system follows the standard 10-20 electrode system which was adopted by the International Federation in Electroencephalography and Clinical Neurophysiology in 1958 [19]. The system is named as 10-20 system because of the proportional distance of electrodes in percentage between Nasion and Inion. Electrodes are marked as F (Frontal), C (Central), T (Temporal), P (Parietal), O (Occipital). The electrodes are named this way because of the brain region that is underlying. However, note that C (Central) is only for geometrical identification but there is no central lobe in the brain. Odd numbers are assigned to the electrodes which are on the left side and even numbers are assigned to the ones on the right side. This standard 10-20 electrode system can be seen in figure 2.7.

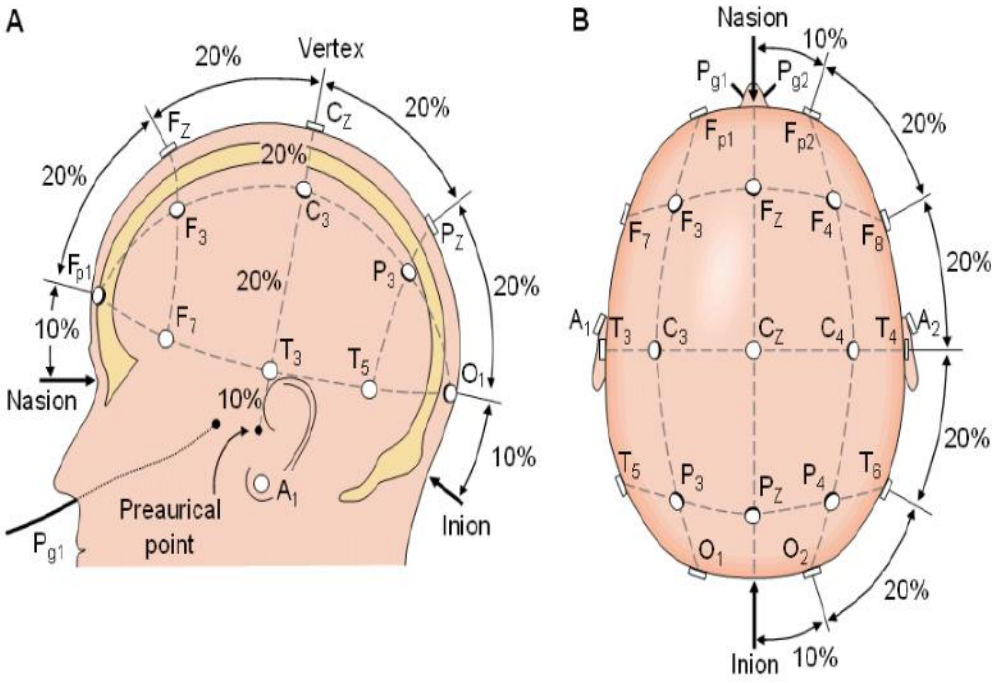

Figure 2.7: The international 10-20 EEG system seen (A) from the left side and (B) from above the head [5]

2.2.2 functional Magnetic Resonance Imaging (fMRI)

fMRI has been widely used to study brain functions. In this section, we will discuss the principle of the Magnetic Resonance Imaging (MRI) and also the physiological background which is measured by fMRI technique.

Principle of Magnetic Resonance Imaging (MRI)

MRI utilizes the inherent magnetic properties in the body to create medical images. The hydrogen nucleus which is a single proton is what is used for imaging because of its wealth in water and fat. MRI scanner consists of magnets with a field strength specified by the unit Tesla, gradient coils which produces a change in field strength from one point to another in the patient's body during the imaging process and radiofrequency (RF) coils which transmits radio wave to the tissue and receives radio wave from the tissue. When the human body is within the magnetic field, the hydrogenous protons are aligned with that magnetic field. But when the RF coil sends the radiofrequency pulse, the alignment of the protons is altered. Afterwards, when the RF pulse is switched off, the protons realign to its original state and this leads to emission of a signal which is also a radio wave. The time that it takes for protons to be realigned and the intensity of the signal that is emitted is dependent on the environment and the types of tissues. With the information, the MRI images are produced [20, 21].

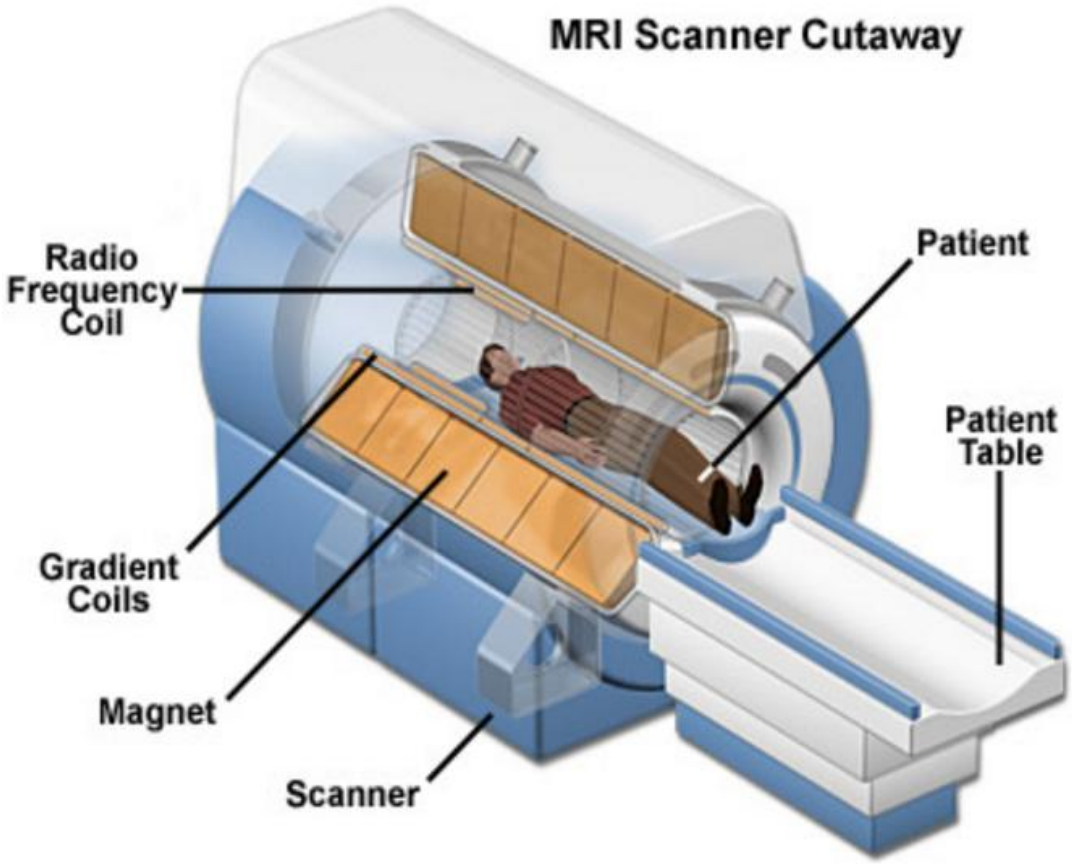

Figure 2.8: The structure of the MRI scanner [6]

Physiological background of the fMRI signal

The conventional MRI technique provides high spatial resolution anatomical images which is 1 mm or better. In the conventional MRI imaging, the difference primarily in the density of water inside tissues and in the way how the water interact with macromolecules such as phospholipids, proteins and fat that is present in tissues produces the contrast in images. However, in the functional MRI imaging (fMRI), it uses the same equipment as the conventional MRI imaging but the contrast within images is generated because of Blood Oxygen Level Dependent (BOLD) changes in the MRI signal. The fMRI images can be obtained while the patient is performing some tasks such as finger tapping, viewing pictures and listening to speech. But they can also be obtained in resting state when the patient is lying on the scanner bed with both eyes closed and not thinking something in particular. fMRI has been widely used to study brain functions because it is non-invasive and safe [22].

fMRI is based on BOLD contrast as mentioned above. There is increased need in oxygen when the neurons are more activated. Therefore, the different ratio of oxyhemoglobin and deoxyhemoglobin in the brain region produces contributes to contrast in BOLD signal [23]. The reason why blood oxygenation level makes BOLD contrast is because of their magnetic properties. Oxygenated hemoglobin is diamagnetic which means that it only reacts with the magnetic field weakly and deoxygenated hemoglobin is paramagnetic which means that it reacts with the magnetic field strongly [24]. The part of the hemoglobin that determines its magnetic properties resides in the ferrous iron ion [25]. The ferrous iron ion is in paramagnetic high-spin state in deoxygenated hemoglobin because the 4 out of 5 electrons in outer shell are not paired. On the other hand, the ferrous iron ion is in diamagnetic low-spin state because the electrons in outer shell are paired with oxygen [26].

In the activated neurons, metabolic demand (oxygen consumption) is increased so that oxygen is taken out from the blood and the amount of deoxygenated hemoglobin in that neuronal area is increased. This causes distortion in the magnetic field because of the paramagnetic characteristic of deoxygenated hemoglobin. That is shown as decreased BOLD signal that you can see in figure 2.9 as 'initial dip' [7]. Afterwards, blood vessels are dilated and the ratio of oxygenated hemoblogin and deoxygenated hemoglobin increases [27]. As a consequence, the BOLD signal increases in that local area [28]. The peak of the BOLD signal is reached in 5-8 s after activation of neurons [29].

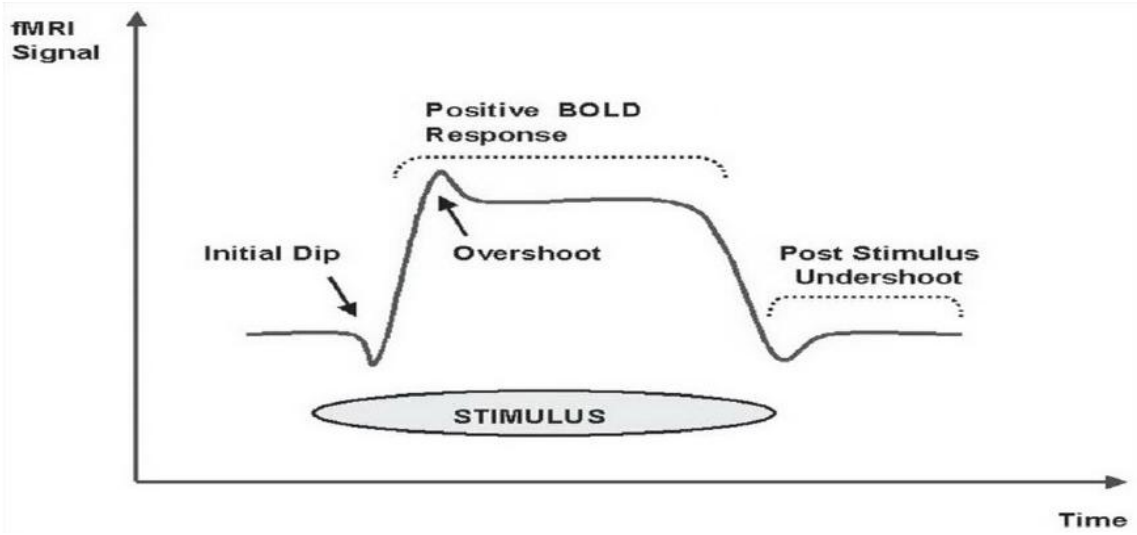

Figure 2.9: BOLD signal shows initial dip and then a more prolonged positive signal [7]

2.2.3 Simultaneous EEG-fMRI

Simultaneous EEG-fMRI has been getting a lot of attention in clinical neuroscience studies as well as in preclinical neuroscience studies. fMRI has high spatial resolution which is millimeter scale but low temporal resolution which is few seconds scale. EEG has low spatial resolution which is centimeter scale but with high temporal resolution of millisecond scale. Due to these characteristics, EEG and fMRI complement each other when used simultaneously.

With high temporal resolution of EEG, it is easy to derive the starting point of pathological brain activities. However, the inverse problem which tries to find the source area of the signal in brain is not straightforward if EEG is used alone. Also only with fMRI, one cannot easily derive when the neuronal activation was started because of the few seconds of delay before BOLD signal reaches its peak. The simultaneous measurement of EEG and fMRI allow us to examine how the epileptic seizure initiates and propagates to other areas [30, 31, 32]. However, there are still some artifacts that are caused to when they are used simultaneously.

We will first discuss the artifacts that are generated on EEG recording due to the fMRI scanning. One example of the artifacts is ballistocardiogram. This is caused by the movement of the body and electrodes because of the cardiac pulse. This artifact is shown at around 10 Hz or below [33, 34]. The ballistocardiogram artifact increases when the magnetic field strength is increased. However, this artifact can be reduced significantly by fixing the EEG electrodes firmly. Another example is the gradient artifacts. This artifact is caused by the gradient switching. They are shown with high amplitudes in the millivolt scale and they are present in the normal EEG frequency range which makes removing the artifacts complicated.

Next, there are also artifacts on fMRI images that are induced by EEG recording. The electrodes

of EEG system should be MR compatible to be used simultaneously with fMRI. However, there is still some interference of magnetic field by the MR compatible electrodes during MR image acquisition and this deteriorates signal to some extent in the brain regions that are close to the EEG electrodes [35].

2.3 Epilepsy

2.3.1 Definition of Epilepsy

The practical (operational) definition of epilepsy aids clinicians for easier communication and diagnosis of epilepsy. This definition was mainly excerpted from the official document of International League Against Epilepsy (ILAE) [36].

"Epilepsy is a disease of the brain defined by any of the following conditions: 1. At least two unprovoked (or reflex) seizures occurring more than 24 h apart 2. One unprovoked (or reflex) seizure and a probability of further seizures similar to the general recurrence risk (at least 60%) after two unprovoked seizures, occurring over the next 10 years 3. Diagnosis of an epilepsy syndrome"

2.3.2 Definition of epileptic seizure

Epileptic seizures are defined below by International League Against Epilepsy (ILAE) and the International Bureau for Epilepsy (IBE) [37].

"An epileptic seizure is a transient occurrence of signs and/or symptoms due to abnormal excessive or synchronous neuronal activity in the brain."

Mode of onset and termination

The beginning and the end of the seizures are clear for the period of seizures. However, it does not always meet this standard. There is also an exceptional condition called status epilepticus where the seizures are continued for more than 5 minutes. These can be easily monitored by EEG recording [37].

Clinical manifestations

Clinical manifestations of seizures can be depicted in a variety of ways. They are relied on several factors such as the position of onset in the brain, patterns of propagation, maturity of the brain, sleep–wake cycle, medical prescriptions, and several other factors. There is a wide range of bodily functions that are affected by seizures such as sensory, motor, and consciousness, emotional state, memory, cognition or behavior [37].

2.3.3 The classification of epilepsy

The classification of epilepsy is highly ambiguous and it is still evolving and being refined constantly. However, for the better clinical assessment and diagnosis, it is worthwhile to have such standard. **Generalized epilepsy** refers to epilepsy with generalized seizures that shows generalized epileptiform EEG patterns. However, they can also involve focal epileptiform EEG patterns too. **The focal epilepsy** refers to epilepsy with focal seizures that are associated with focal EEG epileptiform patterns. The focal seizures can be unifocal or multifocal. It is important to note here that the clear distinction between generalized and focal epilepsy does not exist. Many patients do not belong to just one group [38].

2.3.4 Treatments

Anti-epileptic drugs (AEDs)

Generally, longterm treatment with AEDs is needed for patients with epilepsy and very often, combination of different types of medication is prescribed to those with drug resistant epilepsy [39]. Approximately 25 to 30 % of the epilepsy patients are reported to be drug resistant [39]. It can also be described as pharmacoresistant, medically intractable or refractory. However, the definition of drug resistant epilepsy is perceived intuitively. Therefore, there has been no agreement on definition before the International League Against Epilepsy (ILAE) issued a suggestion. The definition is valuable for medical practitioners, clinical researchers, neurologists, and other people working in this field. ILAE defines drug resistant epilepsy as below [40].

"Failure of adequate trials of two tolerated and appropriately chosen and used AED schedules (whether as monotherapies or in combination) to achieve sustained seizure freedom"

Surgery

Refractory epilepsy patients often undergo resective surgery. The surgery is to remove the seizure onset zone in which seizures are initiated. 60 to 80 percent of patients with temporal epilepsy have been reported to become seizure-free after undergoing the surgery in which the seizure onset zone in the temporal lobe is resected [41, 42, 43]. The safest cases of the surgery are temporal lobe resections. The serious complication rate is no more than 5 percent. The possible complications are cognitive impairment, psychosis, visual field impairment and decrease in verbal abilities [43, 44].

There are different factors that affect surgical outcome. Multiple epileptogenic zones are one of the major factors. The poor surgical outcome of the patients with multifocal seizures could be attributed to these multiple epileptogenic zones. The seizures of these patients have multiple seizure onset zones or they have broader onset zones compared to other patients. Another case that brings poor surgical outcome is when patients have bilateral brain abnormalities [45]. In these cases, surgery in one specific region would not result in seizure freedom. Accordingly, it is of utmost importance to do pre-operative measurements to test the likelihood of successful surgical outcome and to delineate the zone for resection.

Neurostimulation

Neurostimulation is another type of treatment for epilepsy patients who are drug-resistant and are not good candidates for the surgery. We will discuss three different neurostimulation methods which are transcranial magnetic stimulation (TMS), vagus nerve stimulation (VNS) and deep brain stimulation (DBS). First, TMS is the simplest and non-invasive approach. It uses a coil that produces small electric currents within the brain just beneath the coil through electromagnetic induction. This way the targeted regions of brain become stimulated. However, the most common epileptogenic areas are located too deep below the scalp to have successful result with TMS [46]. Second, the direct VNS requires surgical implantation of the stimulator device. The generator of the device is implanted and it sends electric impulses directly to the vagus nerve at certain frequencies [47]. Nevertheless, the effectiveness of the VNS in terms of reducing the frequency and intensity of the seizures is quite different between individuals [46]. Lastly, DBS is the invasive method which requires implantation of the neurostimulator to send electrical impulses via the electrodes to the specific regions in the brain. The DBS is not only used in epilepsy but also on Parkinson's disease, Tourette syndrome and depression for the patients who do not respond to the conventional treatments [48].

Ketogenic diet

The ketogenic diet is a diet which contains high amount of fat and low amount of carbohydrates and proteins. By restricting the consumption of carbohydrates and proteins, the body is forced to use ketone bodies as the main fuel. The ratio of the fat and carbohydrate in the ketogenic diet is 4 to 1. Also the amount of protein is restricted in the diet which leads to the proportion of the amount of fat in the diet as high as 90 %. This treatment option is usually used for children who are drug-resistant [49].

2.4 Animal models of temporal lobe epilepsy (TLE)

There are animal models of epilepsy available. We will discuss temporal lobe epilepsy (TLE) models in this section since it is the most common type of epilepsy in adults. What are the standards of good animal models of epilepsy? First of all, the animal models need to generate corresponding electrophysiological signals as they appear in epileptic human patients. Second, the causes of epilepsies should be similar. Therefore, the animal models of epilepsy should comprise a wide range of human conditions that resulted from injury, genetic inclination, etc. Third, the animal models should also manifest pathological changes such as hippocampal sclerosis. Lastly, the behavioral manifestations in the short and long term should also be similar [50].

Although there is no animal model that possesses all the characteristics of TLE, the Kainic Acid (KA) that was discovered by Ben-Ari et al. [51, 52] and Pilocarpine (PILO) are the two most common animal temporal lobe epilepsy models that have been used for research. On top of that, an electric kindling model is also available. We will take a look at each of these models. But more focus will be given on the KA model which we used in this thesis.

2.4.1 Kainic Acid model (KA)

Kainic Acid (KA) is a neuro-excitatory amino acid that is obtained from a red algae (Digenea simplex) in the beginning of 1950s [8, 53]. There are two different ways of administration of KA which are intracerebral administration and systemic administration. We will discuss each of these ways of administration.

Intracerebral administration of KA

Nadler et al. [54] reported a study presenting the effect of KA on hippocampal neurons. It was proven that pyramidal cells in the hippocampus were degenerated after intraventricular injection of KA at 0.5 nmol in Sprague-Dawley rats. These studies indicated that intracerebral injections of KA, either in hippocampus or in amygdala, could serve as a model of TLE considering that it had resulted in common histopathological characteristic of epileptic patients [52, 55].

0.4-2 µg of KA by intra-hippocampal administration is commonly efficient enough to provoke convulsive seizures in rats [56, 57, 58, 59, 60]. Behavioral manifestations of these seizures are as following; Facial clonus (stage 1), masticatory movements and head nodding (stage 2), wet dog shakes (stage 3), forelimb clonus (stage 4), and rearing and falling (stage 5) are also other subsequent behavioral manifestations [61, 62, 63, 64, 8]. Similar symptoms can be achieved by intra-amygdaloidal injections of KA at 0.4-2 µg in rats. Yet some additional symptoms such as salivation and exophthalmos are present as well [52, 65].

Electrophysiological changes are seen in the KA administered hippocampus prior to the onset of seizures [66, 67, 68]. It was suggested that even when the administration of KA was executed in different areas of brain that are far away from hippocampus, hippocampal formation is vital in the onset and propagation of KA-induced epileptiform activities [69, 8]. However, intra-amygdaloidal injections of

KA do not always result in histopathological alterations in the hippocampus [70, 8]. The epileptiform patterns recorded on EEG after intrahippocampal injection of KA can be seen in figure 2.10.

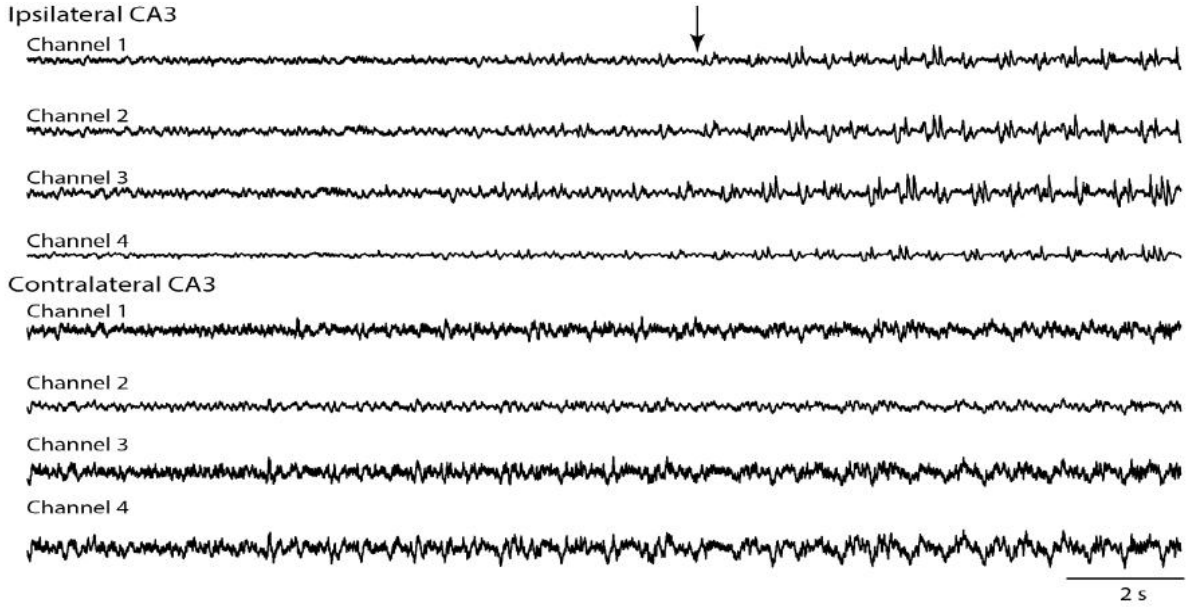

Figure 2.10: Epileptiform patterns represented on EEG after intrahippocampal injection of KA (adapted from [8])

The onset of the seizure is shown by arrow.

Systemic administration of KA

When KA is administered systemically, surgical procedures are not necessary so it shortens the time required for experiments. In addition to them, animals' health does not have to be affected by possible complications that could happen after surgical procedures. But there are also disadvantages that probably several systemic injections may be needed to achieve Status Epilepticus (SE) [8]. Generally, also the clinical manifestations can be spotted in KA treated rats by systemic administration [71].

After 30 min of systemic injection of KA (intraperitoneally, intravenously, subcutaneously), epileptic electrophysiological signals become visible on EEG recordings. It was reported that epileptiform patterns were first observed in the hippocampus in rats who were administered KA systemically [72]. It was found that hippocampus plays a major role in initiating seizure activities which were provoked by KA [73]. Accordingly, these studies indicate that hippocampus holds a principal function in initiation of seizures when KA is administered systemically as well [74, 69].

2.4.2 Pilocarpine model (PILO)

Almost similar epileptic characteristics can be achieved with the pilocarpine model (PILO). However, compared to the KA model, more substantial damages are caused onto the thalamus, dentate hilus, cerebral cortex, olfactory corticles, substantia nigra and the amygdalas [75]. Because of this, the KA model was preferred over the PILO model [76]. An advantage of the PILO model is that it is more reliable than the KA model. It was reported that almost all rats administered with pilocarpine at the amount of 380 mg/kg intraperitoneally began to have acute seizures [77, 78]. PILO model occupies similar behavioral manifestations as in the KA model such as myoclonic twitching, head wobbling and facial automatism (e.g. chewing and eye blinking) [50].

2.4.3 Electric kindling model

In this model, electrical stimulation is iterated for some days and this induces neurons to be chronically excited [79]. It eventually generates severe partial and generalized convulsive seizures [80, 79]. Kindling is superior over other models in the aspect that experimenters can target a certain region of the brain as the seizure onset region and the parameters of stimulation protocols are readily modifiable [81]. On the other hand, the disadvantage of this model is that it does not create similar lesions as in the temporal lobe epileptic patients [82]. Also, since it involves a surgical procedure, it takes more time to experiment and there could be post-surgical damages in the animals.

Chapter 3

Materials and methods

3.1 Overview of the experiments

The overview of all the experiments and rats that were used is shown in table 3.1. In total, 6 rats were used in this thesis work but the rats that died during the experiments were excluded from data analysis. Therefore only the data from 4 rats which are rat 2, rat L1R0, rat L1R1 and rat 3 was analyzed.

Date	**What experiment was performed**	**Rats that were used**
23/11/2015	EEG standalone recording in resting state	Rat1, Rat2
26/11/2015	fMRI standalone scanning in resting state	Rat1, Rat2
27/11/2015	Simultaneous EEG-fMRI measurement in resting state	Rat2 (Rat1 died during the fMRI scanning on 26/11/2015)
02/03/2016	EEG standalone recording in resting state	Rat L1R0, Rat L0R1, Rat L1R1 (Rats were identified by getting their earlobe(s) punched. e.g. Rat L1R0 has only its left earlobe punched)
03/03/2016	fMRI standalone scanning in resting state	Rat L1R0, Rat L0R1, Rat L1R1
04/03/2016	Simultaneous EEG-fMRI measurement in resting state	Rat L1R0, Rat L1R1 (Rat L0R1 died during the fMRI scanning on 03/03/2016)
21/03/2016	fMRI standalone scanning in resting state, Simultaneous EEG-fMRI measurement when seizure induced	Rat3 (Note that this was the only rat used for this session but it was numbered as 3 to be distinguished from the rats of 23/11/2015 dataset)
22/03/2016	Simultaneous EEG-fMRI measurement when seizure induced	Rat3

Table 3.1: The overview of the experiments that were performed

All rats were treated according to guidelines approved by the European Ethics Committee (decree 2010/63/EU). All experimental procedures were approved by the Animal Experimental Ethical Committee of Ghent University Hospital (ECD 13/14). The animals were kept under environmentally controlled conditions (12h normal light/dark cycles, 20–23°C and 40–60 % relative humidity) with food and water ad libitum.

3.2 Animal preparation and handling

3.2.1 Preparation to EEG recording

Before the recording, anesthesia with a mixture of medical O_2 and Isoflurane with a concentration of 5 % was performed on rats in a plastic box. When the rats were fully under anesthesia, they were moved onto the table to prepare for EEG recording. During this, the anesthesia was continued using an air mask. Isoflurane anesthesia was continued with a rate between 1 % and 2 % depending on the breathing rate (between 900 and 1200 ms is the normal range) or the status of the rats. The electrocardiogram (ECG) electrode (Rapid Biomedical, Germany) was placed underneath the chest region of the rats to monitor breathing rate. A heating pad with water of 40°C circulating inside was kept underneath the rats or above the back region of the rats to sustain their normal body temperature. For EEG standalone recording on 23/11/2015, an infrared heating lamp (Philips, Eindhoven, Netherlands) was used instead of the heating pad. The head region of the rats was carefully shaved to decrease impedance between the scalp and electrodes. For the EEG recording on 02/03/2016 and 21/03/2016, depilatory cream (Veet, Reckitt Benckiser, U.S.A.) was also used to lower the impedance further. Afterwards, the region was degreased with 70 % alcohol. Vidisic gel (Bausch and lomb, U.S.A.) was also applied on both eyes of rats to keep them moisturized.

3.2.2 Preparation to MRI acquisition

Anesthesia with a mixture of medical O_2 and isoflurane with a concentration of 5 % was performed on rats in a plastic box. The ECG electrode (Rapid Biomedical, Germany) was positioned underneath the chest region of the rats to keep track of breathing rate. A water-circulating heating pad was placed under the rats to maintain their normal body temperature. The anesthesia by isoflurane was sustained at the rate between 1 % and 2 % through air tubes which are located directly at the head region of rats.

When the rat was fully under anesthesia, it was moved to the bed of 7 T MRI system (Pharmascan 70/16, Bruker, Ettlingen, Germany). During this, the anesthesia was continued using an air mask. Afterwards, sedation by medetomidine was performed. It is known that medetomidine does not suppress brain activities that much unlike isoflurane [83]. The timeline of this sedation protocol [83] can be found in figure 3.1. When the scanning was completed, the rat was injected with atipamezole (0.03 mg/kg) to counter the effect of the medetomidine sedation.

3.3 Seizure induction by KA (Kanic Acid)

Seizures were induced by injecting KA intraperitoneally using a syringe for EEG-fMRI simultaneous measurements on 21/03/2016 and on 22/03/2016. The KA was injected at 5 mg/kg according to the protocol of Hellier et al. [84] just before we put on the EEG cap on the rat.

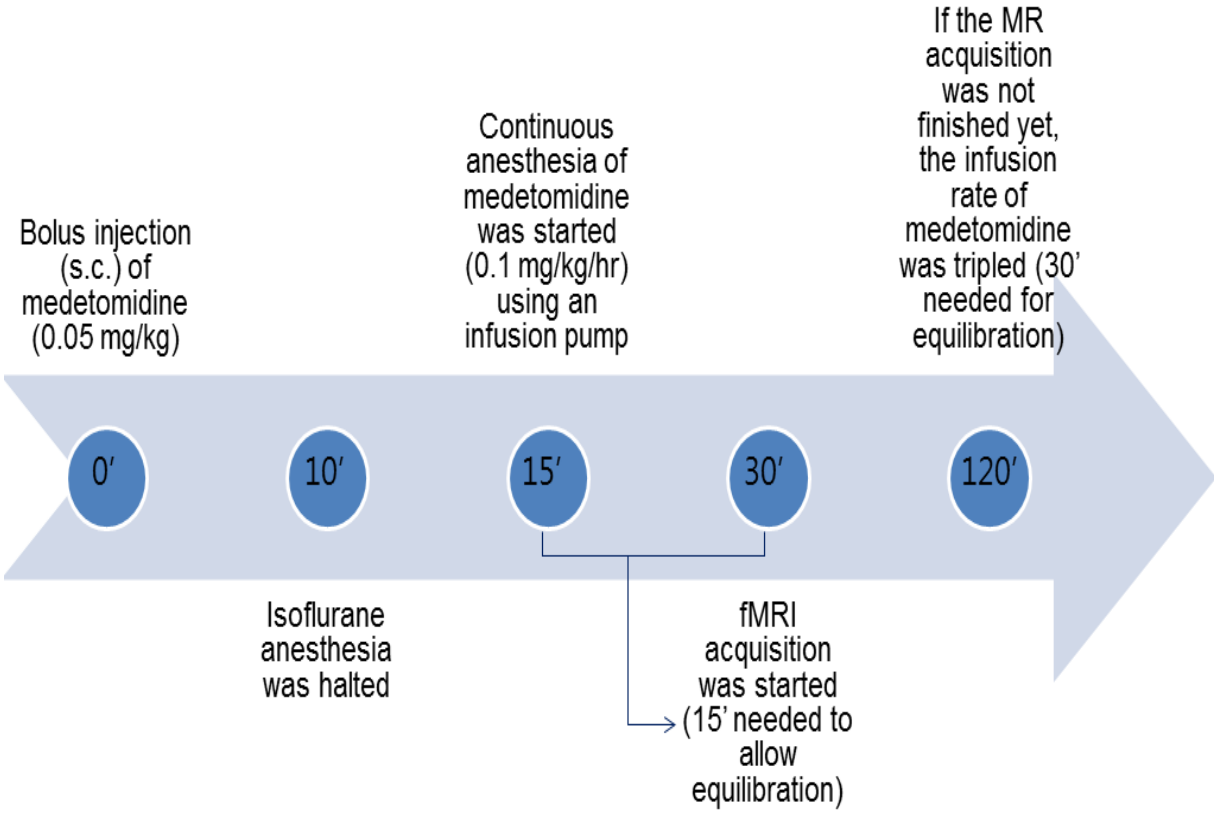

Figure 3.1: Timeline of the medetomidine sedation during MR acquisition
S.c. stands for subcutaneous.

3.4 EEG recording

The EEG cap (length: 36 mm and width: 28 mm) designed by Joachim Ally et al. [9] was connected to an adapter head box which was connected by a flat cable to the MR compatible human EEG system (Brainproducts, Germany) which consisted of a power supply, an amplifier and an USB adapter which was connected to a laptop. The whole system of the EEG recording is described in figure 3.2. The setup of the EEG standalone recording when applied on a rat can be seen in figure 3.3. The spatial distribution of the electrodes of EEG cap on the rat brain can be found in figure 3.4. We found that the spatial distribution suggested by Joachim Ally et al. [9] should be modified since the region of the brain in rats already starts from the nose region. Therefore, considering the approximate location of the hippocampus which is indicated by the red arrow in figure 3.4, 13, 14, 16 and 17 were electrodes of our interest when we analyzed EEG signals since hippocampus is known to be the onset region of the seizures which are induced by KA. In the case of simultaneous EEG-fMRI measurement, the EEG cap, adapter head box, amplifier and power supply were placed in the magnetic shielding room where MRI acquisition was performed. A long optical cable connected the amplifier with the USB adapter and the laptop outside the shielding room.

Next, electrolyte gel which contains 8% of salt (Abralyte 2000, Easycap) was applied using a blunt needle on each electrode of the EEG cap. Then the cap was placed onto the scalp of the rat and then fixed with tape. The fixation way of the EEG cap can be seen in figure 3.5. First, the impedance between the scalp and electrodes was checked. Then the EEG was recorded with sampling frequency of 5000 Hz using the EEG recording software (Brainvision Recorder, Brainproducts, Germany).

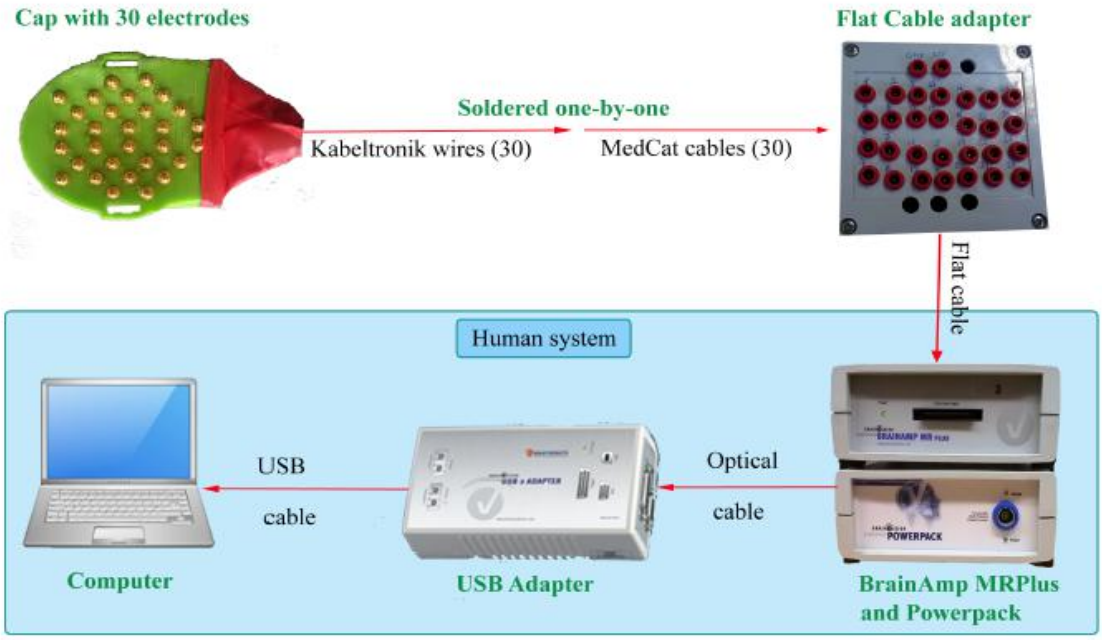

Figure 3.2: The scalp EEG system for rats [9]

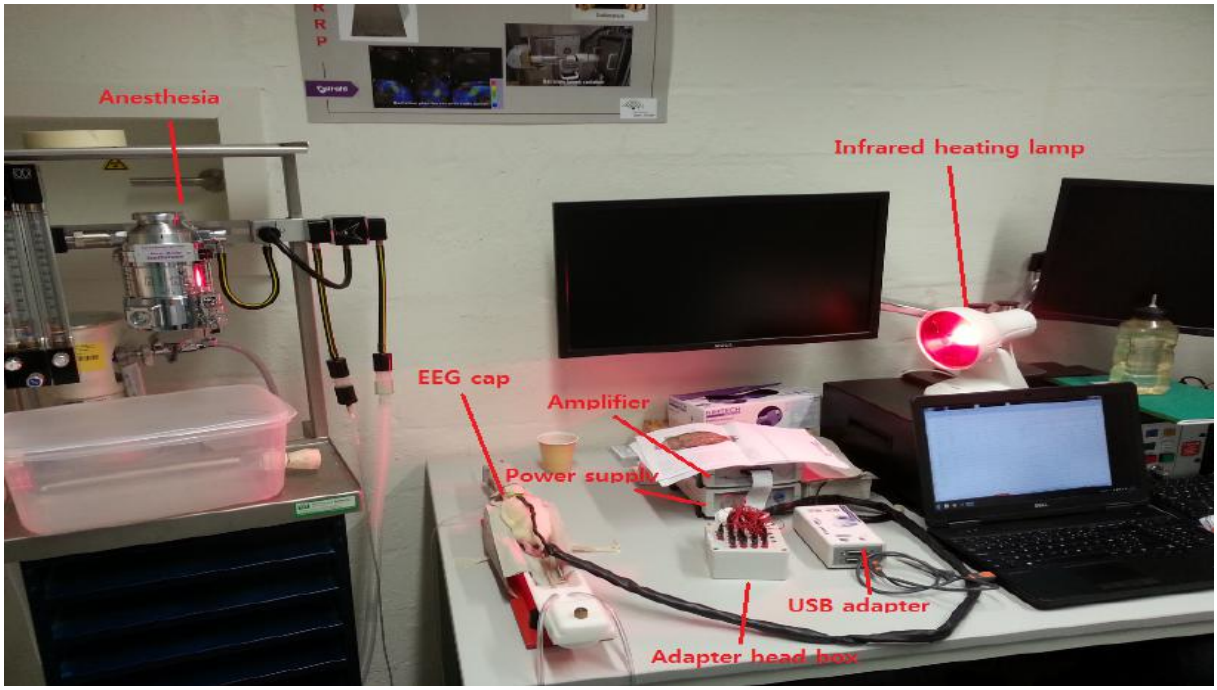

Figure 3.3: Demonstration of EEG standalone recording setup

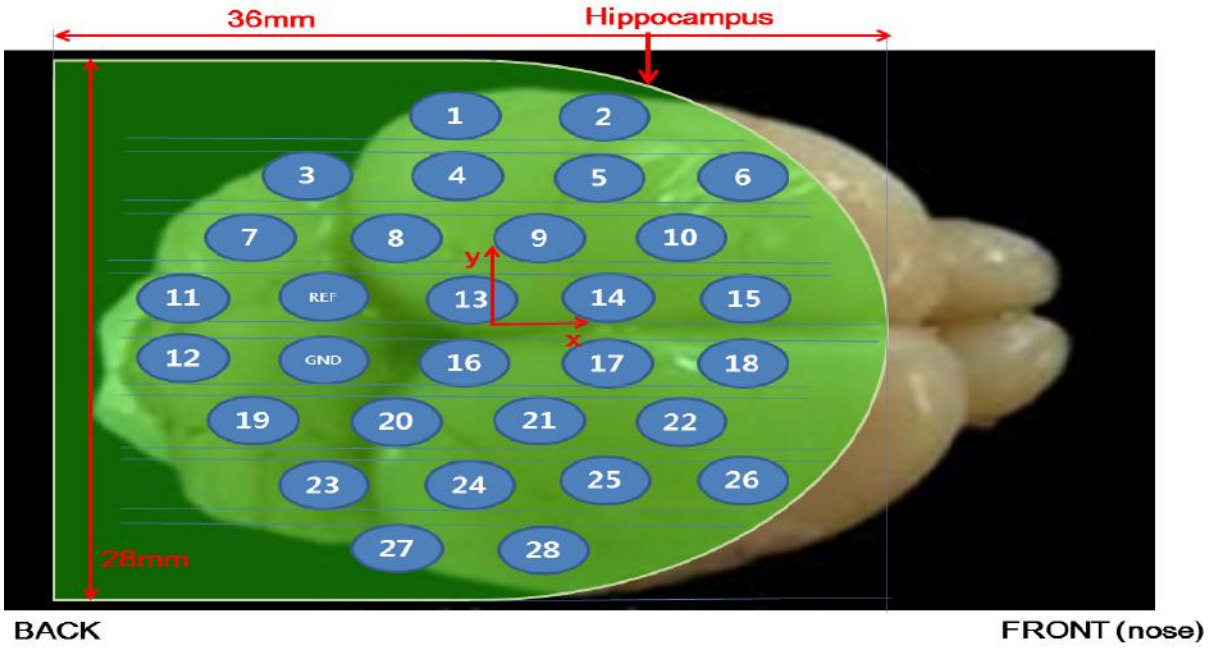

Figure 3.4: Spatial distribution of the electrodes of the EEC cap
The rat brain image was obtained from [85].

Figure 3.5: Fixation way of the cap on the rats [9]
The end of the EEG cap was placed over the region of ears.

3.5 MRI acquisition

The rat was positioned on the bed corresponding to the plane of the rat for imaging. A biting bar (Bruker, Germany) was also used to make it easier to adjust the position of the rat when there was a slight tilt. Before starting MR acquisition, the EEG cap was placed onto the scalp of the rat in the case of simultaneous EEG-fMRI measurements. The demonstration of the EEG-fMRI setup is shown in figure 3.6. Afterwards, a rat head volume coil (Bruker, Germany) was placed around the head of the rat to be

able to image the brain, especially subcortical regions such as the hippocampus. The rat head volume coil can be seen in figure 3.7. Then the acquisition was prepared with the MRI acquisition software Paravision (Bruker, Germany). Before starting the MR acquisition, the first and second order global shimming were performed and then a local first order shimming (MAPSHIM; Multi Angle Projection SHIM) was followed to achieve a homogeneous magnetic field. Afterwards, BOLD fMRI images were acquired making use of a gradient echo echo-planar-imaging sequence (GE-EPI).

The parameters for each fMRI EPI session; number of slices, slice thickness, matrix size, Field Of View (FOV) and voxel size are described in table 3.2. All the fMRI sessions were taken with repetition number of 300 and Time to Repeat (TR) of 2000 ms, so each scan took 10 minutes in total. As an anatomical reference, T2 weighted images were acquired using the Turbo RARE T2 sequence. The parameters for each T2 scan; number of slices, TR, Time to Echo (TE), slice thickness, matrix size, FOV and voxel size are described in table 3.3.

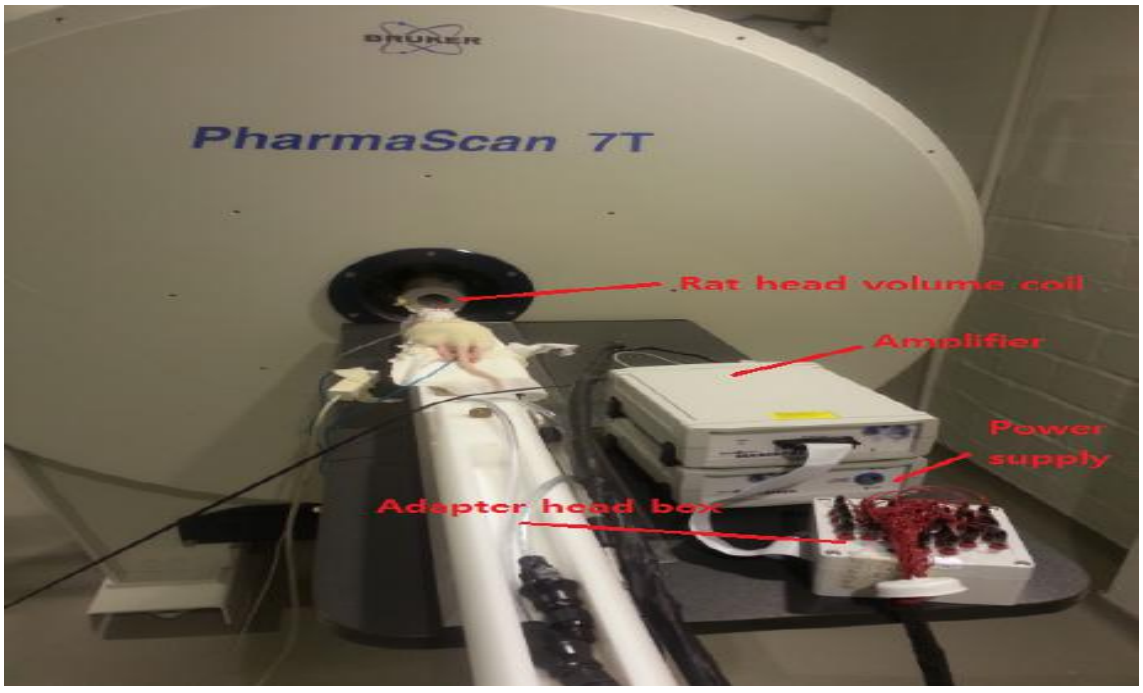

Figure 3.6: The demonstration of EEG-fMRI setup on a rat
This was taken before EEG cap was applied on the rat.

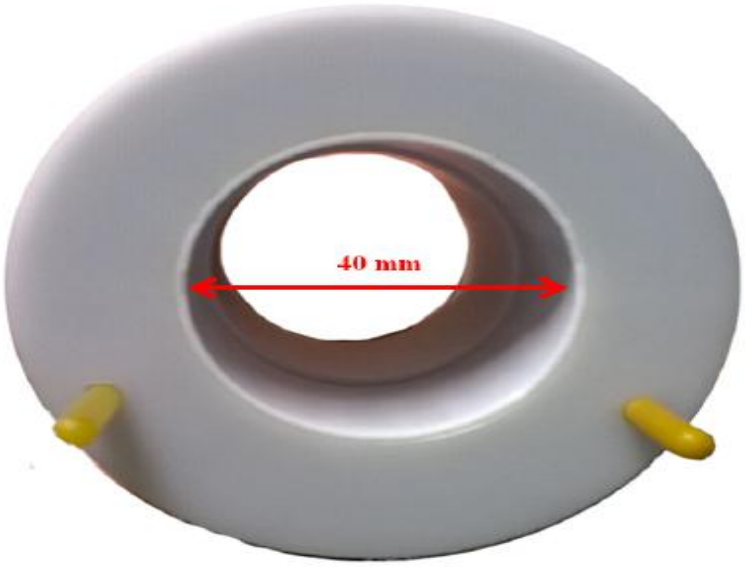

Figure 3.7: MRI rat head volume coil used with 7T MRI scanner [9]

3.6 Processing of the EEG data

Processing of the EEG data was done using the software Brainvision Analyzer (Brain products, Germany). Each EEG recording dataset was processed separately. First, we filtered the data using the Butterworth zero phase filters (Infinite Impulse Response filters) with a low cutoff of 2 Hz, 48 dB/oct and a high cutoff of 25 Hz, 48 dB/oct. Also a notch filter at the frequency of 50 Hz was used to remove the powerline noise. For the manual seizure detection, the power spectrum of the electrodes that is shown by Fast Fourier Transformation (FFT) was investigated to find out when the seizures were evoked. Afterwards, they were checked by a neurology expert, prof. Robrecht Raedt to confirm whether they actually represented seizures.

3.7 Processing of the fMRI data

3.7.1 Preprocessing

Preprocessing of the fMRI data was done using the software DPABI (DPARSF 4.0 (for Rat Data)) [86] for each dataset. It is a pipeline fMRI analysis toolbox and it also provides a module specifically for rat data. First, all datasets went through voxel augmentation which augments voxel size to 10 times using the function 'Voxel Size Augmentor' on DPABI. This has been done only because most available fMRI analysis toolkits are designed for human data and the voxel size for rat MRI data is too small for using those toolkits [86]. The voxel augmentation does not change the data but only augment the voxel size. All datasets were first realigned to remove motion-related artifacts using a least squares approach and a 6 parameter (rigid body) spatial transformations. All the functional EPI images were coregistered to the anatomical T2 weighted images. Note that the functional images of all simultaneous EEG-fMRI datasets were coregistered to the anatomical T2 weighted scan of the fMRI standalone scanning dataset of the corresponding rat for a clear anatomical reference. Afterwards, smoothing was performed using the Full Width Half Maximum (FWHM) of 6 x 6 x 6 mm3. This was chosen as twice the size as the augmented voxel size of rat data which was between 2.5 mm and 3 mm [87]. No masks were applied to any of MRI images. Lastly, a band pass filter between 0.01-0.1 Hz was applied on all fMRI EPI images to reduce physiological noise mainly coming from cardiac pulses and breathing.

EPI Sessions	Number of slices	Slice thick-ness [mm]	Matrix size [cm2]	FOV [cm2]	Voxel size [mm3]
26/11/2015, RS, Rat1	12	1	96 x 96	2.56 x 2.56	0.267 x 0.267 x 1
26/11/2015, RS, Rat2	12	1	96 x 96	2.56 x 2.56	0.267 x 0.267 x 1
27/11/2015, RS, w/EEG, Rat2	12	1.1	96 x 96	4 x 4	0.267 x 0.267 x 1
03/03/2016, RS, Rat L0R1	16	1	96 x 96	2.56 x 2.56	0.267 x 0.267 x 1
03/03/2016, RS, Rat L1R1	16	1	96 x 96	3 x 3	0.312 x 0.312 x 1
03/03/2016, RS, Rat L1R0	12	1	96 x 96	3 x 3	0.313 x 0.313 x 1
04/03/2016, RS, w/EEG, Rat L1R1	16	1	96 x 96	3 x 3	0.313 x 0.313 x 1
04/03/2016, RS, w/EEG, Rat L1R0	17	1	96 x 96	3 x 3	0.313 x 0.313 x 1
21/03/2016, RS, Rat3	12	1	96 x 96	2.56 x 2.56	0.267 x 0.267 x 1
21/03/2016, Seizure, w/EEG, Rat3	12	1	96 x 96	3 x 3	0.313 x 0.313 x 1
22/03/2016, Seizure, w/EEG, Rat3	16	1	96 x 96	3 x 3	0.313 x 0.313 x 1

Table 3.2: Parameters of each fMRI EPI dataset

RS stands for Resting State. Also we used 'Seizure' in the first column to indicate they are the EPI sessions which are taken when the seizure was induced. 'w/EEG' indicates that the EPI session was performed simultaneously with EEG recording.

T2-weighted anatomical sessions	Number of slices	TR [ms]	TE [ms]	Slice thickness [mm]	Matrix size [cm2]	FOV(Field Of View) [cm2]	Voxel size [mm3]
26/11/2015, RS, Rat1	16	2500	11	1	256 x 256	4 x 4	0.117 x 0.117 x 1
26/11/2015, RS, Rat2	16	2500	11	1	256 x 256	4 x 2.56	0.1 x 0.156 x 1
27/11/2015, RS, w/EEG, Rat2	17	2500	11	0.95	256 x 256	4 x 4	0.156 x 0.156 x 0.95
03/03/2016, RS, Rat L0R1	16	2866.1	33	1	256 x 256	2.56 x 2.56	0.1 x 0.1 x 1
03/03/2016, RS, Rat L1R1	16	2500	33	1	256 x 256	3 x 3	0.117 x 0.117 x 1
03/03/2016, RS, Rat L1R0	17	2500	11	0.938	256 x 256	3 x 3	0.117 x 0.117 x 0.938
04/03/2016, RS, w/EEG, Rat L1R1	17	2500	11	0.938	256 x 256	3 x 3	0.117 x 0.117 x 0.938
04/03/2016, RS, w/EEG, Rat L1R0	16	2500	11	1	256 x 256	3 x 3	0.117 x 0,117 x 1
21/03/2016, RS, Rat3	16	2500	33	1	256 x 256	2.56 x 2.56	0.1x 0.1 x 1
21/03/2016, Seizure, w/EEG, Rat3	12	2500	33	1	256 x 256	3 x 3	0.117 x 0.117 x 1
22/03/2016, Seizure, w/EEG, Rat3	16	2500	33	1	256 x 256	3 x 3	0.117 x 0.117 x 1

Table 3.3: Parameters of each anatomical T2 dataset

RS stands for Resting State. Also we used 'Seizure' in the first column to indicate they are the T2 sessions which are taken when the seizure was induced. 'w/EEG' indicates that the T2 session was performed simultaneously with EEG recording.

3.7.2 Postprocessing

Region Of Interest (ROI) drawing

ROIs were drawn manually using the software MRIcron (NeuroDebian, McCausland Center for Brain Imaging, University of South Carolina, U.S.A.) on coregistered structural T2 images for the ROI correlation analysis. The atlas of the brain regions was referred to the Waxholm Space Sprague Dawley rat atlas [88, 89, 90]. All ROIs were drawn right side and left side to see bi-laterality. In total, 10 ROIs were drawn for each rat that was used in this thesis work. The list of ROIs can be found in table 3.4. After the drawing was done, each ROI was saved into a NIfTI file (.nii). All ROIs that are overlaid on the structural T2 image for each rat can be found in figure 3.8, 3.9, 3.10, 3.11. Note that ROIs were drawn on multiple slices where the region was located.

The order of ROIs	The region of the brain	Abbreviation
1	L-Auditory cortex	L-AuD
2	R-Auditory cortex	R-AuD
3	L-Cingulate cortex	L-Cg
4	R-Cingulate cortex	R-Cg
5	L-Hippocampus	L-Hp
6	R-Hippocampus	R-Hp
7	L-Striatum	L-Str
8	R-Striatum	R-Str
9	L-Thalamus	L-Th
10	R-Thalamus	R-Th

Table 3.4: The order and the region of the brain of ROIs
ROI 1-6 were chosen because they are the regions which are believed to be the regions that are activated in the resting state in rats [91]. ROI 7-10 were chosen since they are located near the hippocampus.

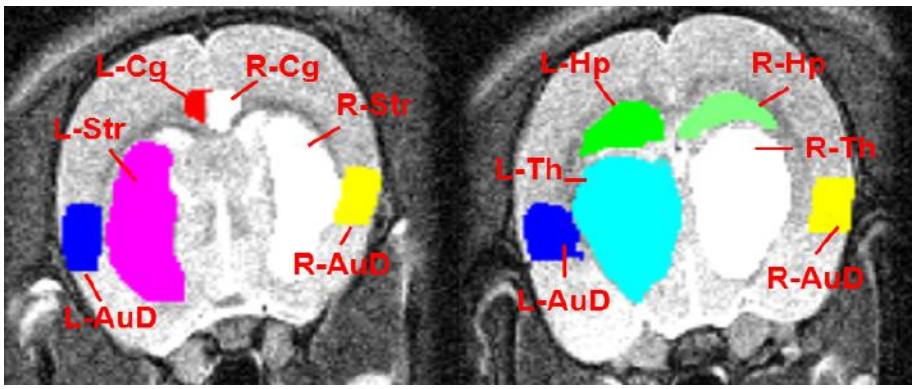

Figure 3.8: ROI drawing of the rat 2 of 26/11/2015 and 27/11/2015 dataset

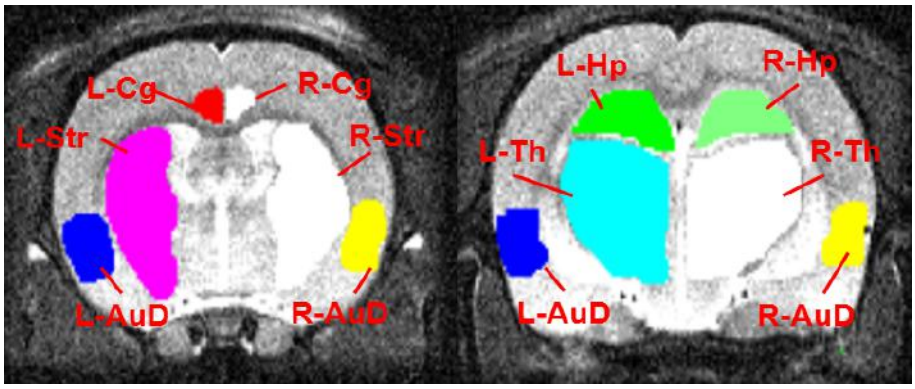

Figure 3.9: ROI drawing of the rat L1R0 of 03/03/2016 and 04/03/2016 dataset

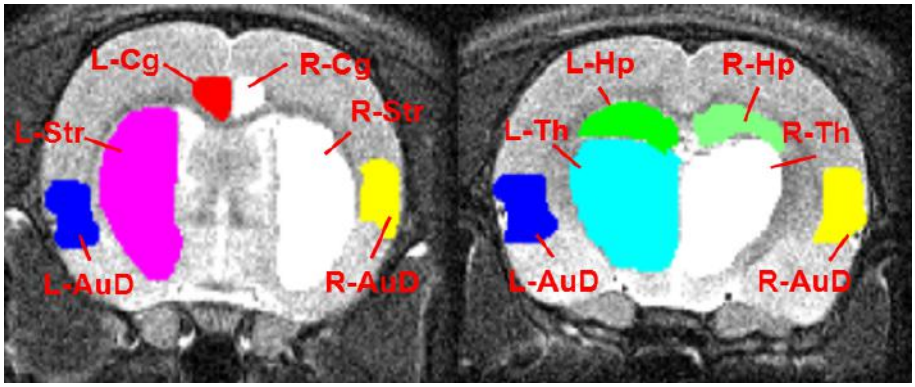

Figure 3.10: ROI drawing of the rat L1R1 of 03/03/2016 and 04/03/2016 dataset

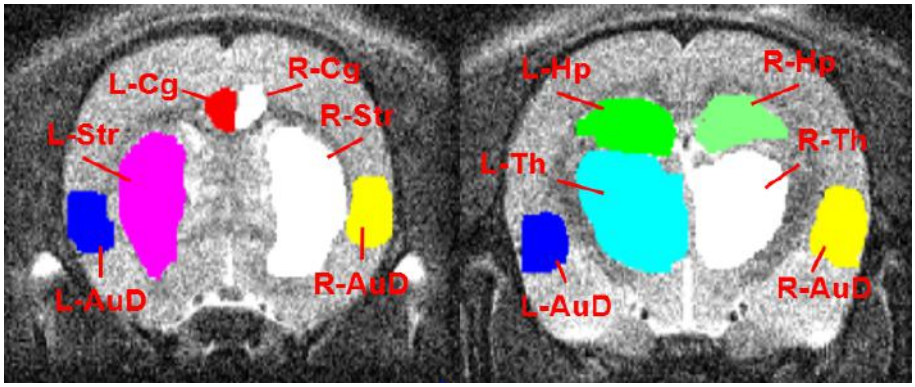

Figure 3.11: ROI drawing of the rat 3 of 21/03/2016 and 22/03/2016 Seizure dataset

10 x 10 ROI correlation analysis

The 10 x 10 ROI correlation analysis was performed using the software DPABI (DPARSF 4.0 (for Rat Data)) [86] for all resting state and seizure fMRI dataset. All ROI files (.nii) that were drawn before were loaded as seed series and the timecourse from the ROIs were extracted from the functional images. Then the 10 x 10 matrix that consists of correlation coefficient between all ROIs was created. For visualization, the correlation matrix that was created previously was loaded in Matlab (R2010b, MathWorks, Natick, MA, U.S.A.) and a color correlation matrix was created with a legend added.

GLM analysis

For the seizure fMRI dataset, GLM analysis was performed using the software SPM 12 (Statistical Parametric Mapping, Wellcome Trust Centre for Neuroimaging, London, UK). Since the seizures were induced by KA which leads to the status epilepticus, it was not possible to have discrete seizures within the seizure fMRI EPI sessions. Therefore, we incorporated some scans of seizure fMRI EPI sessions into the scans of the resting state fMRI EPI session to make a block design in the design matrix. To do so, the seizure fMRI EPI scans were resliced to be compatible with the resting state fMRI EPI scans. The seizure fMRI EPI scans were defined as a condition of seizure with onset and duration specified. The design matrix of GLM was built in seconds option instead of in scans option. In SPM, the timepoint of the first scan in GLM design is regarded as 0 instead of 1. Therefore, the onset was set at 18 instead of 20 for 20 seconds resting - 40 seconds seizure – 20 seconds resting designs and at 38 instead of 40 for 40 seconds resting – 20 seizure – 40 seconds resting designs. The condition of the seizure was convolved with Hemodynamic Response Function (HRF) basis function. The realignment parameter for the scans in the design was added as multiple regressors. Afterwards, the model was estimated. For visualization of the statistical map, a t-contrast of 1 was applied on the column of seizure condition and the p-value was Family Wise Error (FWE) corrected and the threshold was set at the conventional value of 0.05. Then the result was overlaid on the mean functional image of the resting state fMRI scanning dataset.

ICA analysis

ICA was performed for the seizure fMRI datasets of using GIFT v 3.0a (Group ICA of fMRI toolbox). Unlike the model-driven GLM analysis, ICA analysis is not dependent on HRF and it is data-driven. The infomax algorithm was selected to set up the ICA analysis. For visualization, the Z-threshold value was set at 4.0 to have the clear separation of the activation clusters and also to reduce noise. Negative Z value was also chosen to be seen. The result of GLM analysis served as a guidance to select the correct independent component that showed activation on the brain regions. Result was overlaid on the coregistered anatomical scan of the resting state fMRI standalone dataset on 21/03/2016.

Chapter 4

Results

4.1 EEG data analysis

We analyzed EEG recording of simultaneous EEG-fMRI sessions on 21/03/2016 and on 22/03/2016 to see if the scalp EEG cap was able to show seizure activity. The same rat (rat 3) was used for both sessions and KA was injected just before we put on the scalp EEG cap. As can be seen in figure 3.4 and as we knew the hippocampus would be the onset region of the seizure which is induced by KA, the signal from electrodes 13, 14, 16 and 17 that were located over the region of hippocampus was particularly within our interest. Therefore, these electrodes were shown in power spectrum on the right side of the figures. In the power spectrum, the orange color represents the delta frequency region (0.5-4 Hz), yellow color represents the theta frequency region (4-8 Hz), green color represents the alpha frequency region (8-13 Hz) and blue color represents the beta frequency region (13-30 Hz). Epileptic activities are characterized by spikes and sharp waves with high amplitude, approximately at 1-2 Hz in delta frequency region and at 5-8 Hz in theta frequency region [92, 93, 94].

4.1.1 Simultaneous EEG-fMRI measurement when seizure induced, 21/03/2016, Rat 3

First, figure 4.1 shows the EEG data in resting state before fMRI EPI session started. There were breathing artifacts shown approximately at 1 Hz. They are clearly visible especially on the electrode 7 and they are marked by red circles in the figure. Only the normal EEG signal was shown here that represented normal neuronal activity. On the other hand, in figure 4.2 which shows the EEG data before the first fMRI EPI session began, we could clearly see the seizure activity started. When we looked at the power spectrum on the right side, we could observe the sharp highest peak in the delta frequency region at around 2 Hz. This was more pronounced on electrodes 16 and 17. Also, in figure 4.3 which shows the EEG data during the first fMRI EPI session, the seizure activities were more intense since these were observed with higher amplitude in the power spectrum. In addition to this, also in figure 4.4 which shows the EEG data during the second fMRI EPI session, the seizure activities were spotted as well. The seizure activities were manifested with spikes and sharp waves. During the EEG recording, the artifact from fMRI scanning was not discernable so it was not marked in the figure.

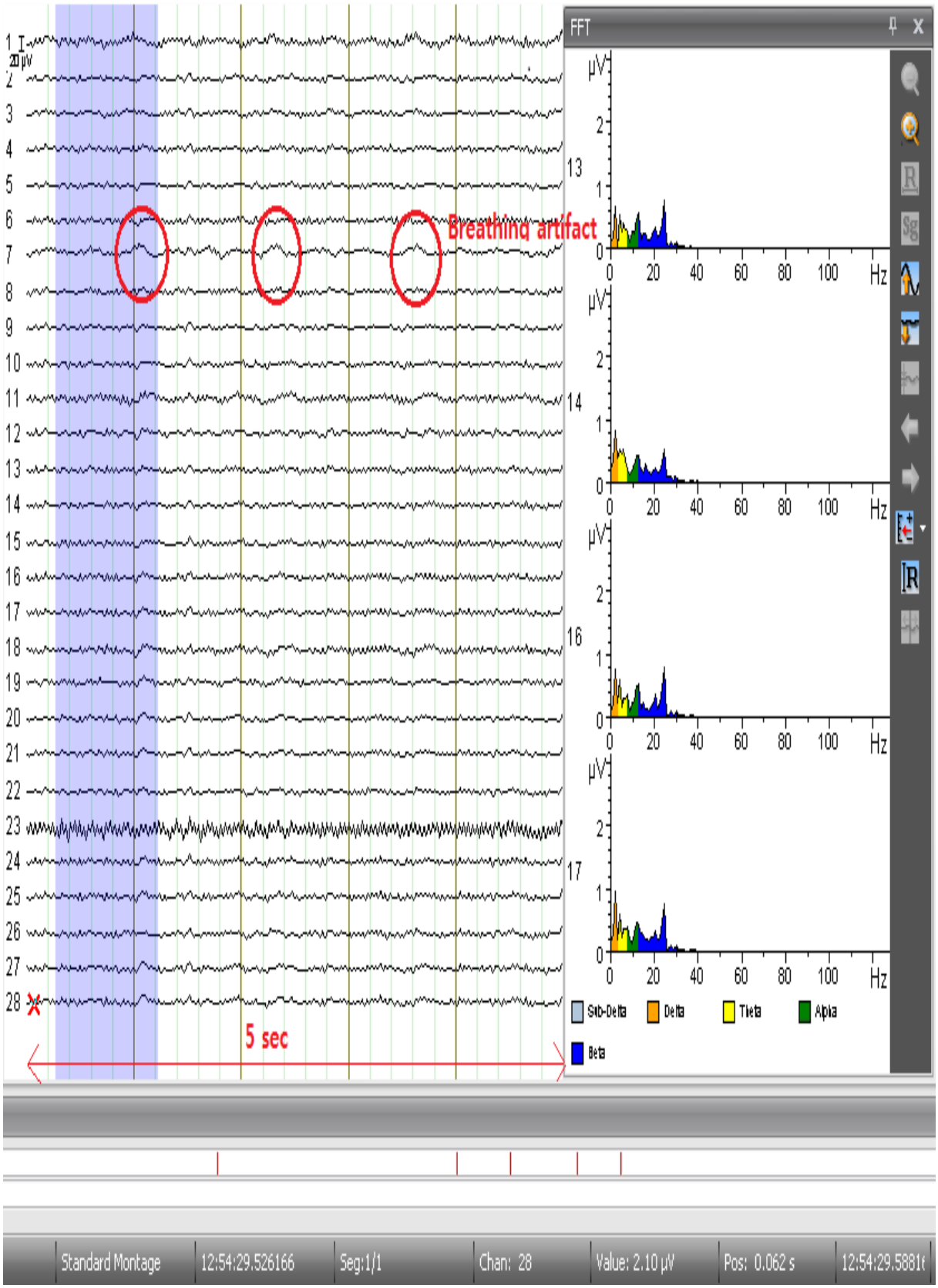

Figure 4.1: Resting state before fMRI EPI session was started

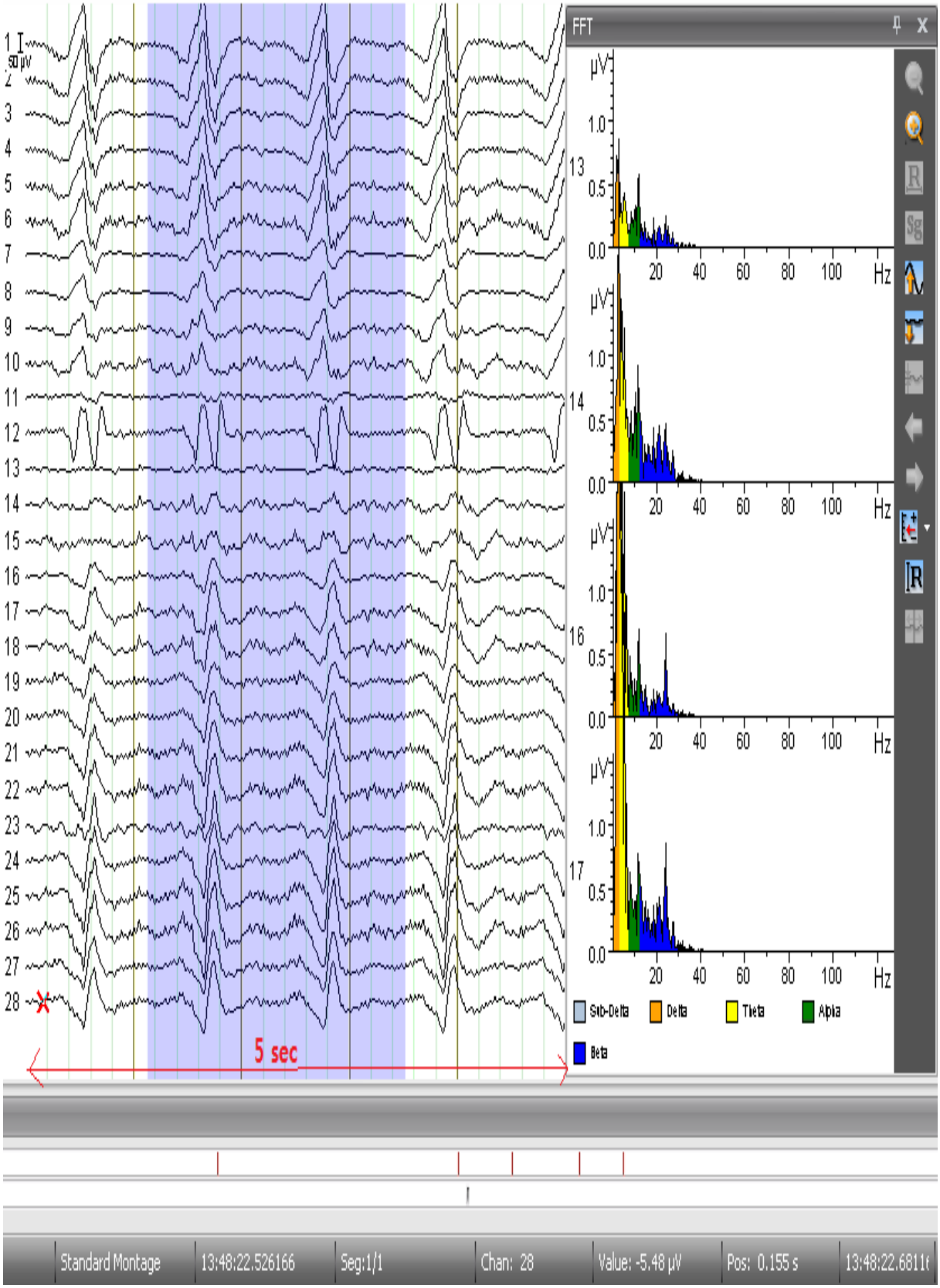

Figure 4.2: Seizure started before fMRI EPI session was started

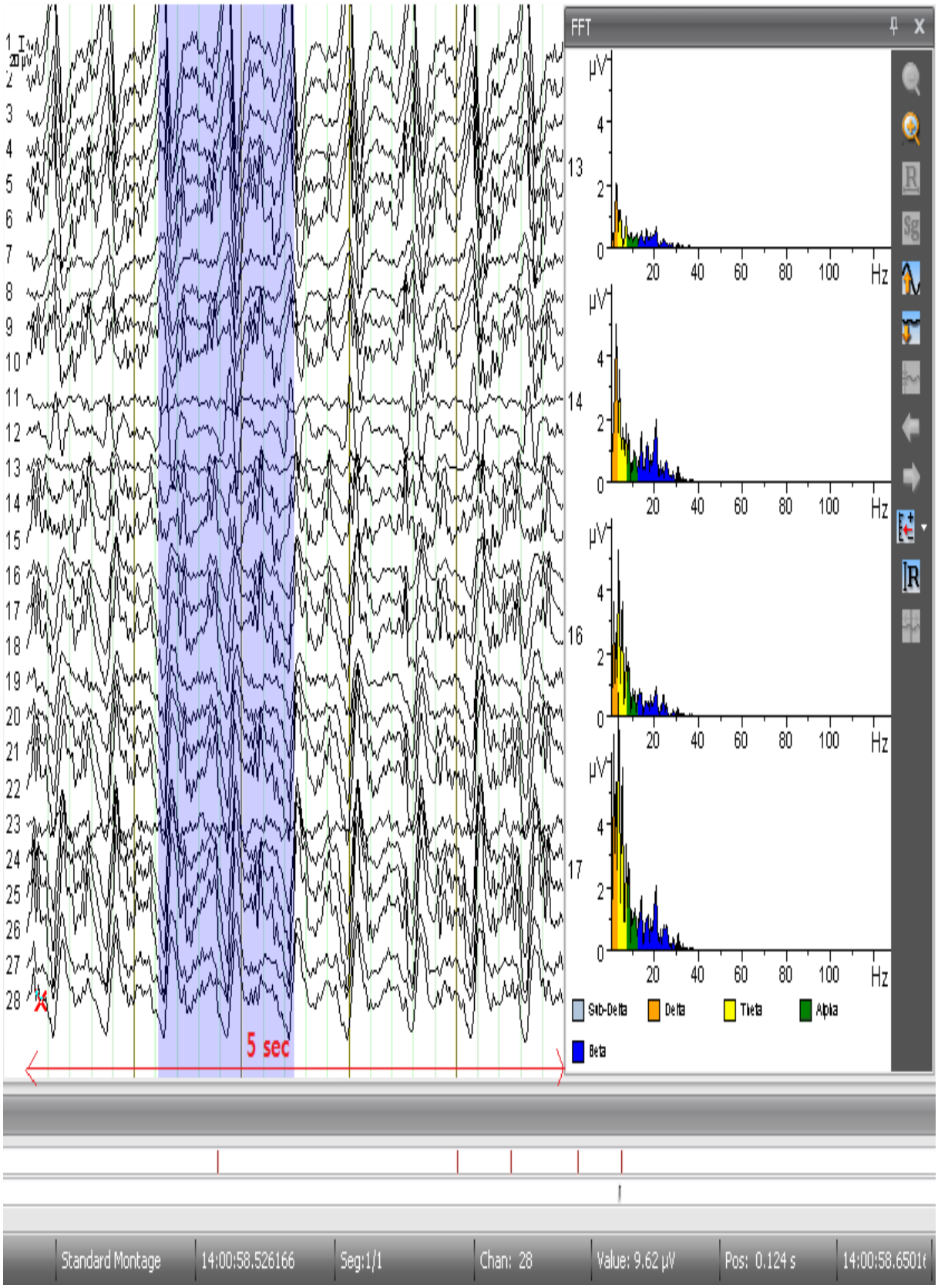

Figure 4.3: Seizure shown during the first fMRI EPI session

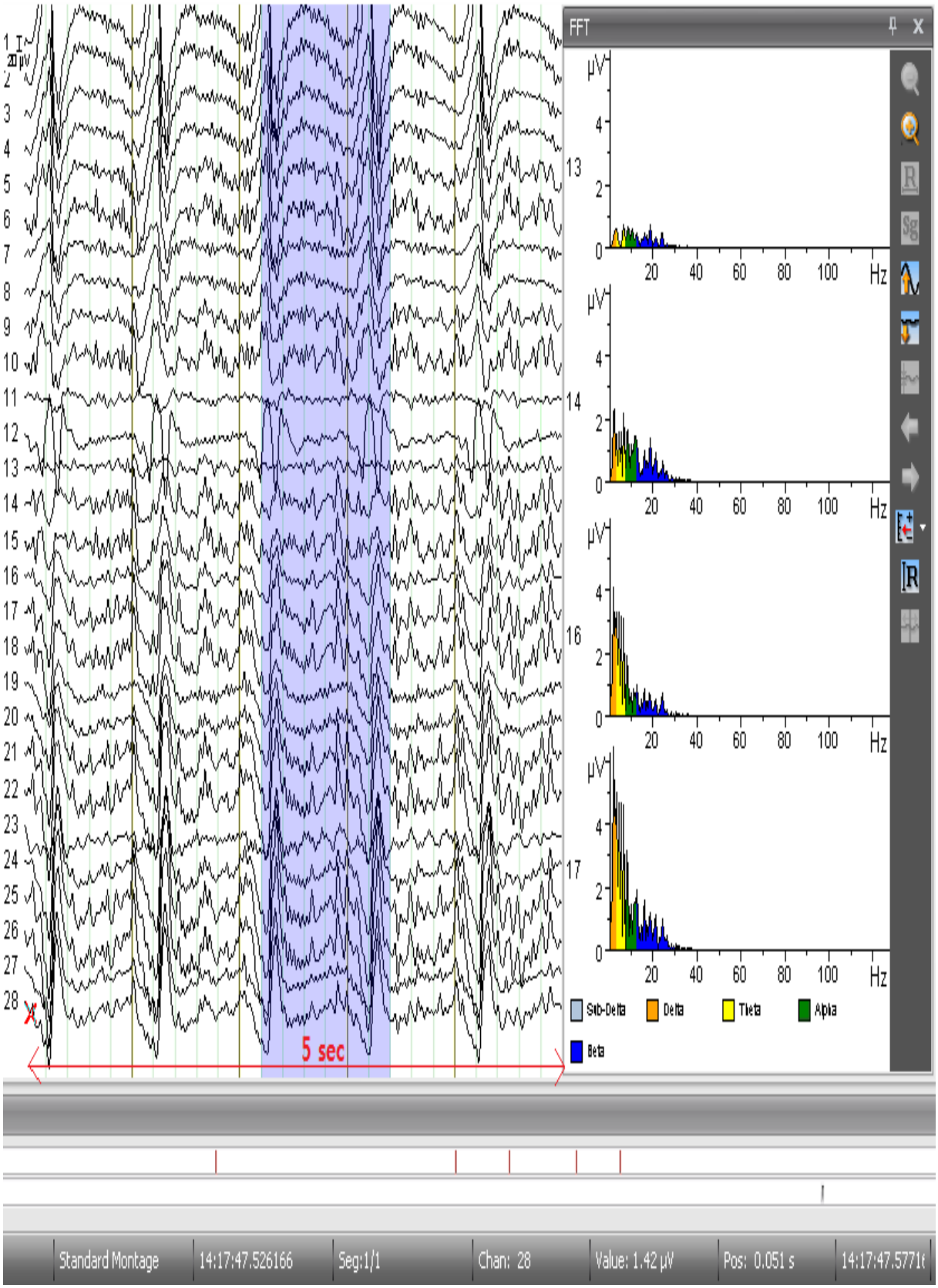

Figure 4.4: Seizure shown during the second fMRI EPI session

4.1.2 Simultaneous EEG-fMRI measurement when seizure induced, 22/03/2016, Rat 3

Figure 4.5 shows EEG data at the very beginning of the EEG recording. It can be seen that seizure activity from the KA injection which was performed the day before (21/03/2016) was still present. The seizures were more pronounced after another KA injection which was executed before the start of EEG recording on that day (22/03/2016). This can be seen in figure 4.6. figure 4.7, figure 4.8 and figure 4.9 show the EEG data during the first fMRI EPI session, the second fMRI EPI session and the third fMRI EPI session respectively. It was obviously shown that seizures were being continued as status epilepticus. The gradient artifact from MR acquisition was distinguishable on the electrode 12 and 23 in figure 4.7, 4.8, 4.9. However, it was not removed since it did not disturb seizure detection.

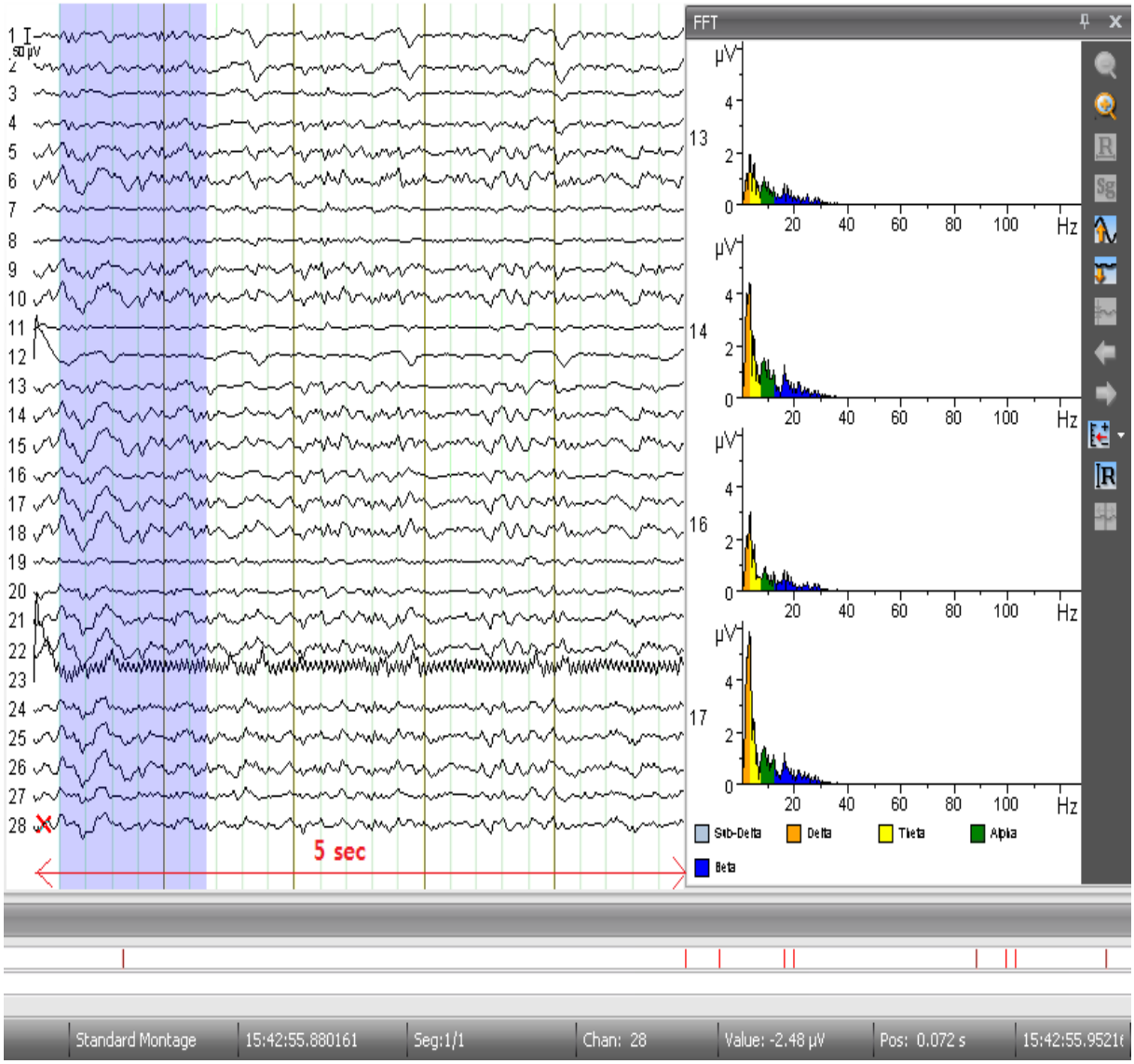

Figure 4.5: Residual seizure activity shown at the beginning of EEG before fMRI EPI session started

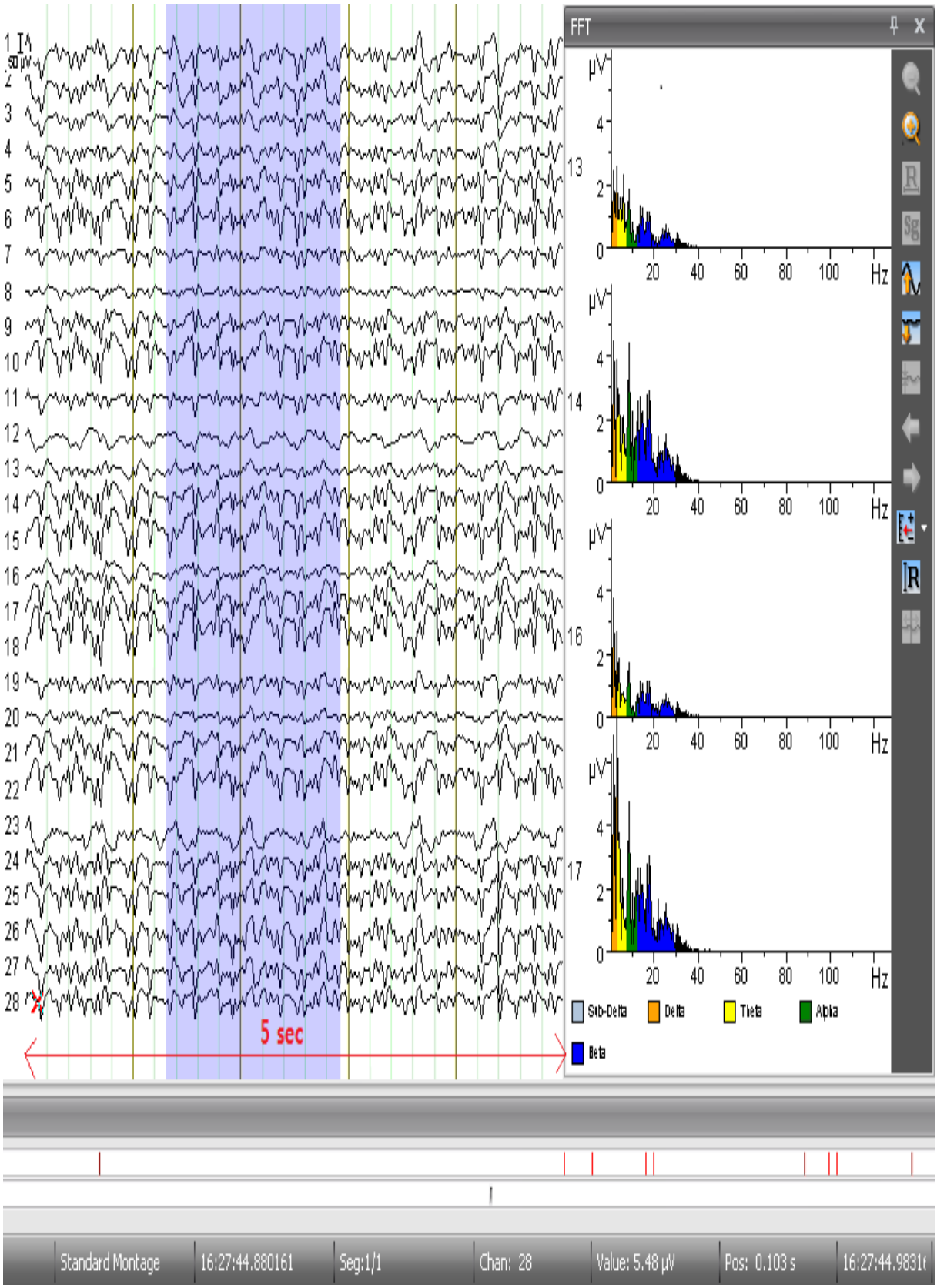

Figure 4.6: After 50 minutes more pronounced seizure shown before fMRI EPI session started

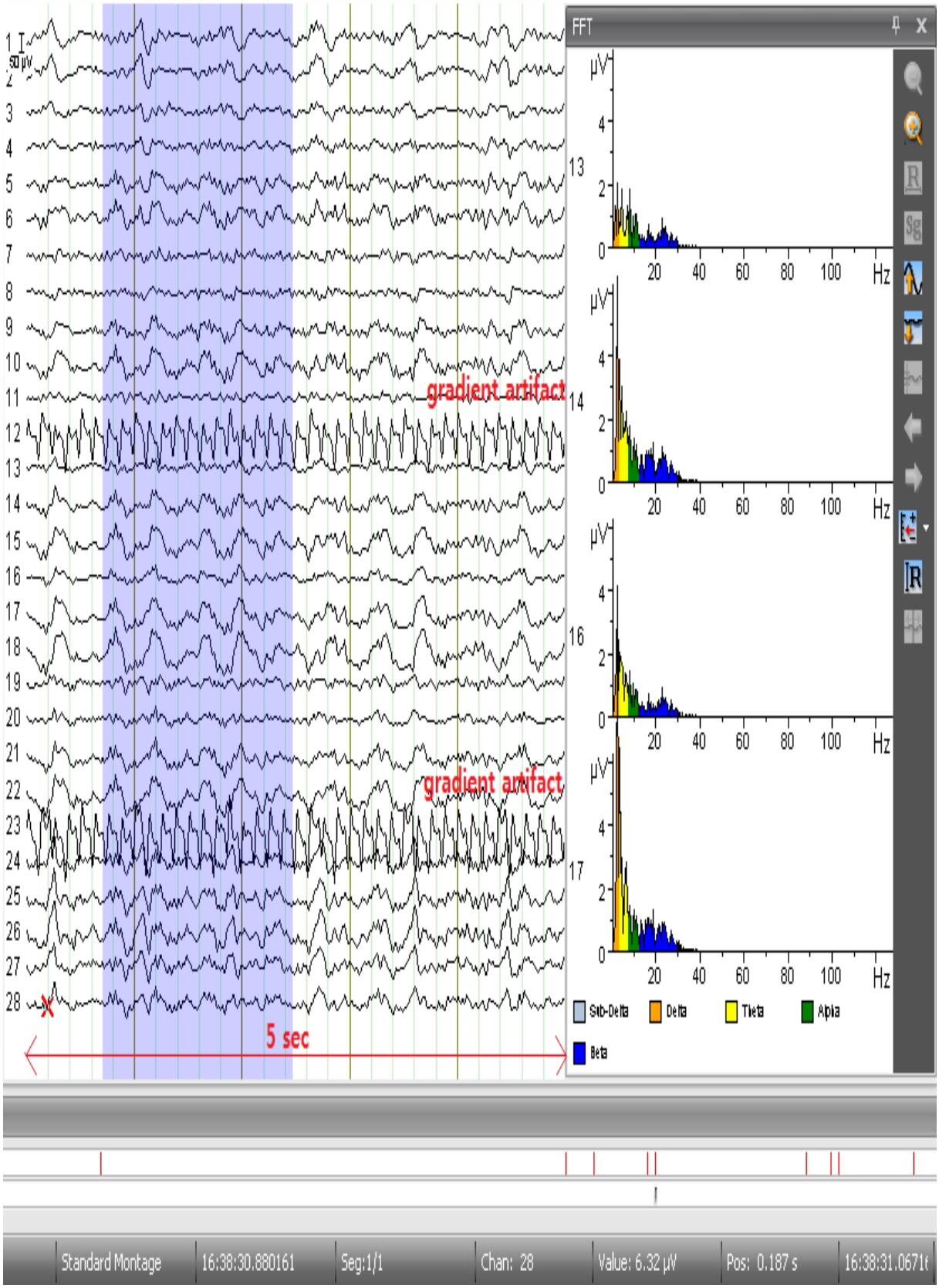

Figure 4.7: Seizure shown during the first fMRI EPI session

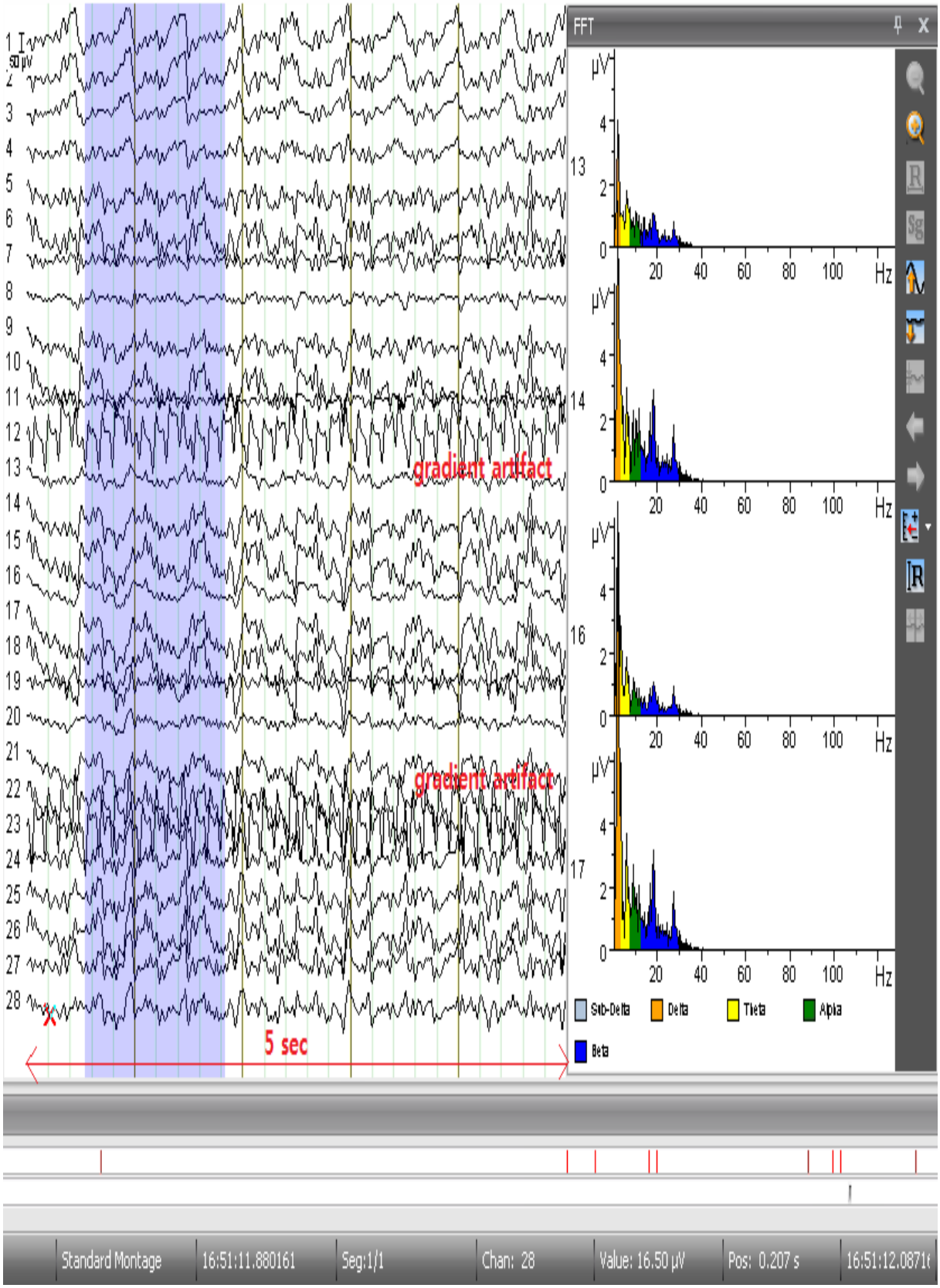

Figure 4.8: Seizure shown during the second fMRI EPI session

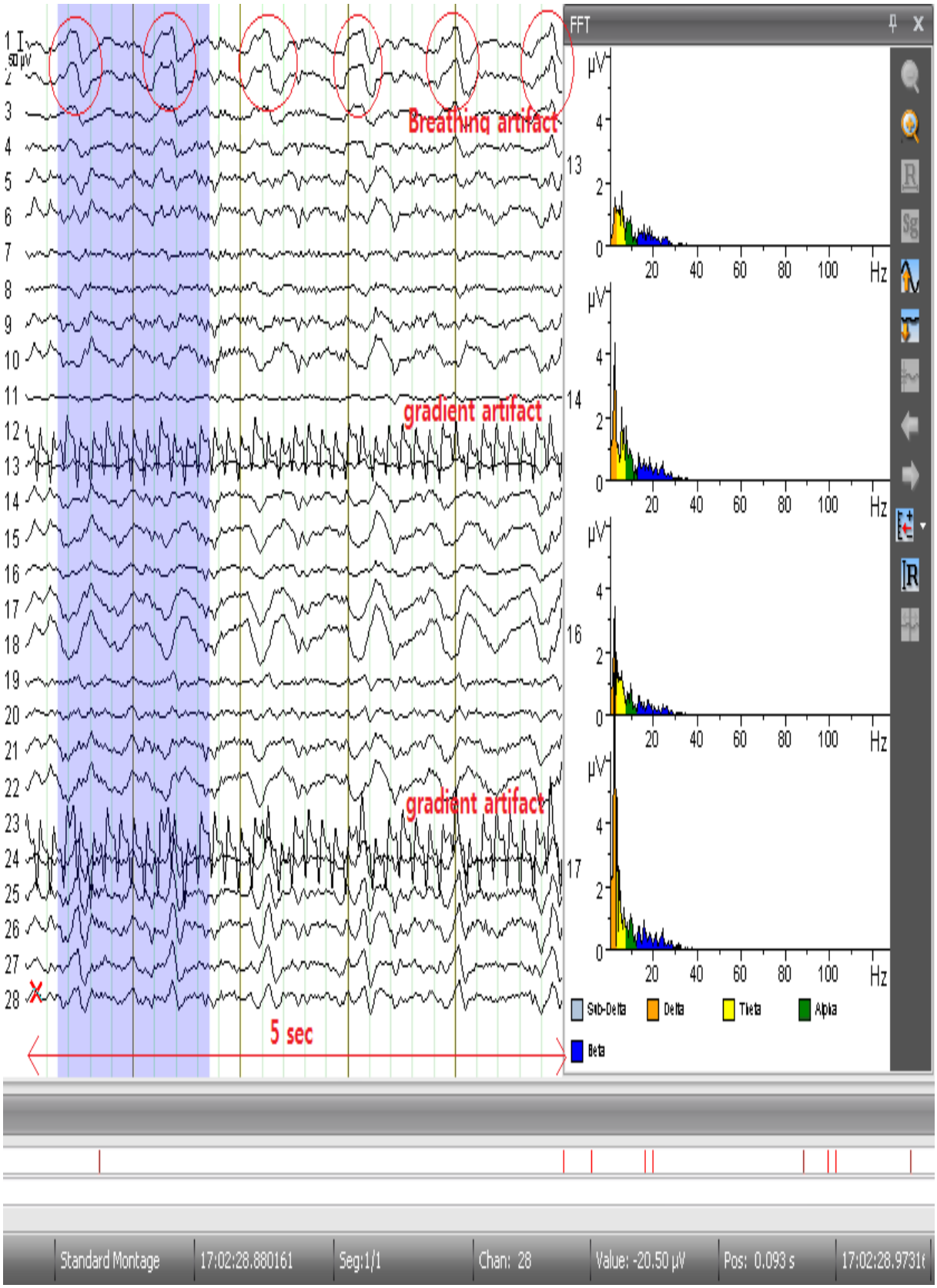

Figure 4.9: Seizure shown during the third fMRI EPI session

4.2 10 x 10 ROI correlation analysis

The 10 x 10 matrix of correlation coefficients between each ROI was visualized as a color map. The list of ROIs is shown next to each correlation map. Also the ROIs that are overlaid on the structural image can be found in chapter 3.7.2 on page 26. The correlation coefficient above 0.7 was considered as high.

4.2.1 fMRI standalone scanning in resting state, 26/11/2015, Rat 2

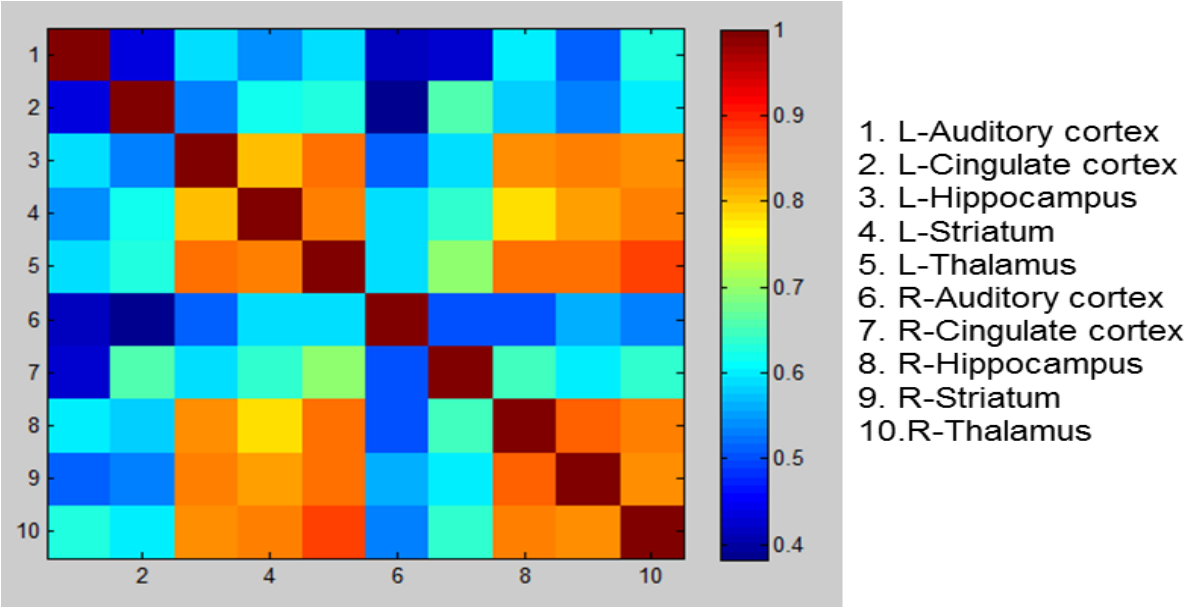

Figure 4.10: ROI correlation matrix of fMRI standalone scanning in resting state, 26/11/2015, Rat 2

The ROI correlation matrix of the fMRI standalone scanning in resting state on 26/11/2015 can be found in figure 4.10. The brain regions with high correlation between left side and right side can be seen in table 4.1. Other inter-regional high correlation values were investigated as well. This can be seen in table 4.2.

ROI	Correlation coefficient
Hippocampus	0.8287
Striatum	0.8256
Thalamus	0.87

Table 4.1: The regions that showed high correlation bilaterally, fMRI standalone scanning on 26/11/2015, Rat 2

Region1	Region2	Correlation coefficient
L-Hippocampus (3)	L-Striatum (4)	0.7975
L-Hippocampus (3)	L-Thalamus (5)	0.8541
L-Hippocampus (3)	R-Striatum (9)	0.8436
L-Hippocampus (3)	R-Thalamus (10)	0.8267
L-Striatum (4)	L-Thalamus (5)	0.8362
L-Striatum (4)	R-Hippocampus (8)	0.7863
L-Striatum (4)	R-Thalamus (10)	0.8426
L-Thalamus (5)	R-Hippocampus (8)	0.8517
L-Thalamus (5)	R-Striatum (9)	0.8467

Table 4.2: Inter-regional high correlation value of fMRI standalone scanning on 26/11/2015, Rat2

4.2.2 Simultaneous EEG-fMRI measurement in resting state, 27/11/2015, Rat 2

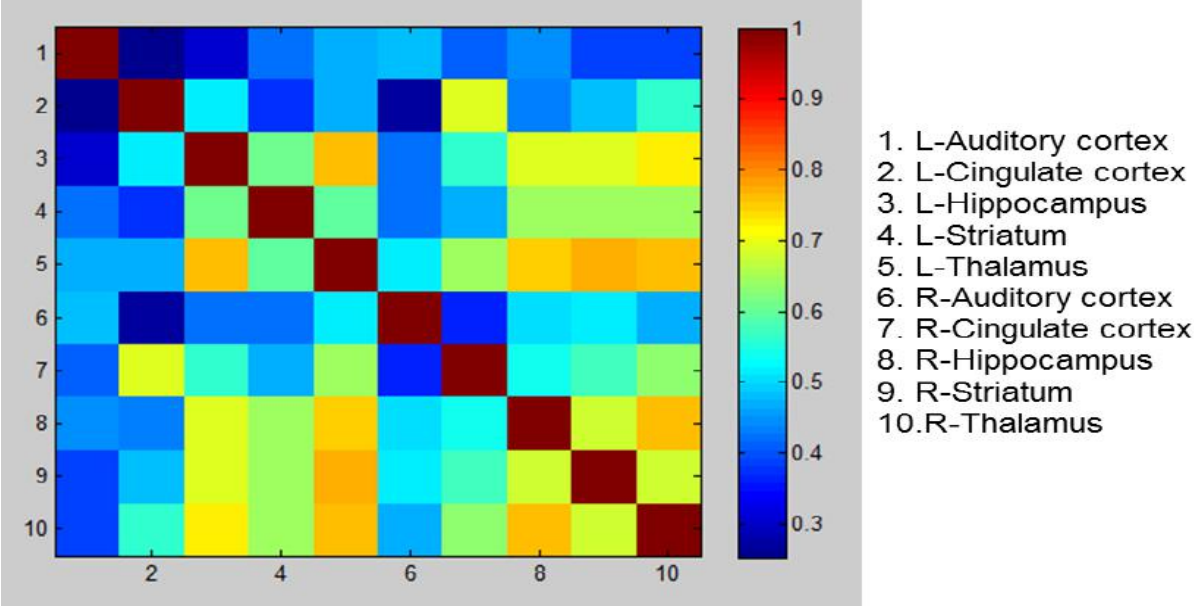

Figure 4.11: ROI correlation matrix of simultaneous EEG-fMRI measurement in resting state, 27/11/2015, Rat 2

The correlation matrix of the simultaneous EEG-fMRI measurement in resting state, 27/11/2015, Rat2 can be seen in figure 4.11. In table 4.3, the brain regions with high correlation between left side and right side are described. Table 4.4 shows inter-regional high correlation values between ROIs.

ROI	Correlation coefficient
Thalamus	0.7551

Table 4.3: The regions that showed high correlation bilaterally, simultaneous EEG-fMRI measurement in resting state, 27/11/2015, Rat 2

Region1	Region2	Correlation coefficient
L-Hippocampus (3)	L-Thalamus (5)	0.7591
L-Hippocampus (3)	R-Thalamus (10)	0.7219
L-Thalamus (5)	R-Hippocampus (8)	0.7470
L-Thalamus (5)	R-Striatum (9)	0.7729

Table 4.4: Inter-regional high correlation value of Simultaneous EEG-fMRI measurement in resting state, 27/11/2015, Rat 2

4.2.3 fMRI standalone scanning in resting state, 03/03/2016, Rat L1R0 and Rat L1R1

Rat L1R0

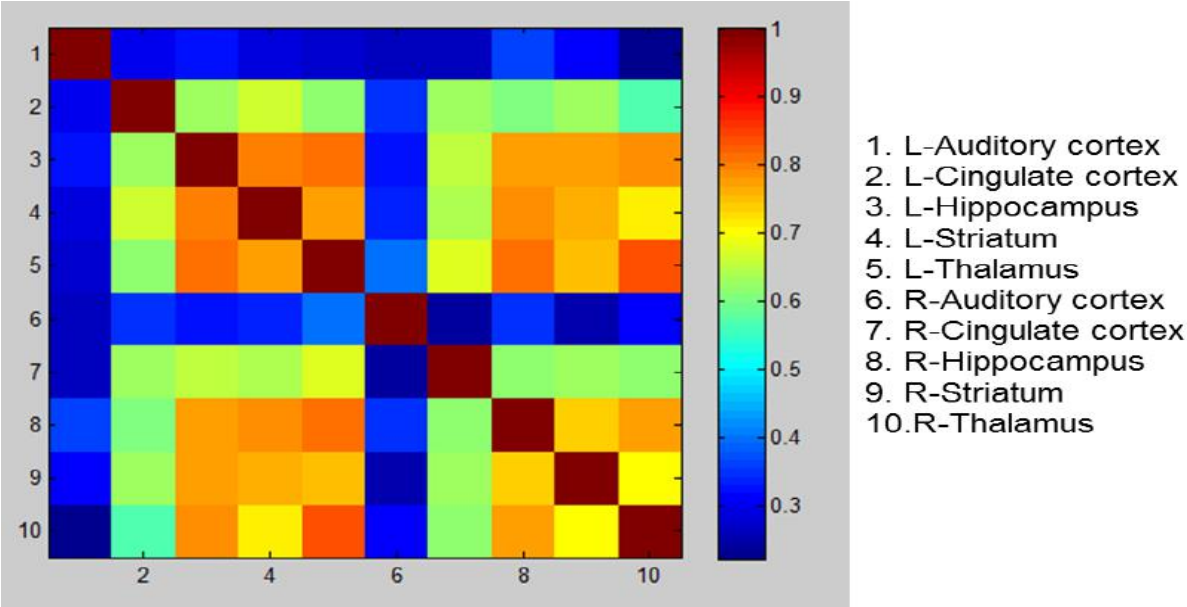

Figure 4.12: ROI correlation matrix of the fMRI standalone scanning in resting state, 03/03/2016, Rat L1R0

Figure 4.12 shows the ROI correlation matrix of the fMRI standalone scanning in resting state, 03/03/2016, Rat L1R0. The brain regions that are highly correlated between left side and right side are indicated in table 4.5. Also, the regions that are highly correlated with other regions of the brain are described in table 4.6.

ROI	Correlation coefficient
Hippocampus	0.7752
Striatum	0.7645
Thalamus	0.8376

Table 4.5: The regions that showed high correlation bilaterally, the fMRI standalone scanning in resting state, 03/03/2016, Rat L1R0

Region1	Region2	Correlation coefficient
L-Hippocampus (3)	L-Striatum (4)	0.7943
L-Hippocampus (3)	L-Thalamus (5)	0.8174
L-Hippocampus (3)	R-Striatum (9)	0.7768
L-Hippocampus (3)	R-Thalamus (10)	0.7930
L-Striatum (4)	L-Thalamus (5)	0.7795
L-Striatum (4)	R-Hippocampus (8)	0.7896
L-Striatum (4)	R-Thalamus (10)	0.7145
L-Thalamus (5)	R-Hippocampus (8)	0.8107
L-Thalamus (5)	R-Striatum (9)	0.7533
L-Thalamus (5)	R-Hippocampus (8)	0.7470
L-Thalamus (5)	R-Striatum (9)	0.7729

Table 4.6: Inter-regional high correlation value of the fMRI standalone scanning in resting state, 03/03/2016, Rat L1R0

Rat L1R1

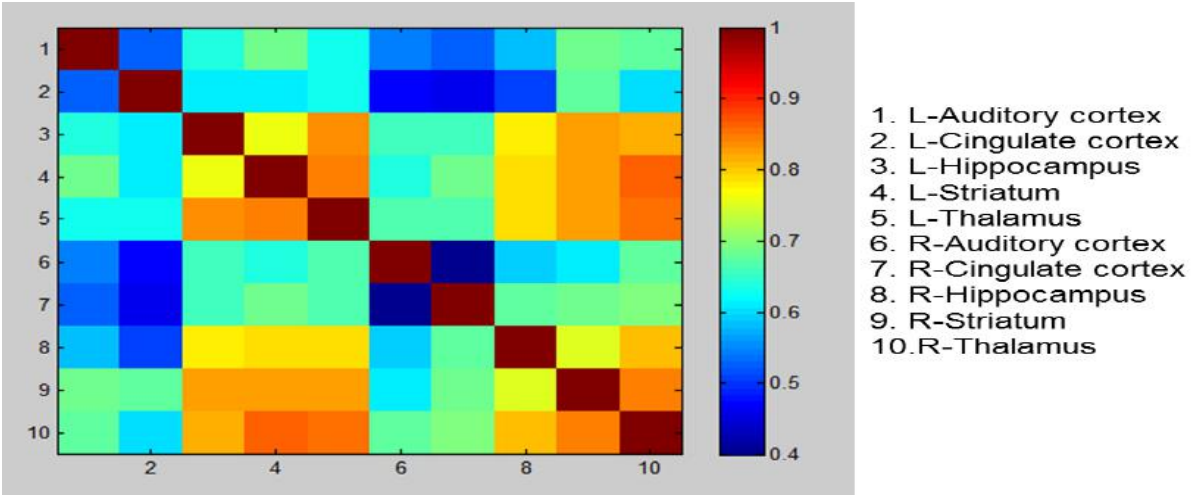

Figure 4.13: ROI correlation matrix of the fMRI standalone scanning in resting state, 03/03/2016, Rat L1R1

The ROI correlation matrix of the fMRI standalone scanning in resting state, 03/03/2016, Rat L1R1 can be found in figure 4.13. The brain regions with bilateral high correlation values can be seen in table 4.7. Other inter-regional high correlation values were examined as well. This can be seen in table 4.8.

ROI	Correlation coefficient
Hippocampus	0.7756
Striatum	0.8256
Thalamus	0.8543

Table 4.7: The regions that showed high correlation bilaterally, the fMRI standalone scanning in resting state, 03/03/2016, Rat L1R1

Region1	Region2	Correlation coefficient
L-Hippocampus (3)	L-Striatum (4)	0.7575
L-Hippocampus (3)	L-Thalamus (5)	0.8326
L-Hippocampus (3)	R-Striatum (9)	0.8298
L-Hippocampus (3)	R-Thalamus (10)	0.8149
L-Striatum (4)	L-Thalamus (5)	0.8410
L-Striatum (4)	R-Hippocampus (8)	0.7850
L-Striatum (4)	R-Thalamus (10)	0.8634
L-Thalamus (5)	R-Hippocampus (8)	0.7889
L-Thalamus (5)	R-Striatum (9)	0.8224

Table 4.8: Inter-regional high correlation value of the fMRI standalone scanning in resting state, 03/03/2016, Rat L1R1

4.2.4 Simultaneous EEG-fMRI measurement in resting state, 04/03/2016, Rat L1R0 and Rat L1R1

Rat L1R0

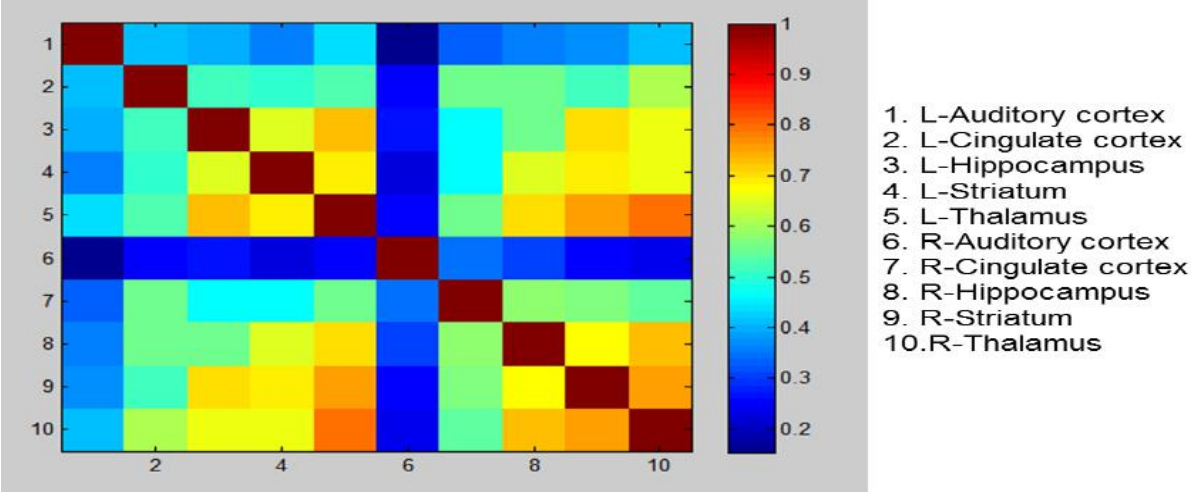

Figure 4.14: ROI correlation matrix of the simultaneous EEG-fMRI measurement in resting state, 04/03/2016, Rat L1R0

Figure 4.14 shows the ROI correlation matrix of the simultaneous EEG-fMRI measurement in resting state, 04/03/2016, L1R0. The brain regions with bilateral correlation coefficient above 0.7 were described in table 4.9. Other inter-regional high correlation values were explored as well which can be found in table 4.10.

ROI	Correlation coefficient
Thalamus	0.7929

Table 4.9: The regions that showed high correlation bilaterally, the simultaneous EEG-fMRI measurement in resting state, 04/03/2016, Rat L1R0

Region1	Region2	Correlation coefficient
L-Hippocampus (3)	L-Thalamus (5)	0.7264
L-Thalamus (5)	R-Striatum (9)	0.7576
R-Hippocampus (8)	R-Thalamus (10)	0.7272
R-Striatum (9)	R-Thalamus (10)	0.7597

Table 4.10: Inter-regional high correlation value of the simultaneous EEG-fMRI measurement in resting state, 04/03/2016, Rat L1R0

Rat L1R1

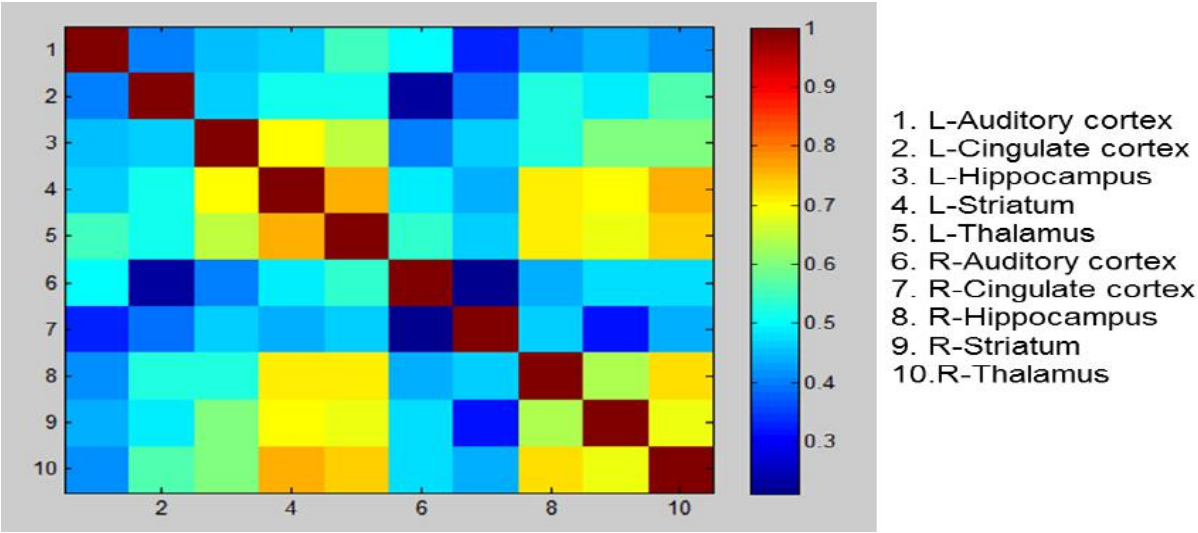

Figure 4.15: ROI correlation matrix of the simultaneous EEG-fMRI measurement in resting state, 04/03/2016, Rat L1R1

The ROI correlation matrix of the simultaneous EEG-fMRI measurement in resting state, 04/03/2016, Rat L1R1 is visualized in figure 4.15. The brain regions of which left side and right side are greatly correlated can be seen in table 4.11. Furthermore, other inter-regional correlation values were inspected and the regions with high correlation coefficient are specified in table 4.12.

ROI	Correlation coefficient
Thalamus	0.7318

Table 4.11: The regions that showed high correlation bilaterally, the simultaneous EEG-fMRI measurement in resting state, 04/03/2016, Rat L1R1

Region1	Region2	Correlation coefficient
L-Striatum (4)	L-Thalamus (5)	0.7657
L-Striatum (4)	R-Hippocampus (8)	0.7050
L-Striatum (4)	R-Thalamus(10)	0.7618
L-Thalamus (5)	R-Hippocampus (8)	0.7096
R-Hippocampus (8)	R-Thalamus (10)	0.7182

Table 4.12: Inter-regional high correlation value of the simultaneous EEG-fMRI measurement in resting state, 04/03/2016, Rat L1R1

4.2.5 fMRI standalone scanning in resting state, 21/03/2016, Rat 3

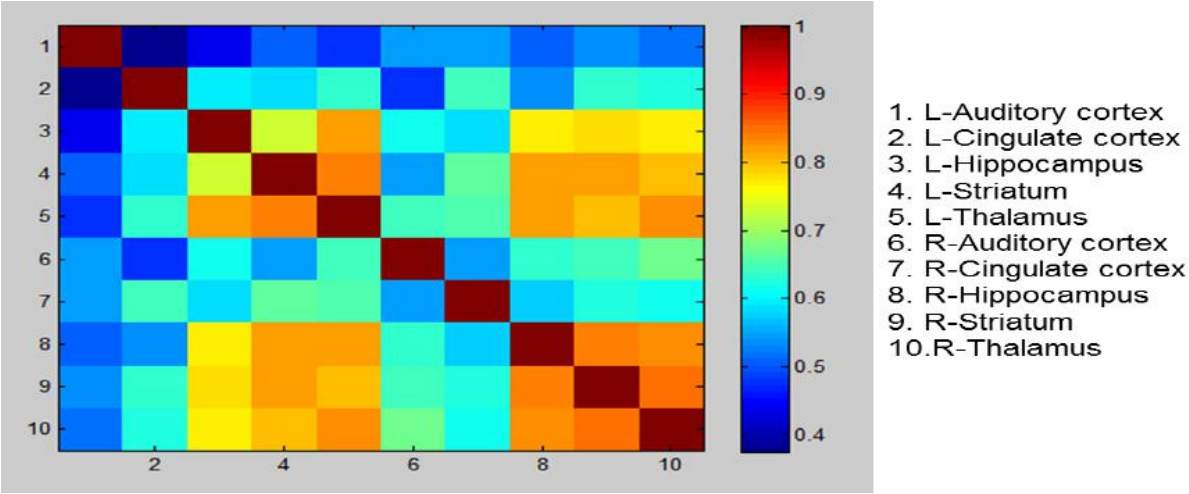

Figure 4.16: ROI correlation matrix of the fMRI standalone scanning in resting state, 21/03/2016, Rat 3

The ROI correlation matrix of the fMRI standalone scanning in resting state, 21/03/2016, Rat 3 can be observed in figure 4.16. The bi-lateral brain regions are described in table 4.13 and regions with inter-regional high correlation values can be seen in table 4.14.

ROI	Correlation coefficient
Hippocampus	0.7688
Striatum	0.8154
Thalamus	0.8253

Table 4.13: The regions that showed high correlation bilaterally, fMRI standalone scanning in resting state, 21/03/2016, Rat 3

Region1	Region2	Correlation coefficient
L-Hippocampus (3)	L-Striatum (4)	0.7290
L-Hippocampus (3)	L-Thalamus (5)	0.8239
L-Hippocampus (3)	R-Striatum (9)	0.7812
L-Hippocampus (3)	R-Thalamus (10)	0.7710
L-Striatum (4)	L-Thalamus (5)	0.8384
L-Striatum (4)	R-Hippocampus (8)	0.8197
L-Striatum (4)	R-Thalamus(10)	0.8038
L-Thalamus (5)	R-Hippocampus (8)	0.8211
L-Thalamus (5)	R-Striatum (9)	0.8023

Table 4.14: Inter-regional high correlation value of fMRI standalone scanning in resting state, 21/03/2016, Rat 3

4.2.6 Simultaneous EEG-fMRI measurement when seizure induced, 21/03/2016, Rat 3

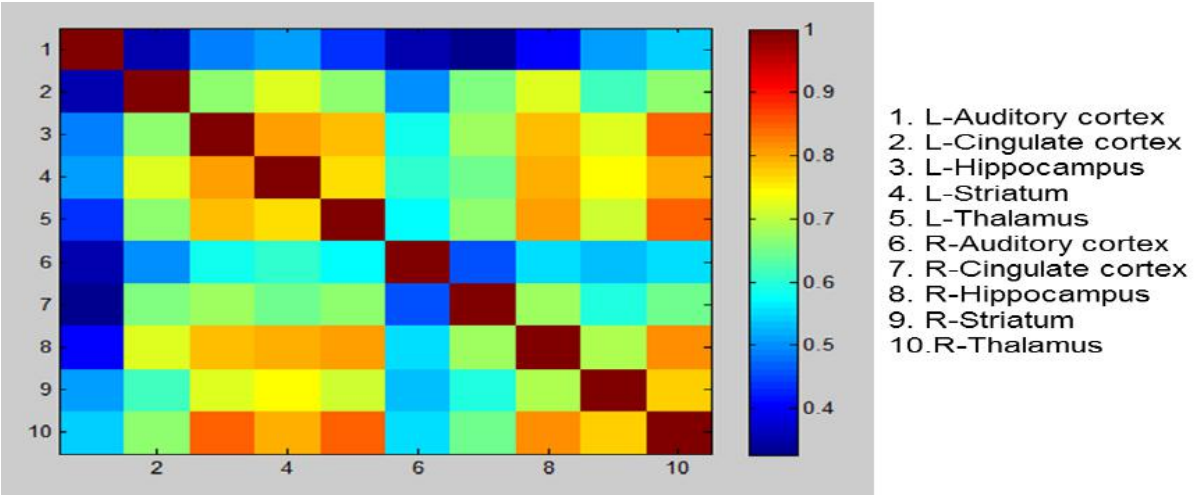

Figure 4.17: ROI correlation matrix of the simultaneous EEG-fMRI measurement when seizure induced, 21/03/2016, Rat 3

Figure 4.17 shows the ROI correlation matrix of the simultaneous EEG-fMRI measurement when seizure induced, 21/03/2016, Rat 3. The regions with intra-regional high correlation coefficients are described in table 4.15. Plus, other inter-regional high correlation values were examined as well which can be seen in table 4.16.

ROI	Correlation coefficient
Hippocampus	0.7892
Striatum	0.7400
Thalamus	0.8498

Table 4.15: The regions that showed high correlation bilaterally, simultaneous EEG-fMRI measurement when seizure induced, 21/03/2016, Rat 3

Region1	Region2	Correlation coefficient
L-Auditory cortex (2)	L-Striatum (4)	0.7164
L-Auditory cortex (2)	R-Hippocampus (8)	0.7254
L-Hippocampus (3)	L-Striatum (4)	0.8097
L-Hippocampus (3)	L-Thalamus (5)	0.7887
L-Hippocampus (3)	R-Striatum (9)	0.7195
L-Hippocampus (3)	R-Thalamus (10)	0.8464
L-Striatum (4)	L-Thalamus (5)	0.7647
L-Striatum (4)	R-Hippocampus (8)	0.7899
L-Striatum (4)	R-Thalamus(10)	0.7988
L-Thalamus (5)	R-Hippocampus (8)	0.8025
L-Thalamus (5)	R-Striatum (9)	0.7134

Table 4.16: Inter-regional high correlation value of simultaneous EEG-fMRI measurement when seizure induced, 21/03/2016, Rat 3

4.2.7 Simultaneous EEG-fMRI measurement when seizure induced, 22/03/2016, Rat 3

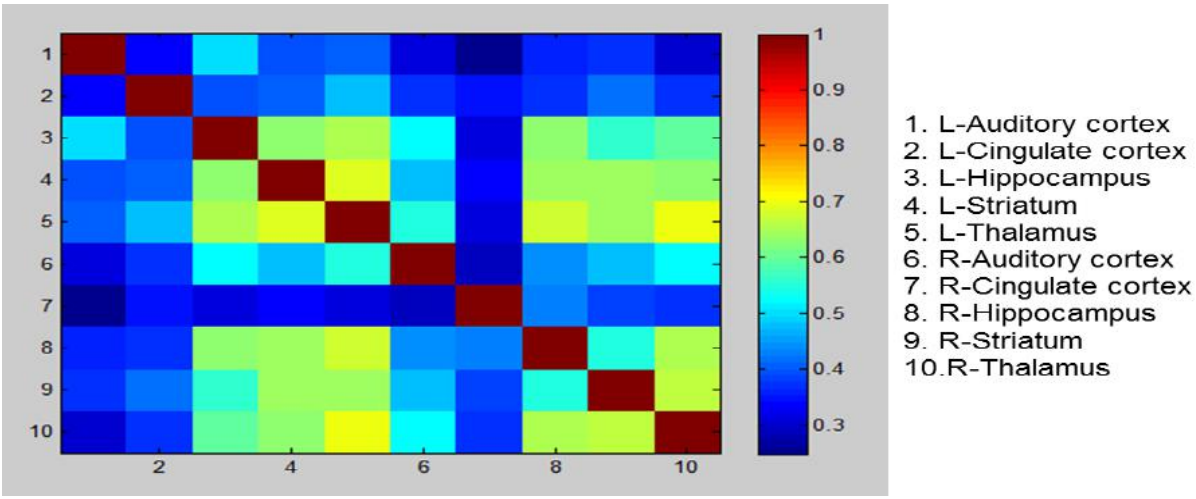

Figure 4.18: ROI correlation matrix of the simultaneous EEG-fMRI measurement when seizure induced, 22/03/2016, Rat 3

The ROI correlation matrix of the simultaneous EEG-fMRI measurement when seizure induced, 22/03/2016, Rat 3 can be found in figure 4.18. Note that this rat was injected by KA the day before so it was second seizure induction for this rat. The brain regions that presented to be highly correlated between their left side and right side can be found in table 4.17. Also, the brain regions that are shown to be highly correlated with other brain regions are investigated as well. But no regions with high inter-regional correlation coefficient were discovered.

ROI	Correlation coefficient
Thalamus	0.7060

Table 4.17: The regions that showed high correlation bilaterally, simultaneous EEG-fMRI measurement when seizure induced, 22/03/2016, Rat 3

4.3 GLM analysis

GLM analysis was performed using the dataset of fMRI standalone scanning in resting state, 21/03/2016, Rat 3, simultaneous EEG-fMRI measurement when seizure induced, 21/03/2016, Rat 3 and simultaneous EEG-fMRI measurement when seizure induced, 22/03/2016, Rat 3. Note that these three dataset used the same rat (Rat 3) and seizure was induced for two consecutive days.

4.3.1 Simultaneous EEG-fMRI measurement with seizure induced, 21/03/2016

First GLM analysis was performed using 20 scans (40 sec) of resting state, next 10 scans (20 sec) during evoked seizures and then another 20 scans (40 sec) of resting state. The design matrix of this 40 sec-20 sec-40 sec model is shown in figure 4.19. The resulted t-statistical parametric map can be found in figure 4.20. The high T-value was seen in neocortex, cingulate cortex, striatum, corpus callosum and hippocampus. Second GLM analysis was carried out using 10 scans (20 sec) of resting state followed by 20 scans (40 sec) during evoked seizures and another 10 scans (20 sec) of resting state. Figure 4.21 shows the design matrix of this 20 sec-40 sec-20 sec model. The model resulted in a t-statistical parametric map which can be found in figure 4.22. As the result of first GLM analysis, second GLM analysis also resulted to show high T-value in neocortex, cingulate cortex, striatum, corpus callosum and hippocampus. For both models, the high T-value shown out of brain region might be some artifact. In the design matrix, the first column is the seizure condition and from second to seventh column represents the realignment parameter that is included as multiple regressors. The last column is the constant.

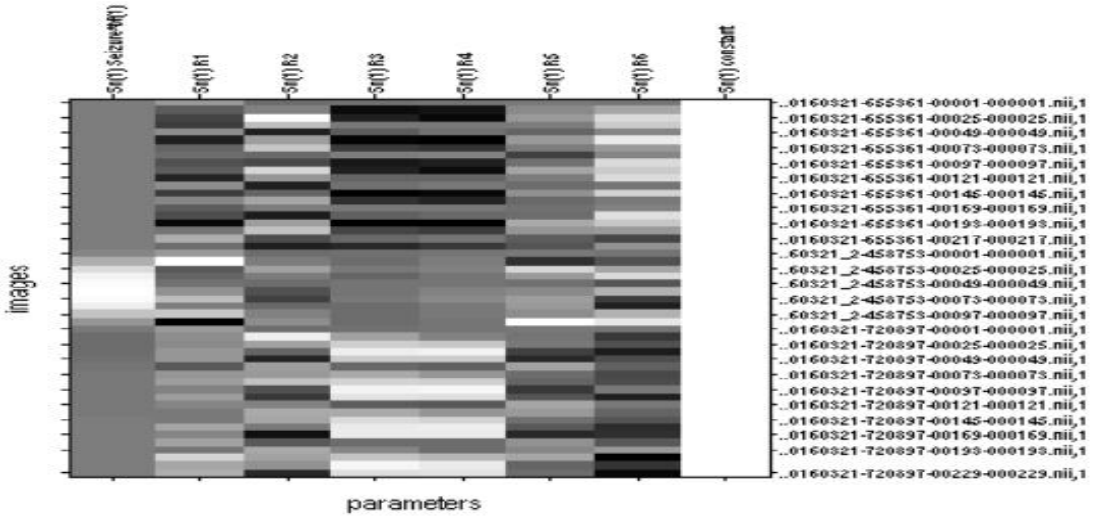

Figure 4.19: The 40sec-20sec-40sec design matrix of the simultaneous EEG-fMRI measurement when seizure induced dataset, 21/03/2016

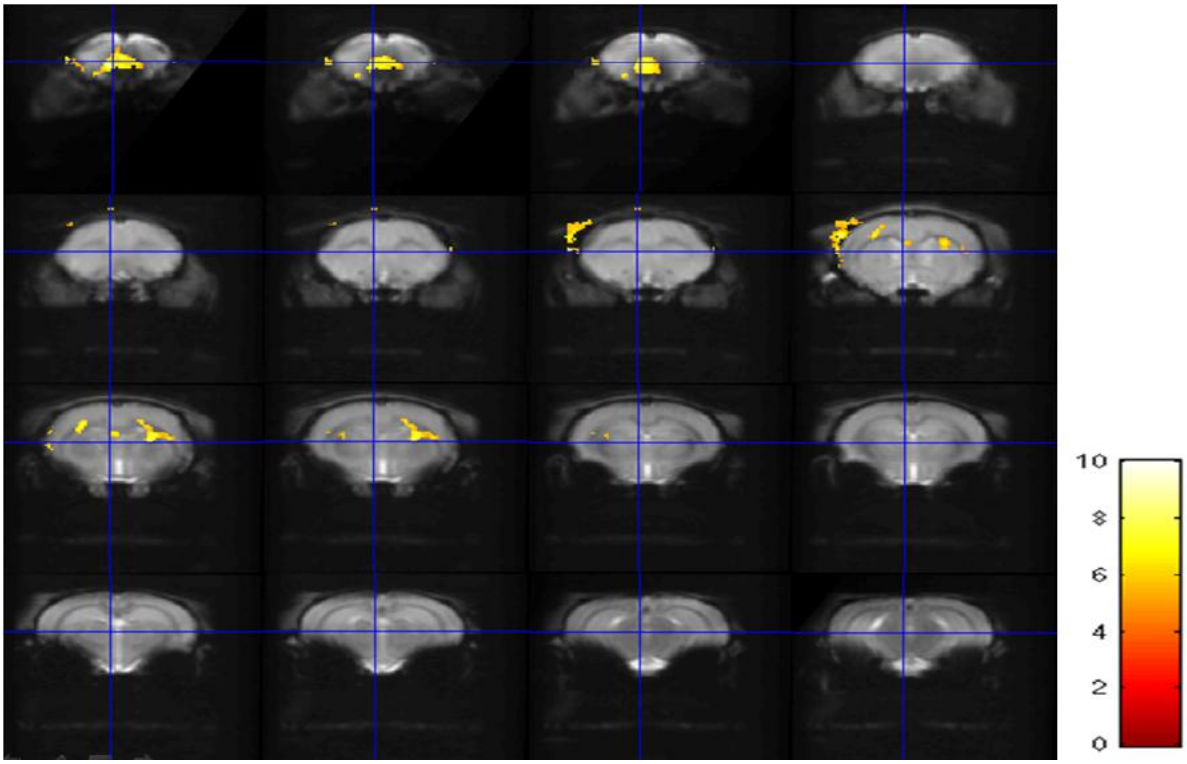

Figure 4.20: GLM result of the 40sec-20sec-40sec model of the simultaneous EEG-fMRI measurement when seizure induced dataset, 21/03/2016

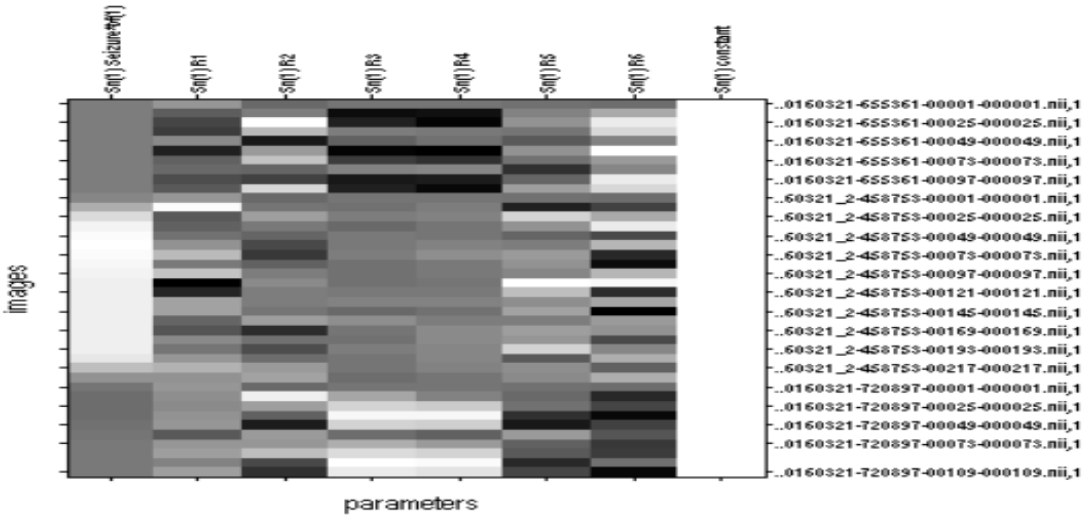

Figure 4.21: The 20sec-40sec-20sec design matrix of the simultaneous EEG-fMRI measurement when seizure induced dataset, 21/03/2016

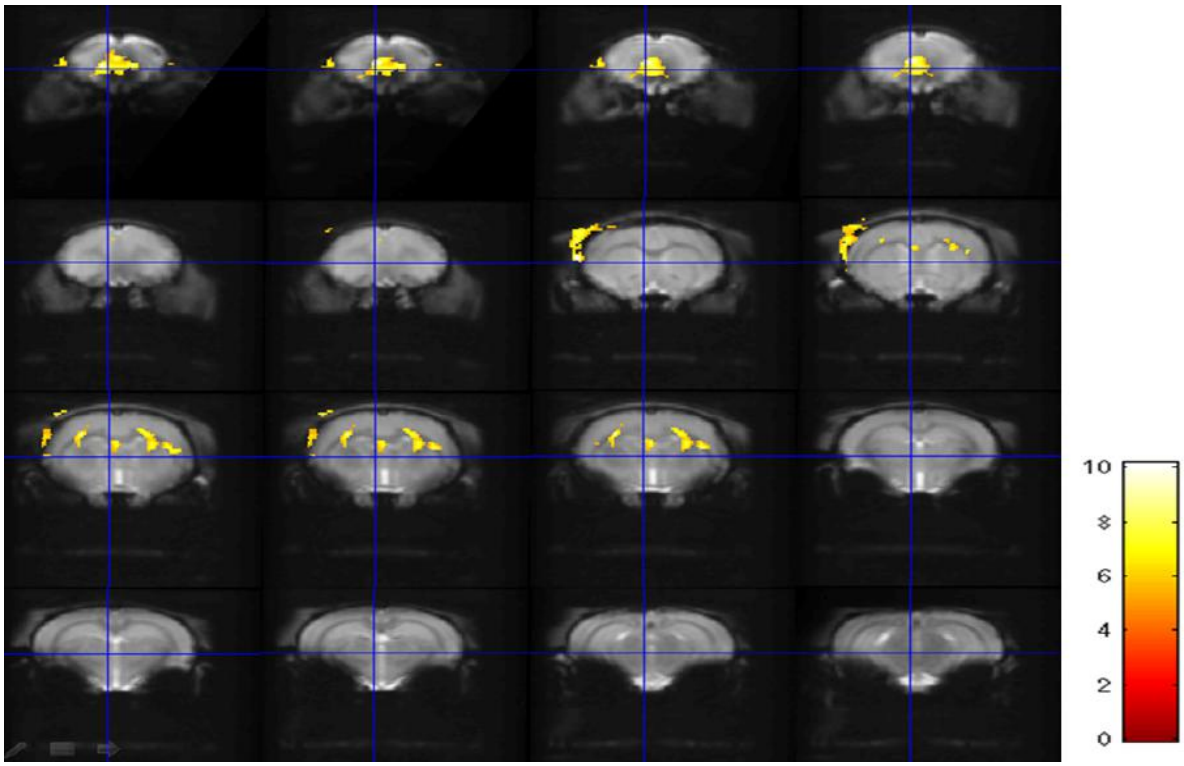

Figure 4.22: GLM result of the 20sec-40sec-20sec model of the simultaneous EEG-fMRI measurement when seizure induced dataset, 21/03/2016

4.3.2 Simultaneous EEG-fMRI measurement with seizure induced, 22/03/2016

First GLM analysis was performed using 20 scans (40 sec) of resting state, 10 scans (20 sec) during evoked seizures and another 20 scans (40 sec) of resting state. The design matrix of this 40 sec-20 sec-40 sec model is shown in figure 4.23 which resulted in a t-statistical parametric map that can be found in figure 4.24. The high T value was observed only in neocortex but in no other brain regions. Second GLM analysis was executed using 10 scans (20 sec) of resting state and 20 scans (40 sec) during evoked seizures and another 10 scans (20 sec) of resting state. The design matrix of this 20 sec-40 sec-20 sec model is shown in figure 4.25. This model led to a t-statistical parametric map which can be found in figure 4.26. Likewise, second GLM analysis, high T-value was observed only in parts of neocortex but in no other brain regions. In the design matrix, the first column is the seizure condition and from second to seventh column represents the realignment parameter that is included as multiple regressors. The last column is the constant.

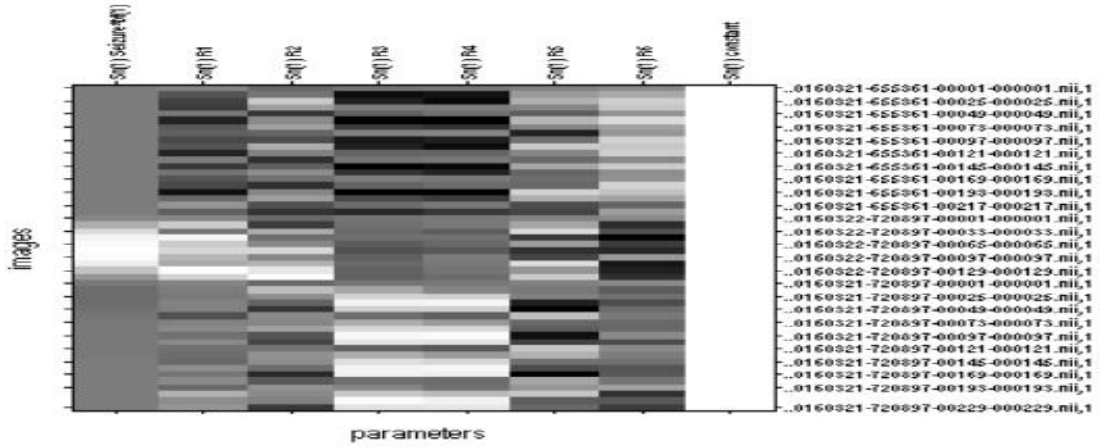

Figure 4.23: The 40sec-20sec-40sec design matrix of the simultaneous EEG-fMRI measurement when seizure induced dataset, 22/03/2016

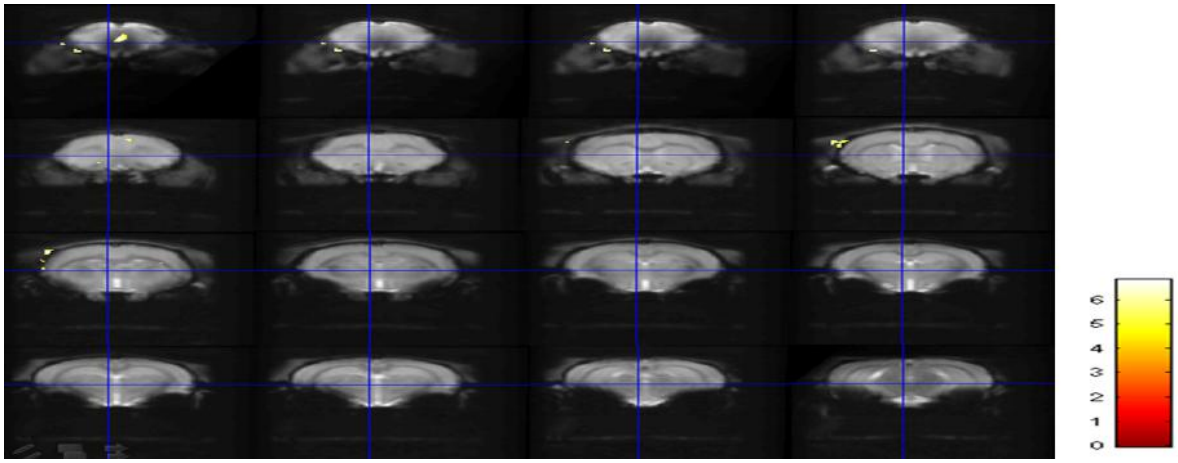

Figure 4.24: GLM result of the 40sec-20sec-40sec model of the simultaneous EEG-fMRI measurement when seizure induced dataset, 22/03/2016

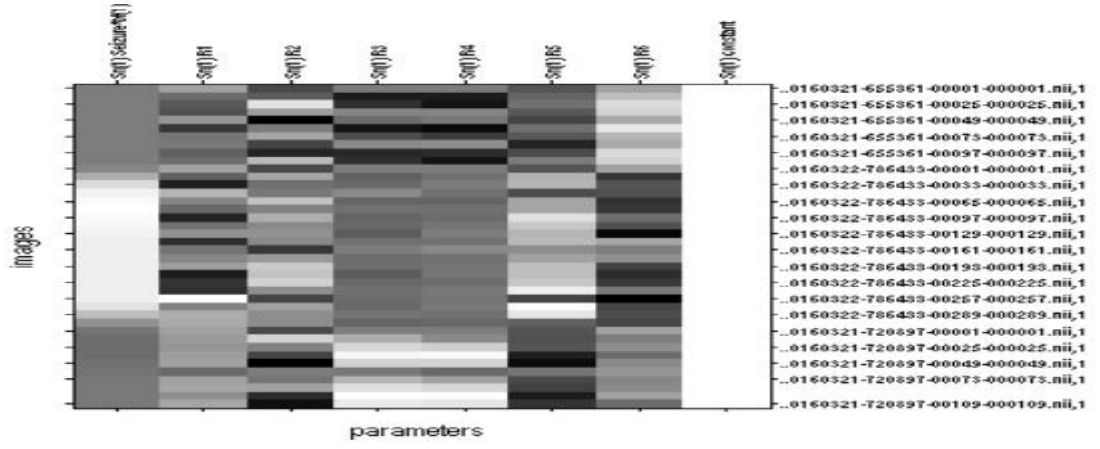

Figure 4.25: The 20sec-40sec-20sec design matrix of the simultaneous EEG-fMRI measurement when seizure induced dataset, 22/03/2016

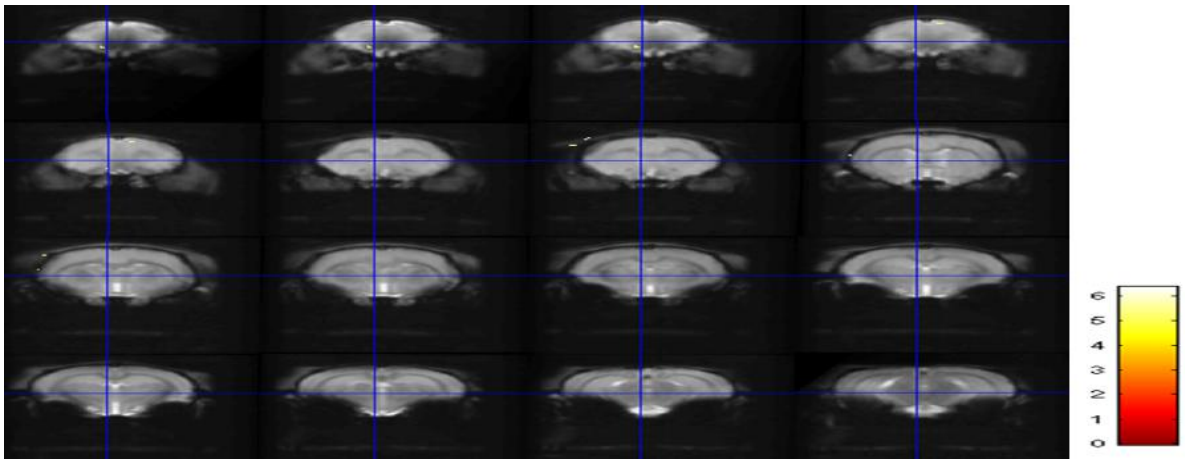

Figure 4.26: GLM result of the 20sec-40sec-20sec model of the simultaneous EEG-fMRI measurement when seizure induced dataset, 22/03/2016

4.4 ICA analysis

ICA analysis was performed using the two seizure fMRI EPI datasets (simultaneous EEG-fMRI measurement when seizure induced, 21/03/2016, Rat 3 and simultaneous EEG-fMRI measurement when seizure induced, 22/03/2016, Rat 3). The result was overlaid on the coregistered anatomical scan of the resting state fMRI standalone dataset of 21/03/2016. Note that the same rat (Rat 3) was used for these three dataset and seizure was induced for two consecutive days. After trying to run with different number of independent components, we found out that when the independent component number was specified at 2, best results for both datasets were found. Then, by comparing them with the ones of GLM results, only the component that corresponded to the activation on the brain was selected.

4.4.1 Simultaneous EEG-fMRI measurement when seizure induced, 21/03/2016

Figure 4.27 shows high Z score over the threshold value in neocortex, cingulate cortex, septal region, thalamus and hippocampus. There was no negative Z score observed in this dataset.

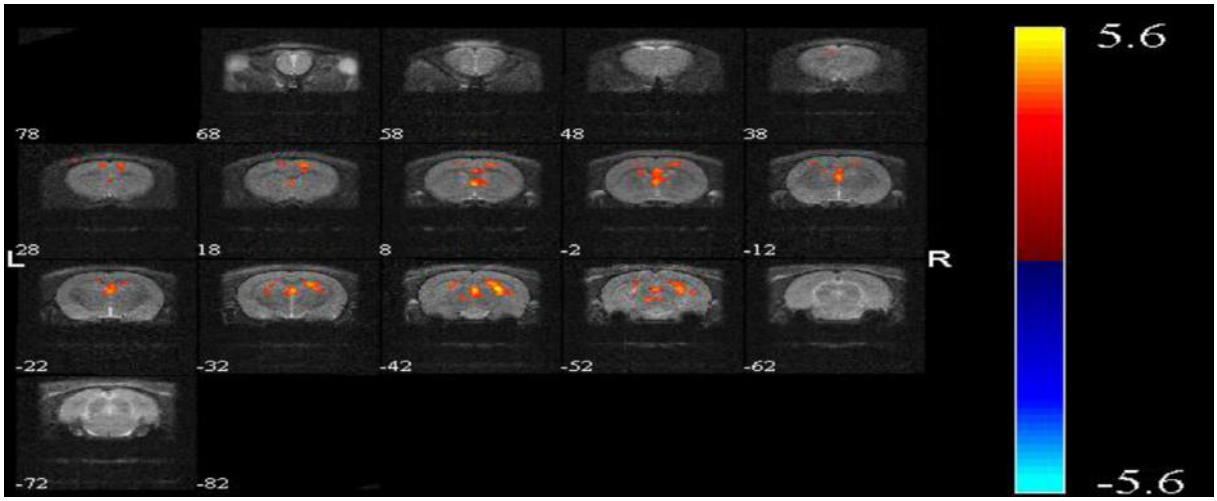

Figure 4.27: BOLD fMRI response map of the simultaneous EEG-fMRI measurement when seizure induced dataset, 21/03/2016

4.4.2 Simultaneous EEG-fMRI measurement with seizure induced, 22/03/2016

Unlike the result of GLM analysis, ICA analysis was able to show high Z score over the threshold value in some brain regions such as neocortex, septal region, cingulate cortex, hippocampus, thalamus and hypothalamus. This can be seen in figure 4.28. There were no brain regions that showed negative Z score in this dataset.

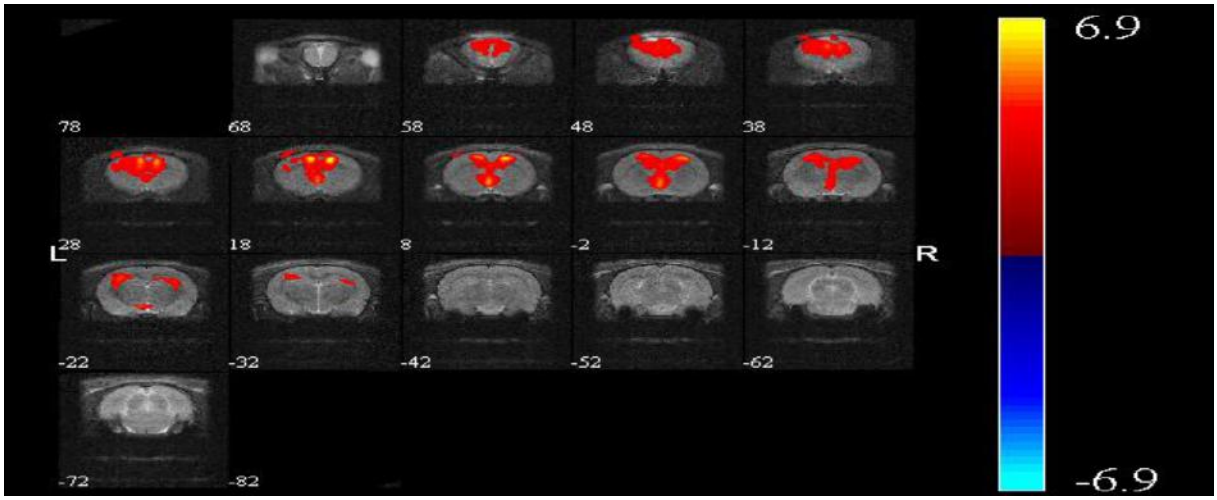

Figure 4.28: BOLD fMRI response map of the simultaneous EEG-fMRI measurement when seizure induced dataset, 22/03/2016

Chapter 5

Discussion

The aim of the thesis was to examine the possibility of the scalp EEG cap if it could detect seizures and also further aid in EEG-fMRI preclinical epilepsy studies. Finally, we assess whether the scalp EEG cap for rats is useful as an experimental platform to bridge the gap between preclinical EEG-fMRI epilepsy studies and clinical EEG-fMRI epilepsy studies. In this chapter, we will interpret the results that we achieved after the data analysis and discuss limitations of the thesis work and possible future works.

5.1 EEG data analysis

To see whether it was possible to record seizure activity with the scalp EEG cap, the power spectrum of the EEG recording was investigated. The resting state EEG signal which can be seen in figure 4.1 did not have any epileptic waveforms such as a sequence of spikes and sharp waves. The amplitude did not exceed 1 microvolt. Later, in figure 4.2, spiking activity was recorded with amplitude higher than 1 microvolt and they were manifested with the high peaks in the delta frequency region at around 2 Hz. This can be checked in the power spectrum on the right side. In the later stage, during the first fMRI EPI session as can be seen in figure 4.3, seizure activity was even more clearly visible on the EEG recording and the amplitude of electrodes 16 and 17 was higher than 4 microvolt. Throughout the first fMRI EPI session, the seizure activity was present. During the second fMRI EPI session as can be seen in figure 4.4, the seizures were still continued in the form of status epilepticus.

On the EEG recording of the second seizure induction day (22/03/2016) as can be seen in figure 4.5, the EEG signals at the beginning showed that seizure activity still remained due to the intraperitoneal KA injection of the day before (21/03/2016). This can be easily noticed when we investigated the power spectrum since sharp waves at 2 Hz were visible. The amplitude of the signal was higher than 4 microvolt for electrodes 14, 16 and 17. The gradient artifact caused by MR scanning was only discernable on electrodes 12 and 23 so it did not interfere with seizure detection. The waveform of the seizures high amplitude spikes corresponds to the characteristic of the epileptiform activity that are seen in KA epilepsy rat models [95].

5.2 fMRI data analysis

For the resting state fMRI datasets, we performed ROI correlation analysis and for the seizure fMRI datasets we performed ROI correlation analysis, GLM analysis and ICA analysis to study functional connectivity. Functional connectivity does not measure directly the connectivity but it measures the similarities in patterns of brain activity of the regions. The functional connectivity that was found in the resting state dataset and in the seizure dataset is compared for ROI correlation analysis. Also the functional connectivity that was discovered in seizure dataset using GLM analysis and ICA analysis was compared.

5.2.1 10 x 10 ROI correlation analysis

Resting state datasets

For rat 2, the simultaneous EEG-fMRI dataset of 27/11/2015 did not show high correlation coefficients between left and right side of the hippocampus and striatum unlike the dataset of fMRI standalone scanning dataset of 26/11/2015. Also the correlation coefficient between left and right side of the thalamus was over 0.7 but lower than the value of fMRI standalone scanning dataset. When we compared the inter-regional correlation value of two datasets, the simultaneous EEG-fMRI dataset had a lower correlation coefficient between all pairs of ROIs. It had high correlation coefficients between L-Hippocampus and L-Thalamus, L-Hippocampus and R-Thalamus, L-Thalamus and R-Hippocampus, L-Thalamus and R-Striatum which were the same case for the fMRI standalone dataset of 26/11/2015 but the values were still lower.

For the rat L1R0 in the dataset of 03/03/2016 fMRI standalone scanning and 04/03/2016 simultaneous EEG-fMRI measurement, for most ROIs, all the intra-regional correlation coefficients were lower in the case of simultaneous EEG-fMRI dataset. Also we observed that the time courses between R-Hippocampus and R-Thalamus, R-Striatum and R-Thalamus were highly correlated in simultaneous EEG-fMRI measurement dataset unlike in the standalone fMRI standalone scanning.

For rat L1R1, in the 04/03/2016 simultaneous EEG-fMRI measurement dataset, the correlation coefficient of left side and right side was lower for all ROIs in contrast to the one in the 03/03/2016 fMRI standalone scanning dataset. But for inter-regional correlation coefficients, R-Hippocampus and R-Thalamus had a higher correlation coefficient but except this pair, all the others were decreased.

The functional connectivity is highly variable for individuals. This is well supported by a lot of studies that have been done [96, 97]. Therefore, we cannot compare the functional connectivity between individuals. However, we observed from the findings above that the functional connectivity shown from the fMRI standalone scanning of a subject differs from the one shown from the simultaneous EEG-fMRI measurement of the subject. The possible reason for this could be because of some artifact caused by EEG recording on BOLD signal during the simultaneous EEG-fMRI measurements [9]. Another possible reason could be difference in mental states of the rat during different MRI acquisition [98].

Seizure datasets

For the dataset of the 21/03/2016 seizure induced, compared to the dataset of 21/03/2016 in resting state, the bilateral correlation coefficient between hippocampus and thalamus was increased while the one between striatum was decreased. For the inter-regional correlation coefficient, L-Auditory cortex and L-Striatum, L-Auditory cortex and R-Hippocampus newly expressed high correlation coefficient. For the dataset of the 22/03/2016 seizure induced, bilateral correlation coefficient was decreased for all ROIs. All inter-regional correlation coefficients were decreased and no values were over 0.7.

In the result of 21/03/2016 seizure induced dataset, increased correlation coefficient was observed for few pairs of ROIs which are discussed above. However, for the 22/03/2016 seizure induced dataset, correlation coefficient was decreased for all pairs of ROIs. It is known that functional connectivity is altered during seizures. It is prevailing hypothesis that functional connectivity is decreased during evoked seizures [99, 99]. On the other hand, there are also other studies that shows increased functional connectivity during seizures [100, 101]. Therefore, a definite conclusion how the functional connectivity of the brain is changed during evoked seizures compared to resting state cannot be made.

5.2.2 GLM analysis and ICA analysis of the seizure datasets

The GLM analysis is the traditional statistical analysis method of studying functional connectivity in the brain. The result of GLM analysis shows voxels of which the time series were highly correlated during the evoked seizures. For the first seizure induction dataset of 21/03/2016, the 40 sec Resting -20 sec Seizure - 40 sec Resting GLM analysis showed us high T-value on voxels of the neocortex, cingulate cortex, striatum, corpus callosum and hippocampus. Also the 20 sec Resting – 40 sec Seizure – 20 sec Resting GLM analysis of the same dataset also showed us high T value for those regions. Therefore, it suggests that neocortex, cingulate cortex, striatum, corpus callosum and hippocampus are the regions that are functionally connected when the seizure was induced in rat 3.

In addition, we performed the ICA analysis for this dataset. The spatial ICA results in showing the voxels that their time series are highly correlated with each other [102]. ICA is a data-driven approach and does not depend on HRF while GLM is a model-driven approach that depends on HRF. The result of ICA analysis for this dataset showed high Z-score over the threshold in neocortex, septal region, cingulate cortex, thalamus and hippocampus. The Z score of the ICA analysis represents the number of standard deviation of the voxel value from the mean voxel value of the map. Therefore, positive Z-score means the value is over the mean and negative Z-score means the value is below the mean. Voxels with Z-score greater than a certain threshold can be considered active voxels for that component that was chosen. Therefore, the voxels with high Z score over the threshold can be considered as active voxels and those voxels mentioned above can be regarded as functionally-connected.

The GLM analysis of the second seizure induction dataset of 22/03/2016 did not result in showing any significantly correlated voxels. However, the ICA analysis was able to show the functionally connected brain regions of this dataset which are neocortex, septal region, cingulate cortex, thalamus, hypothalamus and hippocampus. This is not surprising because it is known that spatial ICA can extract voxels that their time courses are highly correlated while the traditional GLM analysis cannot do so. There have been a lot of studies that compared spatial ICA and GLM and supported this finding [103, 104, 105, 106, 107].

5.3 Limitations of the current work and possible future works

First of all, since there is no literature available about rat EEG-fMRI epilepsy studies using scalp EEG, comparison of the result with existing knowledge was not possible. Most studies opted to use implanted electrodes directly in hippocampus to detect seizures [14, 15]. Therefore, the electrophysiological signal that is coming from hippocampus can be measured directly. However, when using scalp EEG, the inverse problem to know the source of the signal remains unclear since scalp EEG only records the remote effects of electric current produced in the brain. In other words, even if we approximated that EEG signals coming from the electrodes 13, 14, 16 and 17 would be signals from hippocampus but it was not certain. To solve this inverse problem, a lot of ESI (EEG Source Imaging) epilepsy studies using scalp EEG are done with human data to accurately localize seizure onset zone [108, 109]. ESI is the 3D reconstructed functional imaging of the electrophysiological signal from the brain using the EEG and could be used to localize the source of the signal. Using ESI, a better understanding of the pathological process of seizures could be achieved [110]. However, there is only one precedent of developing ESI with rat data [111]. The development of ESI could be attempted in the future taking the advantage of the high density scalp EEG cap that was used in this dissertation.

Second, we induced seizure by injecting KA intraperitoneally which led to status epilepticus. KA injection is one of the most commonly used animal models of epilepsy. However, since the KA evoked continuous seizures, we were not able to make block design within a session. Thus, the block design of the GLM analysis that we used may not be optimal. If we could induce discrete seizures in rats, it

would be possible to detect the onset and duration of each seizure with EEG and incorporate them to make block design as multiple conditions which could bring us more precise result. Therefore, some of the acute seizure models that could possibly induce discrete seizures such as tetanus toxin [112] and repeated penicillin injections [113, 114] may be used in future.

Third, the resting state dataset of rat 3 was performed as standalone fMRI while the seizure datasets of the rat were performed as simultaneous EEG-fMRI. Therefore, there is a certain risk of comparing the functional connectivity for this rat that we inferred from the ROI correlation analysis in resting state and the one in evoked seizure for the rat. The difference in BOLD signal between datasets could be attributed to some artifacts caused by scalp EEG recording on fMRI scanning. This limitation could be improved by optimizing the experimental design. In the future, we could acquire simultaneous EEG-fMRI datasets for each rat both in resting state and in seizure-induced state, using a different approach for intraperitoneal KA injection without having to turn around the rat but only lifting the hind limb [111].

Fourth, since this thesis was a more feasibility study to test the potential usefulness of the scalp EEG cap in assisting simultaneous EEG-fMRI rat epilepsy studies, we have only performed the functional connectivity analysis methods such as ROI correlation analysis, GLM analysis and ICA. However, they do not implicate causality which means that they do not tell us the direction of the connectivity. To be able to infer this, other analysis methods which show the effective connectivity such as structural equation modeling [115, 116] and DCM (Dynamic Causal Modelling) [117] should be performed in future.

Lastly, there are a lot of unexpected factors that can go wrong in preclinical studies and we sacrificed two rats during the experiments. Due to the limited amount of datasets, the result of this thesis might not be able to derive statistical inference. This can be simply solved by acquiring more datasets with experimenters being more experienced in all the experimental procedures.

Chapter 6

Conclusion

The objective of this dissertation was to examine whether the MR compatible scalp EEG cap for rats designed in our lab could be useful in rat epilepsy EEG-fMRI studies and further whether it could bridge the gap between rat and human EEG-fMRI epilepsy studies. For this purpose, we carried out standalone EEG recording in resting state, standalone fMRI scanning in resting state and simultaneous EEG-fMRI measurement in resting state and in evoked seizures. The EEG recordings of the seizure datasets were analyzed to see if the scalp EEG was able to capture seizure activity clearly. In addition, the fMRI datasets were investigated to look at functional connectivity in brain both in resting state and in evoked seizures and evaluate the usefulness of the scalp EEG cap in the data analysis of the fMRI datasets. For this, we executed three data analysis methods which are 10x10 ROI correlation analysis, GLM analysis and ICA. Among these, GLM analysis was the only type of analysis that was informed by EEG recordings. However, the result of GLM analysis served to be a guidance to achieve result of ICA.

The EEG recordings showed the seizure activity with peaks in the delta and theta frequency region and sharp waves. Although there were some artifacts such as breathing artifact and MR gradient artifact, they were not so significant to disturb seizure detection. The result of ROI correlation analysis showed that the correlation coefficients of the standalone fMRI scanning in resting state dataset differed from the ones of simultaneous EEG-fMRI measurement in resting state of the same rat. This might be attributed to some artifacts caused by EEG recording on BOLD signal. But also it could be ascribed to different mental states of the rat during the different experiments. Besides, we observed that the ROI correlation coefficients of the seizure datasets were increased but also decreased compared to the ones of the resting state dataset of the same rat. This corresponded to the existing knowledge that functional connectivity either decreases or increases during the seizures. On top of that, we were able to execute GLM analysis of the seizure datasets by detecting seizures with the scalp EEG and incorporate the seizure scans to make a block design. The result of GLM analysis was able to show the brain regions of the rat which were functionally connected during the evoked seizures compared to resting state. Furthermore, the resulted t-statistical parametric map helped finding the correct component of the ICA. Also, with ICA which is more sensitive than GLM, we found functionally connected brain regions from the second seizure dataset while GLM could not find them.

These findings show that with minor artifacts caused by EEG recording on BOLD signal, we were still able to study functional connectivity of the brain in resting state and in evoked seizures. Also, the EEG was able to clearly show seizures as a standalone but also as a simultaneous EEG-fMRI measurement which allows us to use it as a effective seizure detection device. Thus, we suggest that the scalp EEG cap would be beneficial in rat epilepsy EEG-fMRI studies and it could be used as an experimental platform that is compatible with human EEG-fMRI epilepsy studies.

Bibliography

[1] J. B. Ricki Lewis, David Shier, *Hole's Human Anatomy and Physiology, Ninth Edition*. The McGraw-Hill Companies, 2011.

[2] MD-health.com, "Lobes of the brain." http://www.md-health.com/Lobes-Of-The-Brain.html.

[3] "Portable brain-computer interfaces advance with reconstructed 3d hand motions." http://edgeoftomorrow.wordpress.com/2010/03/02/.

[4] P. Olejniczak, "Neurophysiologic basis of eeg," *Journal of clinical neurophysiology*, vol. 23, no. 3, pp. 186–189, 2006.

[5] "Human electroencephalography." http://ttktamop.elte.hu/online-tananyagok/physiology_practical/ch10s02.html.

[6] "Magnetic resonance imaging (mri)." http://www.iambiomed.com/equipments/mri.php.

[7] C. Kesavadas and B. Thomas, "Clinical applications of functional mri in epilepsy," *The Indian journal of radiology & imaging*, vol. 18, no. 3, p. 210, 2008.

[8] M. Lévesque and M. Avoli, "The kainic acid model of temporal lobe epilepsy," *Neuroscience & Biobehavioral Reviews*, vol. 37, no. 10, pp. 2887–2899, 2013.

[9] J. Ally, "Design of an mri compatible high density cap for scalp eeg in rats," diploma thesis, Ghent University, June 2015.

[10] S. L. Moshé, E. Perucca, P. Ryvlin, and T. Tomson, "Epilepsy: new advances," *The Lancet*, vol. 385, no. 9971, pp. 884–898, 2015.

[11] M. Mula and H. Cock, "More than seizures: improving the lives of people with refractory epilepsy," *European journal of neurology*, vol. 22, no. 1, pp. 24–30, 2015.

[12] C. Rathore and K. Radhakrishnan, "Concept of epilepsy surgery and presurgical evaluation," *Epileptic Disorders*, vol. 17, no. 1, pp. 19–31, 2015.

[13] A. E. Vaudano, P. Avanzini, L. Tassi, A. Ruggieri, G. Cantalupo, F. Benuzzi, P. F. Nichelli, L. Lemieux, and S. Meletti, "Causality within the epileptic network: an eeg-fmri study validated by intracranial eeg," *Frontiers in neurology*, vol. 4, p. 185, 2013.

[14] A. M. Mishra, X. Bai, J. E. Motelow, M. N. DeSalvo, N. Danielson, B. G. Sanganahalli, F. Hyder, and H. Blumenfeld, "Increased resting functional connectivity in spike-wave epilepsy in wag/rij rats," *Epilepsia*, vol. 54, no. 7, pp. 1214–1222, 2013.

[15] B. Van Nieuwenhuyse, R. Raedt, M. Sprengers, I. Dauwe, S. Gadeyne, E. Carrette, J. Delbeke, W. Wadman, P. Boon, and K. Vonck, "The systemic kainic acid rat model of temporal lobe epilepsy: Long-term eeg monitoring," *Brain research*, vol. 1627, pp. 1–11, 2015.

[16] J. D. Power, A. L. Cohen, S. M. Nelson, G. S. Wig, K. A. Barnes, J. A. Church, A. C. Vogel, T. O. Laumann, F. M. Miezin, B. L. Schlaggar, *et al.*, "Functional network organization of the human brain," *Neuron*, vol. 72, no. 4, pp. 665–678, 2011.

[17] O. Sporns, "Brain connectivity," *Scholarpedia*, vol. 2, no. 10, p. 4695, 2007.

[18] "The source of the eeg." http://cognitrn.psych.indiana.edu/busey/eegseminar/pdfs/EEGPrimerCh1.pdf.

[19] H. H. Jasper, "The ten twenty electrode system of the international federation," *Electroencephalography and clinical neurophysiology*, vol. 10, pp. 371–375, 1958.

[20] A. Berger, "How does it work?: Magnetic resonance imaging," *BMJ: British Medical Journal*, vol. 324, no. 7328, p. 35, 2002.

[21] "Magnetic resonance imaging (mri)." https://www.nibib.nih.gov/science-education/science-topics/magnetic-resonance-imaging-mri.

[22] J. C. Gore, "Principles and practice of functional mri of the human brain," *The Journal of clinical investigation*, vol. 112, no. 1, pp. 4–9, 2003.

[23] S. Ogawa, T.-M. Lee, A. R. Kay, and D. W. Tank, "Brain magnetic resonance imaging with contrast dependent on blood oxygenation," *Proceedings of the National Academy of Sciences*, vol. 87, no. 24, pp. 9868–9872, 1990.

[24] L. Pauling and C. D. Coryell, "The magnetic properties and structure of hemoglobin, oxyhemoglobin and carbonmonoxyhemoglobin," *Proceedings of the National Academy of Sciences*, vol. 22, no. 4, pp. 210–216, 1936.

[25] L. Agnati, M. Zoli, I. Strömberg, and K. Fuxe, "Intercellular communication in the brain: wiring versus volume transmission," *Neuroscience*, vol. 69, no. 3, pp. 711–726, 1995.

[26] N. K. Logothetis, "What we can do and what we cannot do with fmri," *Nature*, vol. 453, no. 7197, pp. 869–878, 2008.

[27] P. T. Fox and M. E. Raichle, "Focal physiological uncoupling of cerebral blood flow and oxidative metabolism during somatosensory stimulation in human subjects," *Proceedings of the National Academy of Sciences*, vol. 83, no. 4, pp. 1140–1144, 1986.

[28] R. Turner, D. L. Bihan, C. T. Moonen, D. Despres, and J. Frank, "Echo-planar time course mri of cat brain oxygenation changes," *Magnetic Resonance in Medicine*, vol. 22, no. 1, pp. 159–166, 1991.

[29] G. Aguirre, E. Zarahn, and M. D'esposito, "The variability of human, bold hemodynamic responses," *Neuroimage*, vol. 8, no. 4, pp. 360–369, 1998.

[30] C. Mulert, O. Pogarell, and U. Hegerl, "Simultaneous eeg-fmri: perspectives in psychiatry," *Clinical EEG and neuroscience*, vol. 39, no. 2, pp. 61–64, 2008.

[31] J. Gotman and F. Pittau, "Combining eeg and fmri in the study of epileptic discharges," *Epilepsia*, vol. 52, no. s4, pp. 38–42, 2011.

[32] R. J. Huster, S. Debener, T. Eichele, and C. S. Herrmann, "Methods for simultaneous eeg-fmri: an introductory review," *The Journal of neuroscience*, vol. 32, no. 18, pp. 6053–6060, 2012.

[33] P. J. Allen, G. Polizzi, K. Krakow, D. R. Fish, and L. Lemieux, "Identification of eeg events in the mr scanner: the problem of pulse artifact and a method for its subtraction," *Neuroimage*, vol. 8, no. 3, pp. 229–239, 1998.

[34] G. Bonmassar, P. L. Purdon, I. P. Jääskeläinen, K. Chiappa, V. Solo, E. N. Brown, and J. W. Belliveau, "Motion and ballistocardiogram artifact removal for interleaved recording of eeg and eps during mri," *Neuroimage*, vol. 16, no. 4, pp. 1127–1141, 2002.

[35] K. Mullinger, S. Debener, R. Coxon, and R. Bowtell, "Effects of simultaneous eeg recording on mri data quality at 1.5, 3 and 7 tesla," *International Journal of Psychophysiology*, vol. 67, no. 3, pp. 178–188, 2008.

[36] R. S. Fisher, C. Acevedo, A. Arzimanoglou, A. Bogacz, J. H. Cross, C. E. Elger, J. Engel, L. Forsgren, J. A. French, M. Glynn, *et al.*, "Ilae official report: a practical clinical definition of epilepsy," *Epilepsia*, vol. 55, no. 4, pp. 475–482, 2014.

[37] R. S. Fisher, W. v. E. Boas, W. Blume, C. Elger, P. Genton, P. Lee, and J. Engel, "Epileptic seizures and epilepsy: definitions proposed by the international league against epilepsy (ilae) and the international bureau for epilepsy (ibe)," *Epilepsia*, vol. 46, no. 4, pp. 470–472, 2005.

[38] I. E. Scheffer, S. F. Berkovic, G. Capovilla, M. B. Connolly, L. Guilhoto, E. Hirsch, *et al.*, "The organization of the epilepsies: report of the ilae commission on classification and terminology," *ILAE website*, 2014.

[39] K. D. Laxer, E. Trinka, L. J. Hirsch, F. Cendes, J. Langfitt, N. Delanty, T. Resnick, and S. R. Benbadis, "The consequences of refractory epilepsy and its treatment," *Epilepsy & Behavior*, vol. 37, pp. 59–70, 2014.

[40] P. Kwan, A. Arzimanoglou, A. T. Berg, M. J. Brodie, W. Allen Hauser, G. Mathern, S. L. Moshé, E. Perucca, S. Wiebe, and J. French, "Definition of drug resistant epilepsy: consensus proposal by the ad hoc task force of the ilae commission on therapeutic strategies," *Epilepsia*, vol. 51, no. 6, pp. 1069–1077, 2010.

[41] D. Primrose and G. Ojemann, "Outcome of resective surgery for temporal lobe epilepsy," *Epilepsy surgery*, pp. 181–190, 1992.

[42] J. Engel Jr, "Outcome with respect to epileptic seizures," *Surgical treatment of the epilepsies*, pp. 609–621, 1993.

[43] S. S. Spencer, "Long-term outcome after epilepsy surgery," *Epilepsia*, vol. 37, no. 9, pp. 807–813, 1996.

[44] J. de Tisi, G. S. Bell, J. L. Peacock, A. W. McEvoy, W. F. Harkness, J. W. Sander, and J. S. Duncan, "The long-term outcome of adult epilepsy surgery, patterns of seizure remission, and relapse: a cohort study," *The Lancet*, vol. 378, no. 9800, pp. 1388–1395, 2011.

[45] M. Negishi, R. Martuzzi, E. J. Novotny, D. D. Spencer, and R. T. Constable, "Functional mri connectivity as a predictor of the surgical outcome of epilepsy," *Epilepsia*, vol. 52, no. 9, pp. 1733–1740, 2011.

[46] W. Theodore and R. Fisher, "Brain stimulation for epilepsy," in *Operative Neuromodulation*, pp. 261–272, Springer, 2007.

[47] D. Labar, J. Murphy, E. Tecoma, E. V. S. Group, *et al.*, "Vagus nerve stimulation for medication-resistant generalized epilepsy," *Neurology*, vol. 52, no. 7, pp. 1510–1510, 1999.

[48] E. A. Pereira, A. L. Green, R. J. Stacey, and T. Z. Aziz, "Refractory epilepsy and deep brain stimulation," *Journal of Clinical Neuroscience*, vol. 19, no. 1, pp. 27–33, 2012.

[49] F. Lefevre and N. Aronson, "Ketogenic diet for the treatment of refractory epilepsy in children: a systematic review of efficacy," *Pediatrics*, vol. 105, no. 4, pp. e46–e46, 2000.

[50] M. R. Sarkisian, "Overview of the current animal models for human seizure and epileptic disorders," *Epilepsy & Behavior*, vol. 2, no. 3, pp. 201–216, 2001.

[51] Y. Ben-Ari and J. Lagowska, "[epileptogenic action of intra-amygdaloid injection of kainic acid].," *Comptes rendus hebdomadaires des seances de l'Academie des sciences. Serie D: Sciences naturelles*, vol. 287, no. 8, pp. 813–816, 1978.

[52] Y. Ben-Ari, J. Lagowska, E. Tremblay, and G. L. G. La Salle, "A new model of focal status epilepticus: intra-amygdaloid application of kainic acid elicits repetitive secondarily generalized convulsive seizures," *Brain research*, vol. 163, no. 1, pp. 176–179, 1979.

[53] S. MURAKAMI, T. TAKEMOTO, and Z. SHIMIZU, "Studies on the effective principles of digenea-simplex aq. 1. separation of the effective fraction by liquid chromatography," *YAKUGAKU ZASSHI-JOURNAL OF THE PHARMACEUTICAL SOCIETY OF JAPAN*, vol. 73, no. 9, pp. 1026–1028, 1953.

[54] J. V. Nadler, B. W. Perry, and C. W. Cotman, "Intraventricular kainic acid preferentially destroys hippocampal pyramidal cells," *Nature*, vol. 271, no. 5646, pp. 676–677, 1978.

[55] J. V. Nadler, "Kainic acid: neurophysiological and neurotoxic actions," *Life sciences*, vol. 24, no. 4, pp. 289–299, 1979.

[56] A. Bragin, J. Engel, C. L. Wilson, E. Vizentin, and G. W. Mathern, "Electrophysiologic analysis of a chronic seizure model after unilateral hippocampal ka injection," *Epilepsia*, vol. 40, no. 9, pp. 1210–1221, 1999.

[57] A. Bragin, C. Wilson, and J. Engel, "Chronic epileptogenesis requires development of a network of pathologically interconnected neuron clusters: a hypothesis," *Epilepsia*, vol. 41, no. s6, pp. S144–S152, 2000.

[58] A. Bragin, C. L. Wilson, J. Almajano, I. Mody, and J. Engel, "High-frequency oscillations after status epilepticus: Epileptogenesis and seizure genesis," *Epilepsia*, vol. 45, no. 9, pp. 1017–1023, 2004.

[59] A. Bragin, A. Azizyan, J. Almajano, and J. Engel, "The cause of the imbalance in the neuronal network leading to seizure activity can be predicted by the electrographic pattern of the seizure onset," *The Journal of Neuroscience*, vol. 29, no. 11, pp. 3660–3671, 2009.

[60] G. Carriero, S. Arcieri, A. Cattalini, L. Corsi, V. Gnatkovsky, and M. de Curtis, "A guinea pig model of mesial temporal lobe epilepsy following nonconvulsive status epilepticus induced by unilateral intrahippocampal injection of kainic acid," *Epilepsia*, vol. 53, no. 11, pp. 1917–1927, 2012.

[61] R. J. Racine, "Modification of seizure activity by electrical stimulation: Ii. motor seizure," *Electroencephalography and clinical neurophysiology*, vol. 32, no. 3, pp. 281–294, 1972.

[62] G. Mouri, E. Jimenez-Mateos, T. Engel, M. Dunleavy, S. Hatazaki, A. Paucard, S. Matsushima, W. Taki, and D. C. Henshall, "Unilateral hippocampal ca3-predominant damage and short latency epileptogenesis after intra-amygdala microinjection of kainic acid in mice," *Brain research*, vol. 1213, pp. 140–151, 2008.

[63] F. Pernot, C. Heinrich, L. Barbier, A. Peinnequin, P. Carpentier, F. Dhote, V. Baille, C. Beaup, A. Depaulis, and F. Dorandeu, "Inflammatory changes during epileptogenesis and spontaneous seizures in a mouse model of mesiotemporal lobe epilepsy," *Epilepsia*, vol. 52, no. 12, pp. 2315–2325, 2011.

[64] R. Raedt, A. Van Dycke, D. Van Melkebeke, T. De Smedt, P. Claeys, T. Wyckhuys, K. Vonck, W. Wadman, and P. Boon, "Seizures in the intrahippocampal kainic acid epilepsy model: characterization using long-term video-eeg monitoring in the rat," *Acta neurologica scandinavica*, vol. 119, no. 5, pp. 293–303, 2009.

[65] A. A. Gurbanova, R. G. Aker, S. Sirvanci, T. Demiralp, and F. Y. Onat, "Intra-amygdaloid injection of kainic acid in rats with genetic absence epilepsy: the relationship of typical absence epilepsy and temporal lobe epilepsy," *The Journal of Neuroscience*, vol. 28, no. 31, pp. 7828–7836, 2008.

[66] E. D. French, C. Aldinio, and R. Schwarcz, "Intrahippocampal kainic acid, seizures and local neuronal degeneration: relationships assessed in unanesthetized rats," *Neuroscience*, vol. 7, no. 10, pp. 2525–2536, 1982.

[67] S. Jinde, J. E. Belforte, J. Yamamoto, M. A. Wilson, S. Tonegawa, and K. Nakazawa, "Lack of kainic acid-induced gamma oscillations predicts subsequent ca1 excitotoxic cell death," *European Journal of Neuroscience*, vol. 30, no. 6, pp. 1036–1055, 2009.

[68] A. Medvedev, L. Mackenzie, J. Hiscock, and J. Willoughby, "Kainic acid induces distinct types of epileptiform discharge with differential involvement of hippocampus and neocortex," *Brain research bulletin*, vol. 52, no. 2, pp. 89–98, 2000.

[69] Y. Ben-Ari, E. Tremblay, D. Riche, G. Ghilini, and R. Naquet, "Electrographic, clinical and pathological alterations following systemic administration of kainic acid, bicuculline or pentetrazole: metabolic mapping using the deoxyglucose method with special reference to the pathology of epilepsy," *Neuroscience*, vol. 6, no. 7, pp. 1361–1391, 1981.

[70] M. Berger, H. Lassmann, and O. Hornykiewicz, "Limbic seizures without brain damage after injection of low doses of kainic acid into the amygdala of freely moving rats," *Brain research*, vol. 489, no. 2, pp. 261–272, 1989.

[71] L. Velíšek, H. Kubová, J. Velíšková, P. Mareš, and M. Ortová, "Action of antiepileptic drugs against kainic acid-induced seizures and automatisms during ontogenesis in rats," *Epilepsia*, vol. 33, no. 6, pp. 987–993, 1992.

[72] E. W. Lothman, R. C. Collins, and J. A. Ferrendelli, "Kainic acid-induced limbic seizures electrophysiologic studies," *Neurology*, vol. 31, no. 7, pp. 806–806, 1981.

[73] M. Lévesque, J. P. Langlois, P. Lema, R. Courtemanche, G.-A. Bilodeau, and L. Carmant, "Synchronized gamma oscillations (30–50 hz) in the amygdalohippocampal network in relation with seizure propagation and severity," *Neurobiology of disease*, vol. 35, no. 2, pp. 209–218, 2009.

[74] Y. Ben-Ari and R. Cossart, "Kainate, a double agent that generates seizures: two decades of progress," *Trends in neurosciences*, vol. 23, no. 11, pp. 580–587, 2000.

[75] M. R. Priel, N. F. dos Santos, and E. A. Cavalheiro, "Developmental aspects of the pilocarpine model of epilepsy," *Epilepsy research*, vol. 26, no. 1, pp. 115–121, 1996.

[76] R. S. Sloviter, "The neurobiology of temporal lobe epilepsy: too much information, not enough knowledge," *Comptes rendus biologies*, vol. 328, no. 2, pp. 143–153, 2005.

[77] A. Bortel, M. Lévesque, G. Biagini, J. Gotman, and M. Avoli, "Convulsive status epilepticus duration as determinant for epileptogenesis and interictal discharge generation in the rat limbic system," *Neurobiology of disease*, vol. 40, no. 2, pp. 478–489, 2010.

[78] M. Lévesque, A. Bortel, J. Gotman, and M. Avoli, "High-frequency (80–500hz) oscillations and epileptogenesis in temporal lobe epilepsy," *Neurobiology of disease*, vol. 42, no. 3, pp. 231–241, 2011.

[79] G. V. Goddard, D. C. McIntyre, and C. K. Leech, "A permanent change in brain function resulting from daily electrical stimulation," *Experimental neurology*, vol. 25, no. 3, pp. 295–330, 1969.

[80] G. V. Goddard, "Development of epileptic seizures through brain stimulation at low intensity," *Nature*, vol. 214, pp. 1020–1021, 1967.

[81] Y. H. Raol and A. R. Brooks-Kayal, "Experimental models of seizures and epilepsies.," *Progress in molecular biology and translational science*, vol. 105, pp. 57–82, 2011.

[82] A. K. Sharma, R. Y. Reams, W. H. Jordan, M. A. Miller, H. L. Thacker, and P. W. Snyder, "Mesial temporal lobe epilepsy: pathogenesis, induced rodent models and lesions," *Toxicologic pathology*, vol. 35, no. 7, pp. 984–999, 2007.

[83] C. P. Pawela, B. B. Biswal, A. G. Hudetz, M. L. Schulte, R. Li, S. R. Jones, Y. R. Cho, H. S. Matloub, and J. S. Hyde, "A protocol for use of medetomidine anesthesia in rats for extended studies using task-induced bold contrast and resting-state functional connectivity," *Neuroimage*, vol. 46, no. 4, pp. 1137–1147, 2009.

[84] J. L. Hellier, P. R. Patrylo, P. S. Buckmaster, and F. E. Dudek, "Recurrent spontaneous motor seizures after repeated low-dose systemic treatment with kainate: assessment of a rat model of temporal lobe epilepsy," *Epilepsy research*, vol. 31, no. 1, pp. 73–84, 1998.

[85] K. Yoshizawa, Y. Emoto, Y. Kinoshita, T. Yuri, and A. Tsubura, "N-methyl-n-nitrosourea-induced cerebellar hypoplasia in rats: Effect of arachidonic acid supplementation during the gestational, lactational and post-weaning periods," *Experimental and therapeutic medicine*, vol. 6, no. 3, pp. 627–634, 2013.

[86] C.-G. Yan, X.-D. Wang, X.-N. Zuo, and Y.-F. Zang, "Dpabi: Data processing & analysis for (resting-state) brain imaging," *Neuroinformatics*, 2016.

[87] R. A. Poldrack, J. A. Mumford, and T. E. Nichols, *Handbook of functional MRI data analysis*. Cambridge University Press, 2011.

[88] E. A. Papp, T. B. Leergaard, E. Calabrese, G. A. Johnson, and J. G. Bjaalie, "Waxholm space atlas of the sprague dawley rat brain," *NeuroImage*, vol. 97, pp. 374–386, 2014.

[89] L. J. Kjonigsen, S. Lillehaug, J. G. Bjaalie, M. P. Witter, and T. B. Leergaard, "Waxholm space atlas of the rat brain hippocampal region: Three-dimensional delineations based on magnetic resonance and diffusion tensor imaging," *NeuroImage*, vol. 108, pp. 441–449, 2015.

[90] M. Sergejeva, E. A. Papp, R. Bakker, M. A. Gaudnek, Y. Okamura-Oho, J. Boline, J. G. Bjaalie, and A. Hess, "Anatomical landmarks for registration of experimental image data to volumetric rodent brain atlasing templates," *Journal of neuroscience methods*, vol. 240, pp. 161–169, 2015.

[91] H. Lu, Q. Zou, H. Gu, M. E. Raichle, E. A. Stein, and Y. Yang, "Rat brains also have a default mode network," *Proceedings of the National Academy of Sciences*, vol. 109, no. 10, pp. 3979–3984, 2012.

[92] E. Cavalheiro, M. De Feo, O. Mecarelli, and G. Ricci, "Intracortical and intrahippocampal injections of kainic acid in developing rats: an electrographic study," *Electroencephalography and clinical neurophysiology*, vol. 56, no. 5, pp. 480–486, 1983.

[93] G. L. Holmes and J. L. Thompson, "Effects of kainic acid on seizure susceptibility in the developing brain," *Developmental Brain Research*, vol. 39, no. 1, pp. 51–59, 1988.

[94] E. Cherubini, M. De Feo, O. Mecarelli, and G. Ricci, "Behavioral and electrographic patterns induced by systemic administration of kainic acid in developing rats," *Developmental Brain Research*, vol. 9, no. 1, pp. 69–77, 1983.

[95] C. E. Stafstrom, J. L. Thompson, and G. L. Holmes, "Kainic acid seizures in the developing brain: status epilepticus and spontaneous recurrent seizures," *Developmental Brain Research*, vol. 65, no. 2, pp. 227–236, 1992.

[96] S. Mueller, D. Wang, M. D. Fox, B. T. Yeo, J. Sepulcre, M. R. Sabuncu, R. Shafee, J. Lu, and H. Liu, "Individual variability in functional connectivity architecture of the human brain," *Neuron*, vol. 77, no. 3, pp. 586–595, 2013.

[97] A. Baldassarre, C. M. Lewis, G. Committeri, A. Z. Snyder, G. L. Romani, and M. Corbetta, "Individual variability in functional connectivity predicts performance of a perceptual task," *Proceedings of the National Academy of Sciences*, vol. 109, no. 9, pp. 3516–3521, 2012.

[98] R. L. Buckner, F. M. Krienen, and B. T. Yeo, "Opportunities and limitations of intrinsic functional connectivity mri," *Nature neuroscience*, vol. 16, no. 7, pp. 832–837, 2013.

[99] G. Bettus, E. Guedj, F. Joyeux, S. Confort-Gouny, E. Soulier, V. Laguitton, P. J. Cozzone, P. Chauvel, J.-P. Ranjeva, F. Bartolomei, *et al.*, "Decreased basal fmri functional connectivity in epileptogenic networks and contralateral compensatory mechanisms," *Human brain mapping*, vol. 30, no. 5, pp. 1580–1591, 2009.

[100] D. R. Addis, M. Moscovitch, and M. P. McAndrews, "Consequences of hippocampal damage across the autobiographical memory network in left temporal lobe epilepsy," *Brain*, vol. 130, no. 9, pp. 2327–2342, 2007.

[101] H. Powell, M. P. Richardson, M. R. Symms, P. A. Boulby, P. J. Thompson, J. S. Duncan, and M. J. Koepp, "Reorganization of verbal and nonverbal memory in temporal lobe epilepsy due to unilateral hippocampal sclerosis," *Epilepsia*, vol. 48, no. 8, pp. 1512–1525, 2007.

[102] V. G. van de Ven, E. Formisano, D. Prvulovic, C. H. Roeder, and D. E. Linden, "Functional connectivity as revealed by spatial independent component analysis of fmri measurements during rest," *Human brain mapping*, vol. 22, no. 3, pp. 165–178, 2004.

[103] J. Xu, M. N. Potenza, and V. D. Calhoun, "Spatial ica reveals functional activity hidden from traditional fmri glm-based analyses," *Frontiers in neuroscience*, vol. 7, p. 154, 2013.

[104] V. Calhoun, T. Adali, V. McGinty, J. Pekar, T. Watson, and G. Pearlson, "fmri activation in a visual-perception task: network of areas detected using the general linear model and independent components analysis," *NeuroImage*, vol. 14, no. 5, pp. 1080–1088, 2001.

[105] S. Malinen, Y. Hlushchuk, and R. Hari, "Towards natural stimulation in fmri—issues of data analysis," *Neuroimage*, vol. 35, no. 1, pp. 131–139, 2007.

[106] Y. Tie, S. Whalen, R. O. Suarez, and A. J. Golby, "Group independent component analysis of language fmri from word generation tasks," *Neuroimage*, vol. 42, no. 3, pp. 1214–1225, 2008.

[107] K. K. Kim, P. Karunanayaka, M. D. Privitera, S. K. Holland, and J. P. Szaflarski, "Semantic association investigated with functional mri and independent component analysis," *Epilepsy & Behavior*, vol. 20, no. 4, pp. 613–622, 2011.

[108] P. Mégevand, L. Spinelli, M. Genetti, V. Brodbeck, S. Momjian, K. Schaller, C. M. Michel, S. Vulliemoz, and M. Seeck, "Electric source imaging of interictal activity accurately localises the seizure onset zone," *Journal of Neurology, Neurosurgery & Psychiatry*, vol. 85, no. 1, pp. 38–43, 2014.

[109] G. Pellegrino, T. Hedrich, R. Chowdhury, J. A. Hall, J.-M. Lina, F. Dubeau, E. Kobayashi, and C. Grova, "Source localization of the seizure onset zone from ictal eeg/meg data," *Human brain mapping*, 2016.

[110] S. Vulliemoz, R. Thornton, R. Rodionov, D. W. Carmichael, M. Guye, S. Lhatoo, A. W. McEvoy, L. Spinelli, C. M. Michel, J. S. Duncan, *et al.*, "The spatio-temporal mapping of epileptic networks: combination of eeg–fmri and eeg source imaging," *Neuroimage*, vol. 46, no. 3, pp. 834–843, 2009.

[111] J. Bae, A. Deshmukh, Y. Song, and J. Riera, "Brain source imaging in preclinical rat models of focal epilepsy using high-resolution eeg recordings," *Journal of visualized experiments: JoVE*, no. 100, 2015.

[112] K. E. Nilsen, M. C. Walker, and H. R. Cock, "Characterization of the tetanus toxin model of refractory focal neocortical epilepsy in the rat," *Epilepsia*, vol. 46, no. 2, pp. 179–187, 2005.

[113] H. Ni, Y.-w. Jiang, L.-y. Tao, J.-n. Cen, and X.-r. Wu, "Effects of penicillin-induced developmental epilepticus on hippocampal regenerative sprouting, related gene expression and cognitive deficits in rats," *Toxicology letters*, vol. 188, no. 2, pp. 161–166, 2009.

[114] H. Ni, C. Li, L.-y. Tao, and J.-n. Cen, "Physical exercise improves learning by modulating hippocampal mossy fiber sprouting and related gene expression in a developmental rat model of penicillin-induced recurrent epilepticus," *Toxicology letters*, vol. 191, no. 1, pp. 26–32, 2009.

[115] A. J. Tomarken and N. G. Waller, "Structural equation modeling: Strengths, limitations, and misconceptions," *Annu. Rev. Clin. Psychol.*, vol. 1, pp. 31–65, 2005.

[116] R. Schlösser, T. Gesierich, B. Kaufmann, G. Vucurevic, S. Hunsche, J. Gawehn, and P. Stoeter, "Altered effective connectivity during working memory performance in schizophrenia: a study with fmri and structural equation modeling," *Neuroimage*, vol. 19, no. 3, pp. 751–763, 2003.

[117] K. J. Friston, L. Harrison, and W. Penny, "Dynamic causal modelling," *Neuroimage*, vol. 19, no. 4, pp. 1273–1302, 2003.